AN EXPERIMENTAL STUDY OF HEAT TRANSFER OF A SINGLE HEATED MODULE ON CONDUCTIVE BOARDS IN THE TURBULENT REGION FOR AN IN-LINE ARRAY OF SURFACE MOUNTED CUBIC MODULES IN A HORIZONTAL RECTANGULAR CHANNEL

By

WEN-CHIEH TANG

Master of Science
New Jersey Institute of Technology
Newark, New Jersey
1990

Submitted to the Faculty of the
Graduate College of the
Oklahoma State University
in partial fulfillment of
the requirements for
the Degree of
DOCTOR OF PHILOSOPHY
July, 1997

AN EXPERIMENTAL STUDY OF HEAT TRANSFER OF A SINGLE HEATED MODULE ON CONDUCTIVE BOARDS IN THE TURBULENT REGION FOR AN IN-LINE ARRAY OF SURFACE MOUNTED CUBIC MODULES IN A HORIZONTAL RECTANGULAR CHANNEL

Thesis Approved :

A. J. Ghajar

Thesis Adviser

David G. Lilley

Carl D. Latino

Thomas C. Collins

Dean of the Graduate College

ACKNOWLEDGMENTS

I would like to express my sincere appreciation to my adviser, Dr. A. J. Ghajar, for his direction and advice throughout the progress of this research. My sincere appreciation extends to my committee members, Dr. F. Chambers, Dr. D. Lilley and Dr. C. Latino whose kind suggestions and guidance are invaluable.

I gratefully acknowledge the contributions of Dr. M. Arabzadeh, and Mr. Y. Wang in the design and construction of the apparatus, Mr. M. Rajagopalan in writing the computer programs of data acquisition and reduction. I would also like to thank Mr. D. Kim for his generous help and suggestions.

Moreover, I would like to express my sincere gratitude to my close friends who provided suggestions and assistance for this study: Dr. J. Cai, Dr. L. Tam, Dr. T. Lin, Dr. M. Dong, Dr. Y. Tian and. Dr. G. Chen. Thanks also go to MAE North Lab manager, Mr. J. Davis and MAE Electronic Shop technician, Mr. R. Jackson for their help and kindness.

Most special gratitude and appreciation go to my loving wife Hui-jung Hunag and son Edwin for their patience, sacrifices and support throughout this whole process. I am deeply in debt for the encouragement and financial support given by my parents, Mr. Fan Tang and Mrs. A-fan Lee, Tang, my brother Mr. Wen-hou Tan, and my sister, Ms. Wen-chi Tang.

Finally, I would like to thank the School of Mechanical and Aerospace Engineering for the financial support during more than six and a half years of study.

TABLE OF CONTENTS

LIST OF TABLES

LIST OF FIGURES

Figure Page

NOMENCLATURE

English Letters

A^*	exposed copper foil surface area ratio, dimensionless
$A_{blocked}$	the cross sectional area of the channel blocked by the aluminum modules, cm^2
A_{cross}	cross sectional area of the rectangular channel, cm^2
A_m	exposed module surface area, cm^2
A_k	module contact surface area with the test board, cm^2
D_h	hydraulic diameter of the rectangular channel at a specific channel height, cm
Gr	Grashof number ($= g \beta \Delta T L_c^3/\nu^2$), dimensionless
H	rectangular channel height, cm
h	heat transfer coefficient, W/m^2-K
I	current carried by the test section, Amperes
k	thermal conductivity of the cooling air evaluated at T_∞, W/m-K
k_1	thermal conductivity of pure copper, W / m - °C
k_2	thermal conductivity of the fiberglass, W / m - °C
k_3	thermal conductivity of the commercial plexiglas, W / m - °C
L	module length in streamwise and spanwise direction, 2.54 cm
L_c	characteristic length, cm
Nu	Nusselt number ($= ht/k$), dimensionless

Nu_{ad} Nusselt number of the adiabatic test board, dimensionless

Q_k vertical conduction heat loss, Watts

Q_m equivalent (lumped) convection heat transfer rate of the heat dissipating module, Watts

Q_r radiation heat loss, Watts

Q_t input power to the active (heat dissipating) module, Watts

R gas constant of air, 287 J/kg-K

Re modified Reynolds number (= V* t/ν), dimensionless

R_w the thermal resistance of the test board and channel floor assembly, °C/W

S length between the modules of the in-line array in streamwise and spanwise directions, 2.54 cm

T* copper foil thickness ratio, dimensionless

T_∞ the approaching cooling air temperature of the test fluid or the surroundings air temperature, °C

T_m module temperature, °C

t module height, 2.54 cm

t_1 thickness of the copper foil, cm

t_2 thickness of the fiber glass circuit board, cm

t_3 the thickness of the commercial plexiglas bottom board, cm

V measured channel centerline velocity, m/s

V* modified channel centerline velocity [= $V A_{cross}/(A_{cross} - A_{blocked})$], m/s

V_{local} measured local velocity, m/s

V_{max} maximum measured velocity, m/s

Volt voltage drop across the heat dissipating resistor, volt

x stream-wise distance from the center of a module to the beginning of the

in-line array, m

Greek Symbols

ΔP	pressure difference, in. of water
ΔT	temperature difference, °C
ν	kinematic viscosity of the cooling air flow evaluated at T_∞, m^2/s
ρ	density of the approaching air flow evaluated at T_∞, kg/m^3

Subscripts

adjusted	refers to adjusted
atm	refers to atmospheric
exp	refers to the experimental value
pred	refers to the predicted value
10W	refers to the value when heated with 10 Watts
20W	refers to the value when heated with 20 Watts
∞	refers to far field (inlet of the rectangular channel) or surroundings

CHAPTER I

INTRODUCTION

1.1 Background

Electronic devices have become a vital part of modern civilization. The increase in circuit density of electronic components and corresponding rise in power densities is making electronic cooling (or electronic thermal control) a very challenging part of the evolution of electronic systems. Corporate competitiveness is putting even more pressure on the product-development process for faster turn around time of new systems. Consequently, fundamental knowledge of heat transfer processes in electronic devices has become increasingly important in creating models that can characterize the heat transfer behavior during the developmental stage of the product.

As power dissipation and component density continue to increase in electronic devices, effective cooling technology of electronic equipment has become essential. In some high-capacity power components, the heat dissipation required frequently reaches 50 W/cm^2 and can be as high as 200 W/cm^2 (Peterson and Ortega,1990). Semiconductor chips themselves have steadily become more sophisticated, thus more complicated. The numbers of transistors contained in a chip have increased by several orders of magnitude. Today, thermal control of the circuitry is well recognized as a gating factor in the

development of advanced electronic systems. More rigorous reliability constraints in modern electronic devices demand much better prediction of the temperature field, within and around individual components. It has been found in some investigations that a single component operating 10 °C beyond the manufacturer's maximum specified service temperature, typically between 85 and 100 °C, can reduce the reliability of some systems by as much as 50% (Peterson and Ortega,1990).

Air-cooled, hybrid-cooled, indirect liquid cooled, and direct liquid cooled are cooling technologies applied by the industry. The heat dissipating capacity of each type of cooling technology varies from the lowest of air-cooling to the highest of direct liquid cooling. Air is the working fluid that cools the electronic components packed in electronic devices for air cooling. Hybrid cooling uses air to cool the electronic components and water cooled heat exchangers cool the air. Electronic components are mounted on cold plates cooled by water for indirect liquid cooled systems. Direct liquid cooling immerses the heat dissipating electronic components in the cooling liquid (dielectric coolant).

Air cooled systems do not require an extensive change from original printed circuit board architecture. Consequently, air cooling is the choice of cooling technology by the industry whenever it is possible. The main advantages of air cooled systems are : easy to design, inexpensive to install and operate, and easy to maintain.

There is still not sufficient knowledge in conventional heat transfer analysis for

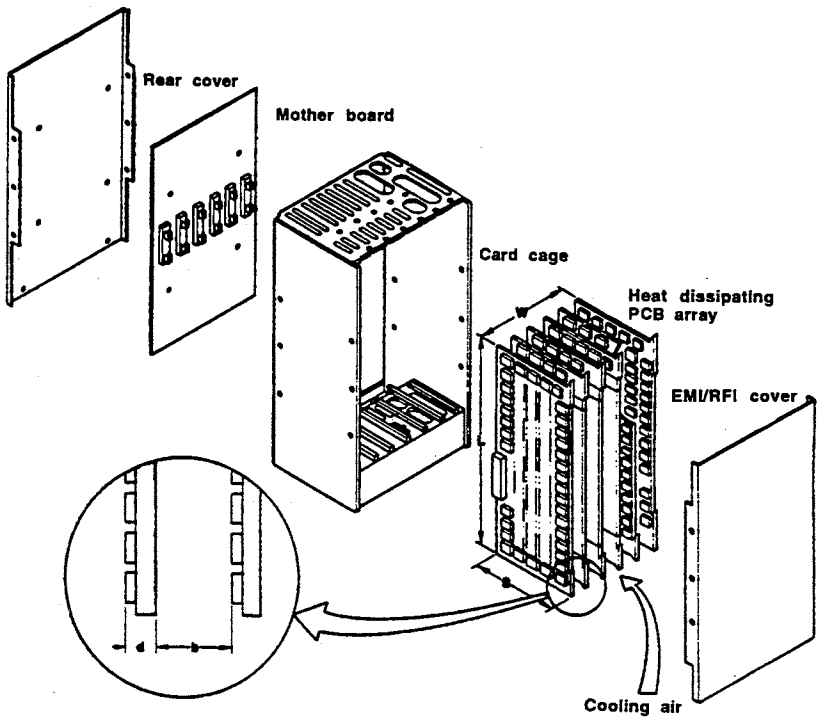

Fig. 1.1a Typical printed circuit board arrangement in electronic equipment (Chung, 1987).

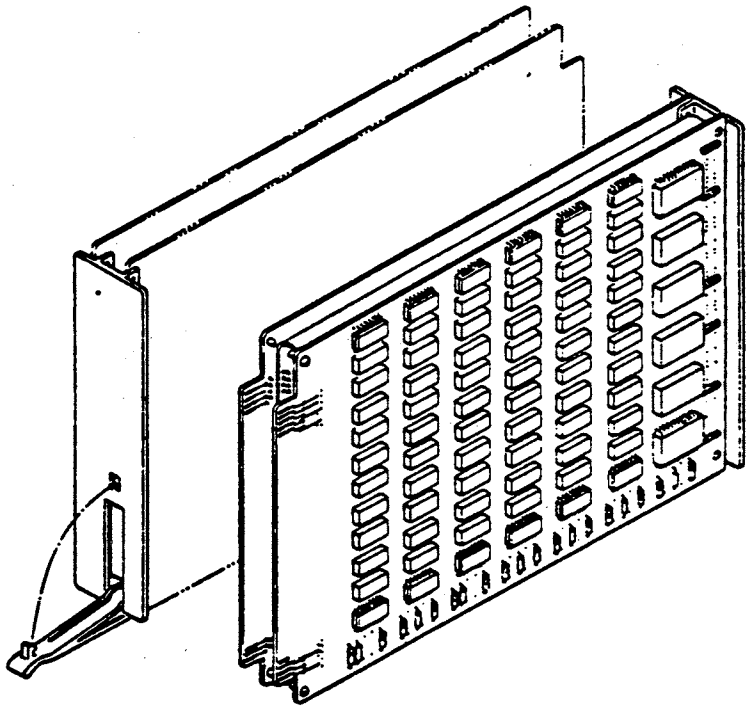

Fig. 1.1b Typical printed circuit board with an in-line array of semi-regular components (Ortega and Moffat, 1986b).

the highly non-uniform situation found in most electronic devices. Inside modern electronic equipment, there may be all kinds of electronic components that vary in size, shape and material, and in the way they are arranged on printed circuit boards. One of the most common modeling problems in electronic cooling is that of cards on board configurations. Fig. 1.1a shows a typical arrangement of printed circuit boards in electronic equipment. A typical printed circuit board with an in-line array of semi-regular components is shown in Fig. 1.1b. Even with an in-line array of semi-regular components instead of irregular components arranged irregularly, the geometry presented in Fig. 1.1b propounds a complex problem in heat transfer analysis. In addition, the heat dissipation from each element in the array may also be different. In real printed circuit boards, there is one or multiple layers of copper foil electric power distribution plane which is also highly conductive thermally. Thus, the process of heat transfer from a single integrated circuit chip package or a similar shape of electronic component mounted on a printed circuit board is a complicated combined mode of conduction and convection (conjugate heat transfer). To be able to address this complex heat transfer problem, fundamental understanding of heat transfer mechanisms in electronic cooling is vital. It is the physical phenomenon more than the practical design that this study is interested in. That is, to understand these fundamental physics, in particular for turbulent air flow over surfaces such as a printed circuit board with arrays of electronic components mounted on its surface.

In the past few years, a number of investigators have been focusing on electronic cooling. Most of these investigators used uniform modules on an adiabatic board to

simulate a printed circuit board (PCB). The previous works related to electronic cooling are either two-dimensional (ribs) or three-dimensional modules and most of the numerical works simplified three-dimensional modules to two-dimensional ribs due to the computational ability of today's computers. There are still not sufficient experimental investigations on the conjugate heat transfer process in electronic cooling available in the literature. Numerical works should be united with experimental data and vice versa to depict a complete picture of this combined heat transfer process.

This research focuses on the combined mode of heat transfer phenomena of a single air-cooled one-sided printed circuit board with heat dissipating electronic components. It is common that these electronic components are arranged in in-line array on a printed circuit board. The board may be vertically (or horizontally) positioned facing the back of an adjacent board or packed in a rectangular metal (or plastic) case by itself. With some idealizations and simplifications, a horizontal rectangular channel with a regular in-line array of cubic modules, which are frequently used to represent typical PCB topologies, was used to characterize the electronic cooling situation mentioned above.

This study is to contribute to the goals of (1) improving the understanding of the fundamental aspects of the combined mode of heat transfer phenomena of real printed circuit boards which have one or more layers of conductive substrate (copper foil), and (2) identifying the important parameters affecting this conjugate heat transfer process based on sound physics and thoughtful experimental investigation. In general, this study is to improve the capability to comprehend this complex heat transfer process.

1.2 Literature Survey

Heat transfer in electronic cooling is a topic that has generated a lot of interest among researchers in recent years. Consequently, this has lead to a good many of research directions and a great variety of studies in electronic cooling have been published. This survey will concentrate on the studies related to the heat transfer of a printed circuit board with an in-line array of electronic components in a rectangular channel. In most of these studies, an array of rectangular blocks (three-dimensional modules) or ribs (two-dimensional modules) were used to characterize the heat-dissipating electronic components.

Arvizu and Moffat (1981) reported an experimental study on the problem of predicting the temperature of each module in an air-cooled array on an adiabatic bottom board. They applied the superposition technique successively to predict the temperature distribution on an array of arbitrarily heated components in forced convection. Heat transfer coefficients and thermal wake profiles of the dimensionless temperature (θ) were measured on regular in-line arrays of cubes of side 1.27 cm with array spacing of S/B (the ratios of the center to center spacing between modules in the stream wise direction to the module height) = 2 and 3. The channel height (H) was varied from H/B= 1 to 4.6, and the velocity was varied from 1.5 to 9.0 m/s. The dimensionless temperature, θ, defined as

$$\theta = \frac{T_{measured} - T_{amb}}{T_{heated\ block} - T_{amb}}$$

where, $T_{measured}$ is the measured temperature of the module of interest. A thermal wake function was modeled as θ (N) = (1/N) θ_1. In this model, N is the number of rows downstream of the heated module and θ_1 is the thermal wake function at N = 1. The thermal wake profiles of θ were then superposed to calculate the predicted temperature distribution on an arbitrary heated array.

Ortega and Moffat (1986a, 1986b) experimentally investigated the problem of predicting the temperature of each module in an air-cooled array in mixed and free convection. They found that when the adiabatic temperature was used as a local descriptor and showed that for $Gr_a / Re^2_B < 0.3$ (Gr_a is the adiabatic Grashof number based on the module height B and the element's adiabatic temperature, and Re_B is the induced flow Reynolds number based on the module height), local buoyancy effects were negligible compared to the local forced convection effects which means that forced convection dominated the heat transfer process. They also successfully applied the superposition technique to free convection flows whenever $Gr_a / Re^2_B < 0.3$.

Copeland (1988) studied heat transfer coefficients and thermal wake functions as a function of channel height, air velocity, and planar spacing with experiments. The thermal wake functions were found to be strongly dependent on velocity and channel height but followed the (1/N) θ_1 model of Arvizu and Moffat (1981).

The previous few paragraphs summarized the works of the researchers who have looked at applications of the superposition technique to electronics cooling. The basic assumption of the superposition technique is the linearity and homogeneity of the energy

equation. The temperature distribution of the thermal wake, namely, forced convection heat transfer mode, can be superimposed to predict the temperature field. That is why most of the experimental works of superposition technique were done with arrays of uniform size of modules on adiabatic boards. The conduction in the board always exists in electronic applications due to the power distribution system which is one or more layers of solid copper foil buried within the board. The adiabatic board assumption is widely applied in electronic cooling research. There is still not yet enough experimental data to either support or dismiss this assumption. Wirtz (1996) argued that after adiabatic board convection mechanisms are suitably quantified, the analysis of electronic cooling can be complete using a standard conduction analyzer in conjunction with separate calculations for convection and radiation heat transfer process. Again, without a sufficient experimental data bank to verify the conduction (due to copper foil in the board) analysis, the analysis will be far from complete. The following researchers did not include superposition technique in their studies yet all assumed adiabatic board conditions.

Chang et al. (1987) studied forced convective heat transfer from surface mounted three-dimensional components to a horizontal channel airflow. Based on the results of their experiments, the Colburn j-factor which is a function of Reynolds number and the ratio of channel height to component height can better characterize the average heat transfer coefficient from heated component. It was also found that the hydrodynamic wake from the upstream component depending on the spacing between two components can cause a large variation in heat transfer on the heated component.

Faghri et al. (1989) performed experiments to study heat transfer and pressure-drop characteristics in forced convection cooling of three-dimensional blocks deployed along one adiabatic wall of a rectangular channel. They introduced a new dimensionless parameter called the packing density which is defined as

$$C = \frac{L^2 B}{(L+S)^2 (B+H)}$$

where L is the length and width of the module , B is the height of the module , S is the distance between modules and H is the difference between the channel and module height. The parameter C is the ratio of the volume of the modules to the total volume of the test section. Both the heat transfer and the pressure-drop data correlate well with the new parameter in the form of

$$St^{0.25} Re^{0.0625} / C^2$$

as a function of C and

$$f^{0.25} Re^{0.0625} / C^2$$

also as a function of C. The dimensionless friction factor (f) defined as

$$f = \frac{\dot{p}(H+B)}{\frac{1}{2}\rho V_{in}^2}$$

where, $\dot{p}$ is the pressure gradient across successive rows of modules, ρ is the density of air at prevailing lab conditions and V_{in} is the inlet air velocity.

Lehmann and Wirtz (1985) conducted experiments with two dimensional ribs at different channel heights and rib spacings. For a given channel spacing and channel Reynolds number, it was shown that the Nusselt number increased with increased spacing

between ribs, as the flow between ribs changed from a driven-cavity-type situation, to a wake-interference regime, to an independent roughness regime. Lehmann and Wirtz showed this transition by smoke wire flow visualization in similar ribbed channels.

Sparrow et al. (1982) used the naphthalene sublimation technique to measure the Sherwood number and infer a Nusselt number for modules. The modules measured 2.67 × 2.67 × 1.0 cm and were spaced 0.67 cm apart for S/L (L = length of module in stream wise direction)= 0.25, and a fixed channel height of 2.67 cm.

Wirtz and Dykshoorn (1984) measured the thermal wake functions downstream of a heated module as well as heat transfer coefficients as a function of channel height (H/B = 1.5 to 4.6) and inlet velocity (V = 1 to 10 m/s). The geometry was a regular in-line array of flat packs (2.54 × 2.54 × 0.635 cm high) with a module spacing S/L, of 2. Wirtz and Dykshoorn's data were correlated by the expression

$$Nu_L = 0.348\ Re_L^{0.6}$$

and the data of Sparrow et al. (1982) were also correlated in a similar form by

$$Nu_L = 0.0935\ Re_L^{0.72}$$

Roeller and Webb (1992) conducted experiments to investigate the heat transfer characteristics of isolated two-dimensional protrusions in channel flow. The experimental study included the effects of channel Reynolds number (based on the channel hydraulic diameter) in the nominal range $1500 \leq Re \leq 10000$. A composite correlation was developed for the two-dimensional data and the three-dimensional protrusion data they

reported previously. A parameter A** was defined which represented the fraction of the channel cross-section open to flow.

$$A^{**} = 1 - (P_w/W) (P_h/H)$$

where P_w and P_h are the module width and height respectively, W and H are the channel width and height respectively. All two-dimensional and three-dimensional data were correlated with the equation

$$\overline{Nu} = 0.150\, Re^{0.632} (A^{**})^{-0.455} (H/P_L)^{-0.727}$$

where P_L is the module length (in the flow direction). The function describes well the average Nusselt number dependence on channel Reynolds number, normalized channel wall spacing, and a parameter quantifying the fraction of channel cross-section open to flow. The empirical correlation predicts their experimental data with an average deviation of 6.6% and a maximum deviation of 27%.

Conductive boards or conduction heat transfer in the printed circuit boards were investigated by the following researchers.

Wagner (1984) reported a two-dimensional finite-difference numerical study on the influence of the thermal conductivity of the substrate material of a printed circuit board on the operating temperature of the integrated circuit chips (ICs) that are attached to it. One of the conclusions is that the thermal conductivity of the substrate material has a profound influence on the operating temperatures of the ICs that are attached to it. It was also found out that the surface area of the substrate has little effect for low

conductivity substrates, but gradually becomes the dominant factor as the conductivity increases. The equivalent thermal conductivity for the five types of circuit boards evaluated in the work of Wagner (1984) is given in Table 1.1. Though these values were numerically calculated based on a simple two-dimensional heat conduction model and not measured directly, they can still be used as reference thermal conductivities for different types of printed circuit boards. The values listed in the table demonstrate the relative magnitudes of thermal conductivities between different types of circuit boards. The test

TABLE 1.1

Equivalent Thermal Conductivity for Four Types of Circuit Boards

Material	Equivalent Thermal Conductivity (W/ m - ^{o}C)
Epoxy-glass (no copper)	0.294
Epoxy-glass (1 oz. copper)	9.11
Epoxy-glass (2 oz. copper)	17.71
Epoxy-glass (4 oz. copper)	35.13

boards used in this study were epoxy-glass 1 oz, 2 oz copper and no copper (adiabatic) boards.

Davalath and Bayazitoglu (1987) considered the effects of conduction to the plate to which the two-dimensional ribs are attached and computed the entrance region for this geometry. The heat transfer through the plate to an adjacent, identical channel was also computed. The Nusselt number over the rib was not affected considerably by decreasing

the plate to fluid thermal conductivity ratio k_{plate} / k_f, from 10 to 1, but the percentage of the total heat generated that was transferred through the bottom surface of the plate into the adjacent channel decreased from 44 to 33 percent. This fact can be considered as a proof that the thermal conductivity of the board will change the heat transfer phenomena.

The above studies were numerical works on the conjugate heat transfer process based on a two-dimensional model. The thermal conductivity of the printed circuit board was simplified to one lumped equivalent value without considering the exposed copper foil area (copper tracking distribution) effect. The experimental studies on the conjugate heat transfer process are presented in the following paragraphs.

Biber and Sammakia (1986) made extensive heat transfer measurements in an array of 20 real PCBs, each densely populated with heat-dissipating modules that could be arbitrarily heated. Three sizes of modules were investigated and every card was populated with an array of uniform sized modules. There were two different PCBs versions, one with two 0.003 in. copper power planes (copper foil) and one without. It was observed that in real PCBs, conduction effects were always important because of the presence of copper power distribution planes within the board. They successively used the superposition approach of Arvizu and Moffat (1982) to predict temperatures of the modules.

Graham and Witzman (1988) carried out experiments to supplement their analytical study of thermal design of electronic packages. Their experiments covered many component package (semiconductor chip in an electronic package) styles. Real FR4

type printed circuit boards and smaller FR4 test coupons were used. These authors discovered that in many designs, 40 to 60 percent of the total heat load would be dissipated through the board into the air stream.

Azar and Moffat (1991) conducted an experimental investigation to measure the heat transfer coefficients on twelve representative components in a simulated electronic circuit pack. They found that the thermal behavior of the simulated electronic circuit pack was strongly affected by conduction, with conduction to the PCB accounting for between 20 to 60 percent of the total power dissipation. It is suggested that the secondary flows, inside the grooves formed by components, might be affected by non-uniform heating and if the mixed convection becomes stronger, $Gr / Re^2 = 0.3$, might impact the heat transfer coefficient h.

Arabzadeh, et al. (1993) examined the effect of Reynolds number, component placement, and board conductivity on the conduction heat transfer to the board, component temperature, and convection heat transfer coefficient. Experiments were conducted in a horizontal rectangular wind tunnel using an array of twelve components (polished aluminum cubes, $2.54 \times 2.54 \times 2.54$ cm) placed in four rows and three columns. Three test boards were used to investigate the board conductivity effect, a solid aluminum board (0.155 cm thick), a fiberglass board (0.16 cm thick) and a balsa wood board (0.645 cm thick). The experimental results indicated that the conduction heat transfer through the board and consequently the thermal behavior of the system were strongly affected by the Reynolds number of the flow, placement of the component, and the board

conductivity. They concluded that board conductivity can have a significant direct effect on the operating temperature of the heated component.

Ortega et al. (1994) used two-dimensional flush-mounted heat sources in their experimental investigation on conjugate forced convection on a plane conducting surface. A flush mounted strip heater 50.8 cm long in the span-wise direction of the wind tunnel was applied to approach a one-dimensional strip source of heat. The heat flow sensor (area dimensions of 2.54 × 5.08 cm) was placed under the span-wise center of the heater above the channel floor of plexiglass (nominal thermal conductivity between 0.18 and 0.2 W/m-K). It was found that the relative magnitude of substrate conduction scales inversely with Reynolds number, varying from about 5% of the total in the fully turbulent regime, to 15% in the laminar regime. In the laminar regime, conduction was significant up to two source length-scales upstream and downstream of the source.

Lohan and Davies (1996) conducted an experimental study by measuring the forced-air junction-to-ambient thermal resistance of a single 160-lead plastic quad flat pack electronic component mounted on a standard SEMI test PCB. The same approach was also applied to a regular in-line array of the same type of components mounted on a larger Double Euro Card test PCB. Copper tracking covered 19% of the total surface area of both PCBs. Several experiments were conducted with and without non-component side insulation. The most influential factors that contributed to an increase in component resistance were the loss of convective heat dissipation from the PCB's non-component side and the existence of powered adjacent components.

Nakayama and Park (1996) investigated both experimentally and analytically the conjugate heat transfer from a single surface-mounted block (31 × 31 × 7 mm) to forced convective air flow (1 – 7 m/s) in a parallel-plate channel. A simulated module consisted of a copper piece (31 × 31 × 4 mm) supported by various materials (acrylic, copper…etc.) with the same dimensions of 31 × 31 × 3 mm. The channel floor (1-mm-thick plate) was also tested with different materials. They concluded that the thermal resistance of the block support is an important parameter that controls the conjugate heat transfer from the floor. It was also found that a good thermal bonding between the block and the floor, with the support's resistance of the order of 0.01 K/W, and a high thermal conductance of the floor (1-mm-thick copper plate), maximizes the conduction heat transfer from the module to the floor to more than 50%.

All the investigators mentioned above have studied the conjugate heat transfer problem of electronic cooling by conducting experiments on either simulated or real PCBs. In general, the conclusions they reached were (1) conduction can be a significant part of PCB conjugate heat transfer, (2) the higher the thermal conductivity of the substrate, the greater the influence of conduction and some researchers also found that (3) the lower Reynolds number, the greater the influence of conduction. The shortcomings of their studies are summarized as follows:

(1) All the simulated PCBs tested consisted of different materials and were fabricated using different contrived techniques. As no two simulated boards were the same, the scope for comparing results was hampered.

(2) With the exception of Lohan and Davies (1996) who qualitatively showed that greater exposed copper foil area promoted conduction heat spread, the majority of experimental studies that used real PCBs failed to examine the important characteristics of PCB conduction heat transfer. For example, the effects of exposed copper foil surface area, the thickness of the copper foil, etc.

Systematic and quantitative studies on the important characteristics of conduction effects of the copper foil in the real printed circuit boards are needed to understand this complex subject.

1.3 Research Objectives

The fast growth of the electronic industry has been creating greater and greater demand on cooling technology. With this in mind, the search for new and better electronic cooling technologies has been intensified but the research in this field is far from complete. Specifically, experimental data of conjugate heat transfer from surface-mounted blocks as well as numerical studies on heat transfer from three-dimensional modules are relatively scarce. This research is primarily an experimental study on the conjugate heat transfer process in the turbulent flow regime. In order to study the conduction effects of the printed circuit boards, real pre-cut copper clad circuit boards were used as test boards. The objectives are outlined to provide the role of this present study and what will be its contributions to this area.

The objectives of this study are as follows:

1) Investigate the effects of the surface area of the conductive substrate (copper foil) on the conjugate heat transfer. The surface area of the substrate is defined as the exposed (to the cooling air flow) surface area ratio, it is the area of the copper foil on a test board (excluding the area covered by the in-line array of modules) divided by the total surface area of the test board (25.4 × 38.1 cm).

2) Investigate the influence of the thickness of the conductive substrate (copper foil) on the conjugate heat transfer process. Three conductive 1 oz and three 2 oz epoxy-glass test boards with the same copper foil distribution pattern and three copper band widths had been studied. The thickness of the copper foil of the 2 oz test boards is double that of the 1 oz boards used in the present study.

3) Investigate the effects of the power dissipated (10W vs. 20 W) by the heated module on the heat transfer coefficient and the conduction heat flow to the surroundings of the heat-dissipating module.

4) Investigate the influences of conduction in the test board on the neighboring modules of the heat-dissipating module, especially the upstream module and the two lateral modules.

5) Gather and compile the data generated through these experiments into a useful data bank for future applications. For example, to provide a set of reliable experimental data as an input for the Computational Fluid Dynamic and Heat Transfer benchmark problems.

6) Finally, develop a general empirical correlation in terms of the involved operating parameters and physical dimensions based on the experimental heat transfer results of this study. This correlation will express the Nusselt number of any single heated cubic component placed in an in-line array of cubic components.

As specified above, by applying systematic investigation to the conductive characteristics of the real printed circuit boards, the present study will hopefully extend our current understanding of the conjugate heat transfer mechanisms, thus increasing our ability to address some of the questions in electronic cooling.

The following Chapter (Chapter II) is a description of the experimental apparatus and procedures. Chapter III is devoted to a discussion of present experimental results. The last Chapter (IV) summarizes the conclusions of this study and recommendations for future work on this subject.

CHAPTER II

EXPERIMENTAL SETUP AND FACILITIES

A schematic diagram of the experimental apparatus for the heat transfer measurements is shown in Fig. 2.1. This versatile experimental setup was built and instrumented by Arabzadeh (1993). The uncertainty analysis of the overall experimental procedures using the method of Kline and McClintock (1953) showed that there was a maximum of 3.8% uncertainty for heat transfer coefficient calculations. The maximum percentage uncertainty in the experimental measurements of the heat transfer coefficient is presented in Appendix A. Presented in this chapter is a description of the test boards and the experimental apparatus used including the necessary instrumentation details. Following the apparatus description is the explanation of the calibration processes. Finally, this chapter will cover the data reduction techniques used in this research.

Experiments were conducted in a horizontal rectangular wind tunnel. This wind tunnel consists of a contraction section , a rectangular test section, a plenum, a section of circular plexiglas duct followed by a blower and sections of circular plexiglas duct to vent the air flow from the blower to the outside of the room. In the following subsections, the test boards of the present study and each part of the experimental setup will be presented.

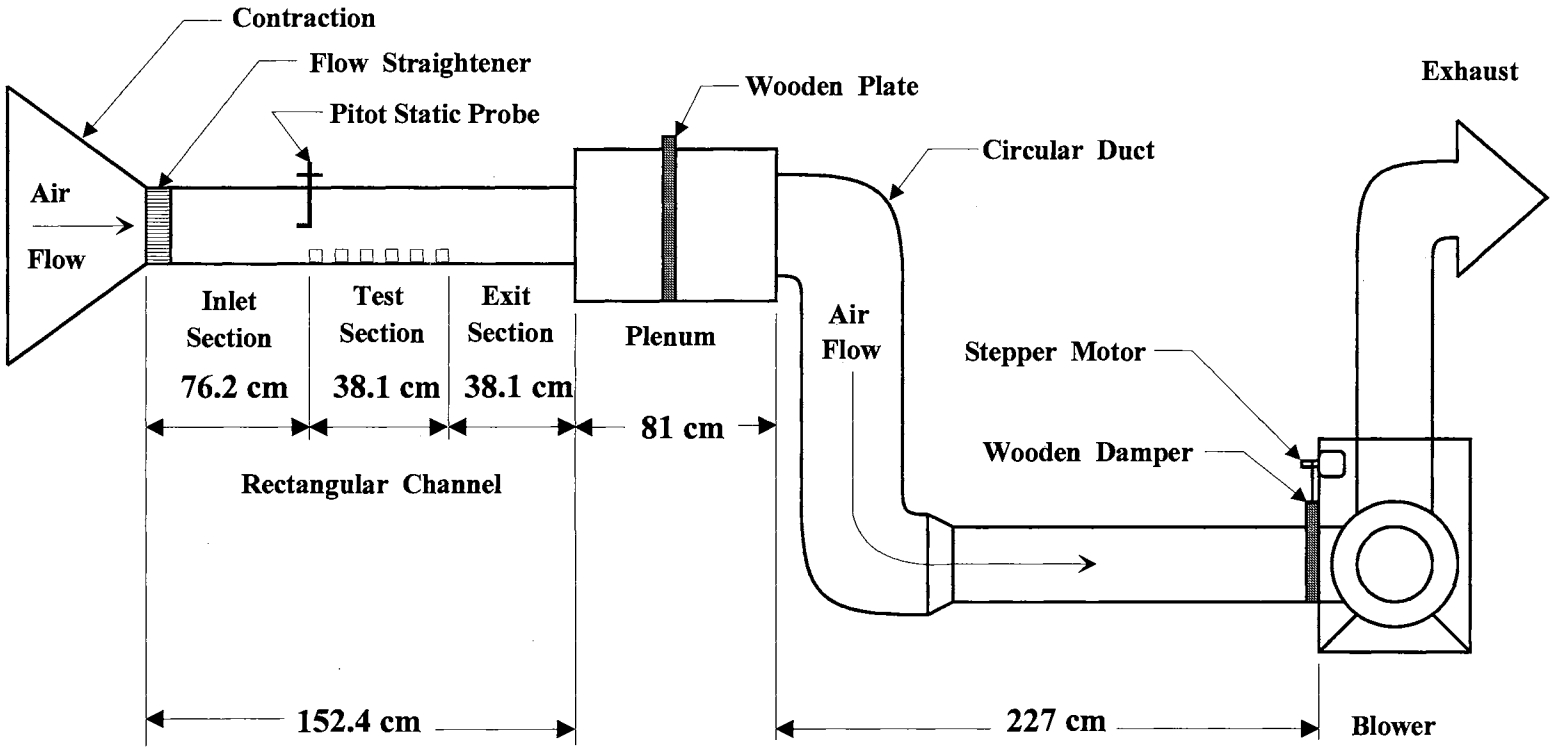

Fig. 2.1 Schematic of the experimental apparatus.

2.1 Description of the Test Boards

In order to systematically investigate the conduction effects of the conductive substrate (copper foil) in the printed circuit boards, a capable approach was needed. After some serious searches for the right approach, it was finally decided that real printed circuit board blanks (1.6mm thick, FR-4 glass epoxy with 1 and 2 oz copper foil by Kepro Circuit Systems, Inc.) would be used as the conductive test boards in the present study. Though real printed circuit boards were used as test boards by some previous researchers, the copper foil in the printed circuit boards was never systematically and quantitatively studied. Designing a pattern to reflect different copper foil distributions is believed to be the first time applied to study different exposed copper foil surface area in printed circuit boards systematically. In this present study, a designed pattern with different connecting band widths was devised to represent the generalized variations of the copper foil distribution of the typical printed circuit boards. The pattern was basically 2.54 cm squares copper foils connected by different widths (2.54, 1.27 and 0.318 cm) of rectangular copper foil bands both in stream-wise and span-wise directions. The schematics of the finished test boards are shown in Fig. 2.2 in which the designed pattern can be clearly seen for the six conductive test boards.

Extra large size (30.3 × 46.6 cm) plastic film negatives were needed to etch the pattern on the pre-cut printed circuit board blanks (25.4 × 38.1 cm). These extra size negatives were made by the Audio Visual Center at Oklahoma State University (OSU). Before the negatives can be made, the pattern had to be generated in a computer and the files of the graphic images for these pattern then given to the Audio Visual Center at

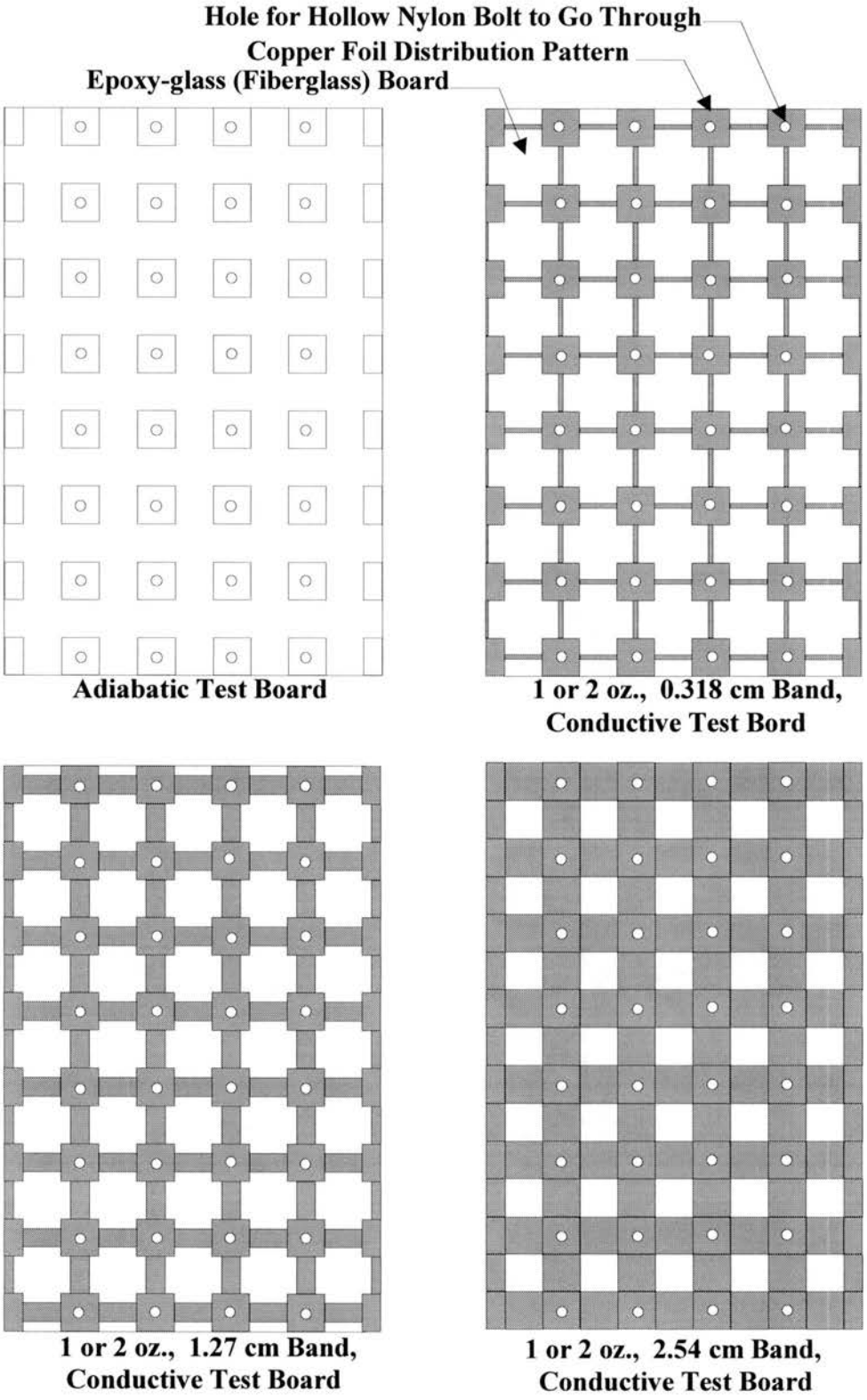

Fig. 2.2 Top view of seven different test boards with the same dimensions of 25.4 by 38.1 cm (10 by 15 in.).

OSU. for enlargement of the images to the exact specified dimensions (25.4 × 38.1 cm) and later these enlarged images were applied to actually print the designed pattern on the plastic films.

The etching process started with exposing the one negative to one copper clad laminate (printed circuit board blank) with an ultra violet fluorescent light source (BX-101 UV Fluorescent by Kepro Circuit Systems, Inc.) for 5 minutes in a dark room. The negative was sandwiched between a piece of glass and the board every time to insure an accurate exposure.

The next procedure of making a conductive test board was developing. The developing process required DFD-12G (Kepro Circuit Systems, Inc.) dry concentrate mixed with hot tap water. After removing the protective film from the board, it was placed in the heated developing solution in a large tray. The tray had to be rocked for at least 1 minute (sometimes longer) to achieve the desired result. Then the board was wiped with a soft wet sponge until the exposed pattern was all that remained.

Etching was the procedure that followed developing. To etch a test board Ferric Chloride liquid E-1G (Kepro Circuit Systems, Inc.) was used. The board had to be constantly agitated in the heated etchant (but can not exceed 43 °C) to accelerate the etchant's reaction to the copper. This procedure usually took at least thirty minutes. Then the test board with the desired copper foil pattern was rinsed with tap water and dried.

Each etched board was then drilled with thirty-two holes 0.992 cm (25/64 in.) in diameter at the specified locations on the test board. These holes were needed for the hollowed nylon bolts used to fasten the full size cubic module to go through. The

adiabatic (base-line) test board was prepared also by drilling the needed holes on it but without any etching procedure. The material of the adiabatic test board was the same as the conductive test board excluding the copper foil. The adiabatic board (25.4 × 38.1 cm) was a 1.6 mm thick plate made of epoxy resin mixed with fiberglass (NEMA G-11 by Polypenco, Inc.)

There was a thin film of photoresist left on every etched board after the etching process. It was left on a finished test board until right before the test board was applied to the experiment to avoid unnecessary oxidation of the copper foil on the board. The photoresist was removed by the same chemical used for developing but with less submerged time.

2.2 Description of the Equipment

2.2.1 Contraction

The large entrance contraction is made of plywood with a flexible lower part that can be moved vertically together with the whole channel floor to adjust to the desired channel (wind tunnel) height from 1.27 to 7.62 cm (0.5 to 3 in.). A perspective view of the contraction with this flexible arrangement is shown in Fig. 2.3. The contraction ratio varies from 14.5 to 82, depending on the channel height. The beginning of the channel floor rests on a wooden flap, which is attached to the flexible lower part of the contraction. The surface of this wooden flap is at the same level as the bottom side of the channel floor with a maximum elevation of 137 cm above the laboratory floor for the minimum channel height. The beginning of each side wall of the channel rests on a

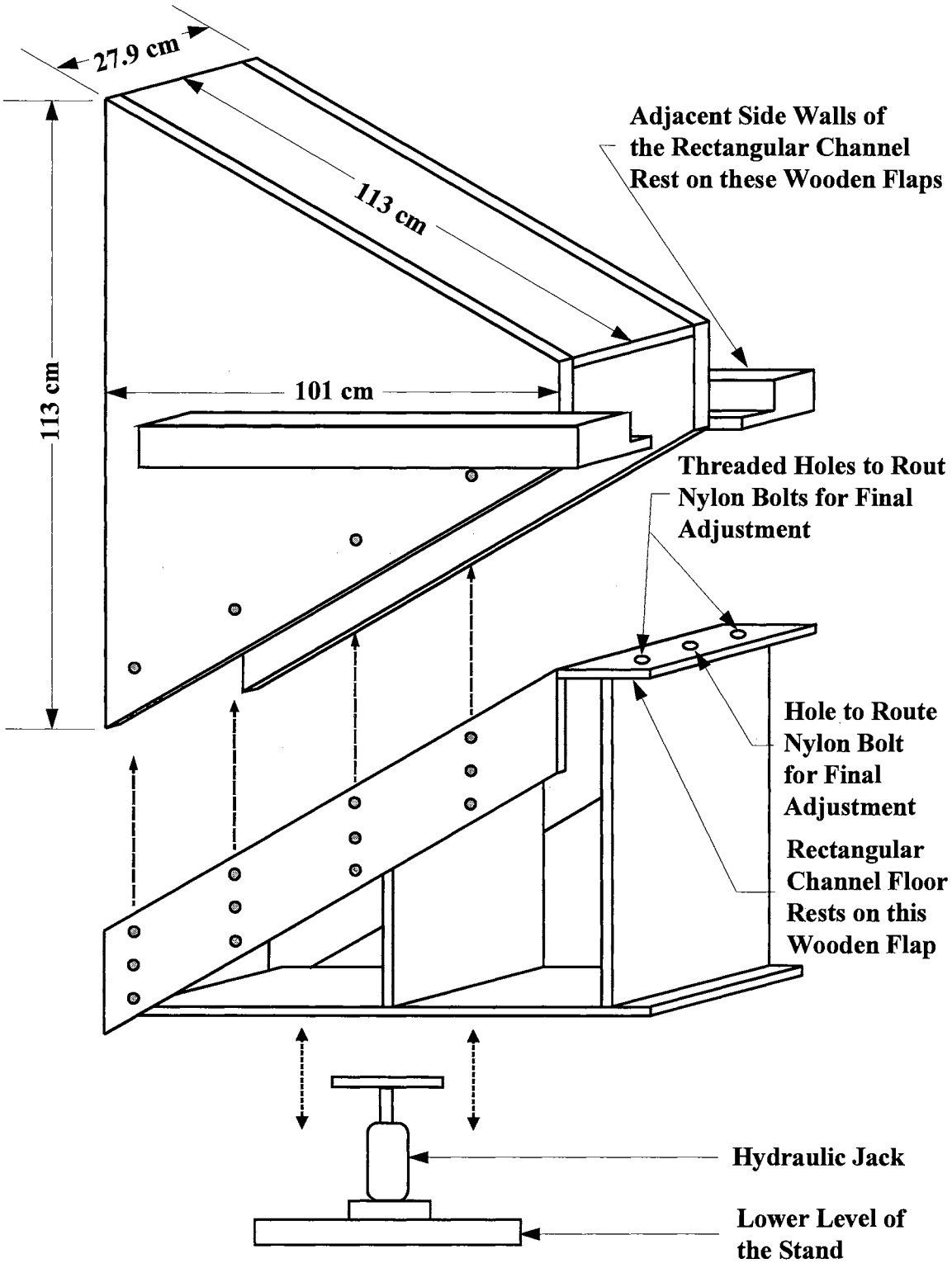

Fig. 2.3 Perspective view of the contraction with the adjustable movement arrangement of its lower part.

separated wooden flap attached to a wooden strip. These two strips are screwed to the fixed side walls of contraction and rest on a right angle iron stand bolted down to the concrete laboratory floor. A small hydraulic jack (maximum capacity 2 ton) is positioned under the bottom plywood board of the flexible lower part of the contraction to help to adjust to a desired channel height and support the contraction. At the interface between the contraction and the rectangular channel, a flow staightener is installed to provide a uniform velocity profile and eliminate any transverse velocities. The flow straightener (0.678 open area ratio) consists of soda straws (0.55 cm inside diameter, 12 cm length) tightly packed between galvanized steel mesh screens (0.044 cm wire diameter, 0.32 cm mesh width). For any desired channel height, an appropriate flow straightener corresponding to the channel height was installed at the beginning of the rectangular channel.

2.2.2 Rectangular Channel

The rectangular channel is 25.4 cm wide and 152.4 cm long and constructed of 1.27 cm commercial-grade plexiglas. A schematic of the rectangular channel is shown in Fig. 2.4. Its height is adjustable from 1.27 to 7.62 cm. The channel is constructed of commercial-grade plexiglas and 152.4 cm in length. It consists of three sections: a 68.6 cm entrance section, a 53.3 cm test section and a 30.5 cm exit section. The ceiling of each of these sections can be removed individually and the entire floor (bottom board) can be removed as well. The floor is supported by two pieces of 1.27 cm plexiglas (24.5 cm long, 16 cm wide) which are fixed to the side walls of the channel. These supports are held in place by nylon screws. Spacers can be placed on these two supports under the

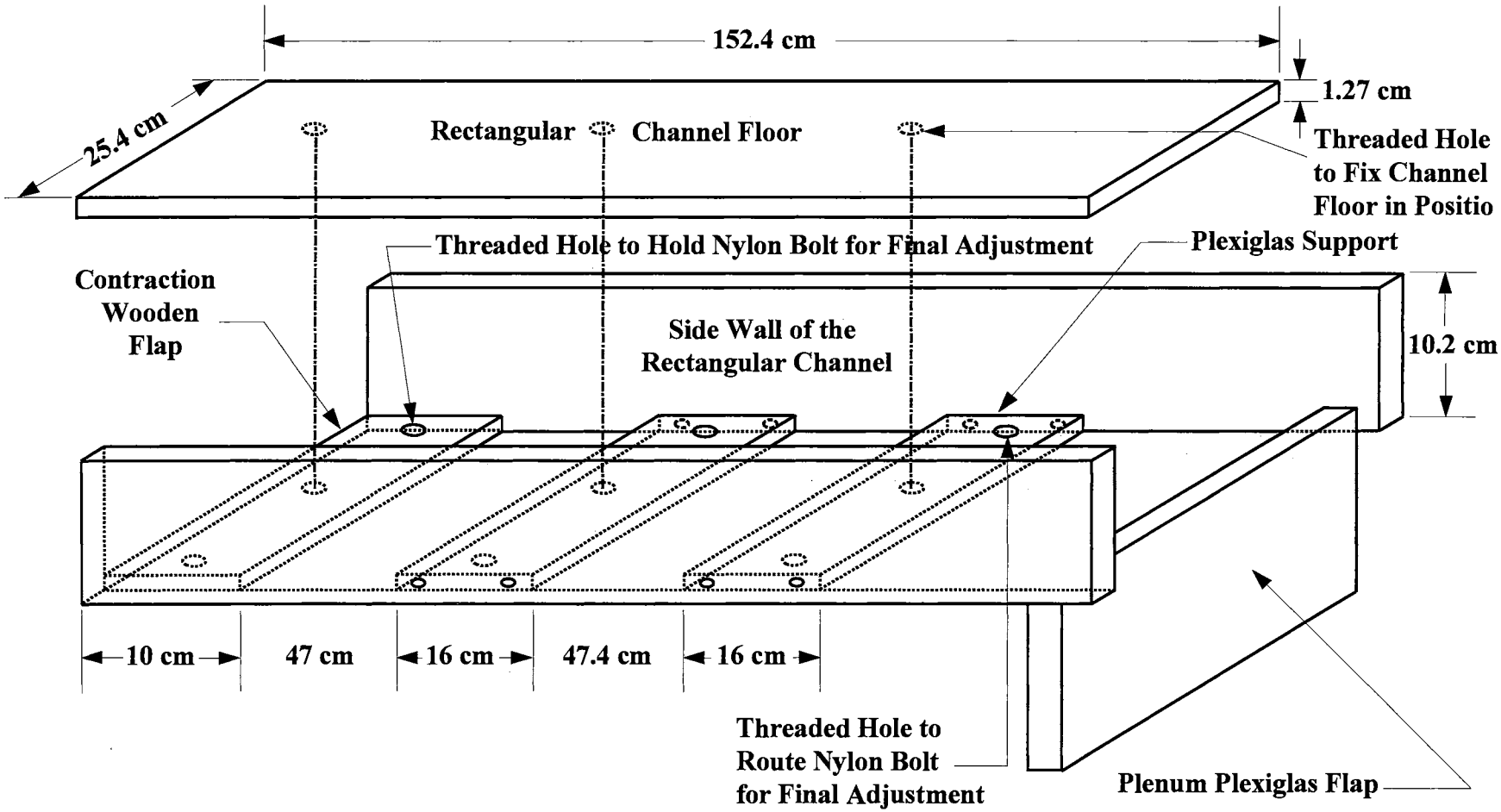

Fig. 2.4 Perspective view of the rectangular channel and the arrangements for final adjustment of the channel floor.

bottom floor of the channel to distribute the weight and avoid buckling. The bottom of the channel is held on these two supports, the wooden flap of the contraction and the plexiglas flap of the plenum. Two threaded holes and one smooth hole are made through each support. Nylon screws are used in these threaded holes to adjust to the desired channel height with an accuracy of 0.025 cm. After the desired channel height is achieved, a set of nylon bolt and nut is used at the center hole on each end and each support. All the bolts and nuts are tightened to secure the channel floor and prevent it shifting from the right position especially at high channel air velocities.

The top portion of the channel consists of three pieces of plexiglas. The contraction side (68.6 × 28 cm) and plenum side (30.5 × 28 cm) are held in place with nylon screws. The ceiling of the test section (53.5 × 28 cm) is the middle piece of the top portion of the channel between the contraction and plenum side. It is held by adhesive tape in its position during experiments so that easy access to the array of modules is possible. For the adiabatic case, the entire channel floor was covered with a 1.6 mm thick plate made of epoxy resin mixed with fiberglass (NEMA G-11 by Polypenco, Inc.), which is the same as the boards actually used in computers but without any copper tracking on it. For conductive cases, the floor of the test section which the array of testing modules were mounted on was covered with real printed circuit boards etched to designed pattern with different copper foil band widths as shown in Fig.2.2. The modules were mounted and tightened through circular holes on the channel floor using hollow nylon bolts for the thermocouple wires and power supply leads to go through.

2.2.3 Test Section

The test section as illustrated in Fig. 2.5, encompasses an array of modules arranged in a regular in-line pattern, the span and stream-wise inter module gaps are identical for three-dimensional modules. The beginning of the test module array is located 76 cm from the entrance of the channel. The dimensions of the test section, the range of the test parameters, and the dimensions of the modules were carefully chosen and constructed in order to perform experiments with different arrangements and configurations. The model geometry consisted of an array of three-dimensional cubical elements mounted on several boards with different thermal conductivities. The geometry chosen for this study may be an idealized representation of a typical configuration presently used in electronic equipment, and the test surfaces also hardly resemble a single printed circuit board with real electronic components. However, the idealization retains three important features: (1) the heat dissipation takes place at discrete locations on the test surface, (2) at these locations, three-dimensional cubic modules introduce a significant impedance to the free flow of cooling air through the channel, and (3) the different test boards induce different degrees of the conjugate heat transfer phenomena.

Each test board used in the present study was mounted with eight rows and four columns of full-size (2.54 cm cube) modules flanked on both sides (in the flow direction) by half-size (2.54×1.27×2.54 cm rectangular aluminum block) modules. Each half-size module was mounted on the side wall adjacent to the channel floor. The idea underlying the employment of the half-size modules is to simulate an infinite wide array more closely (Sparrow, et al., 1982).

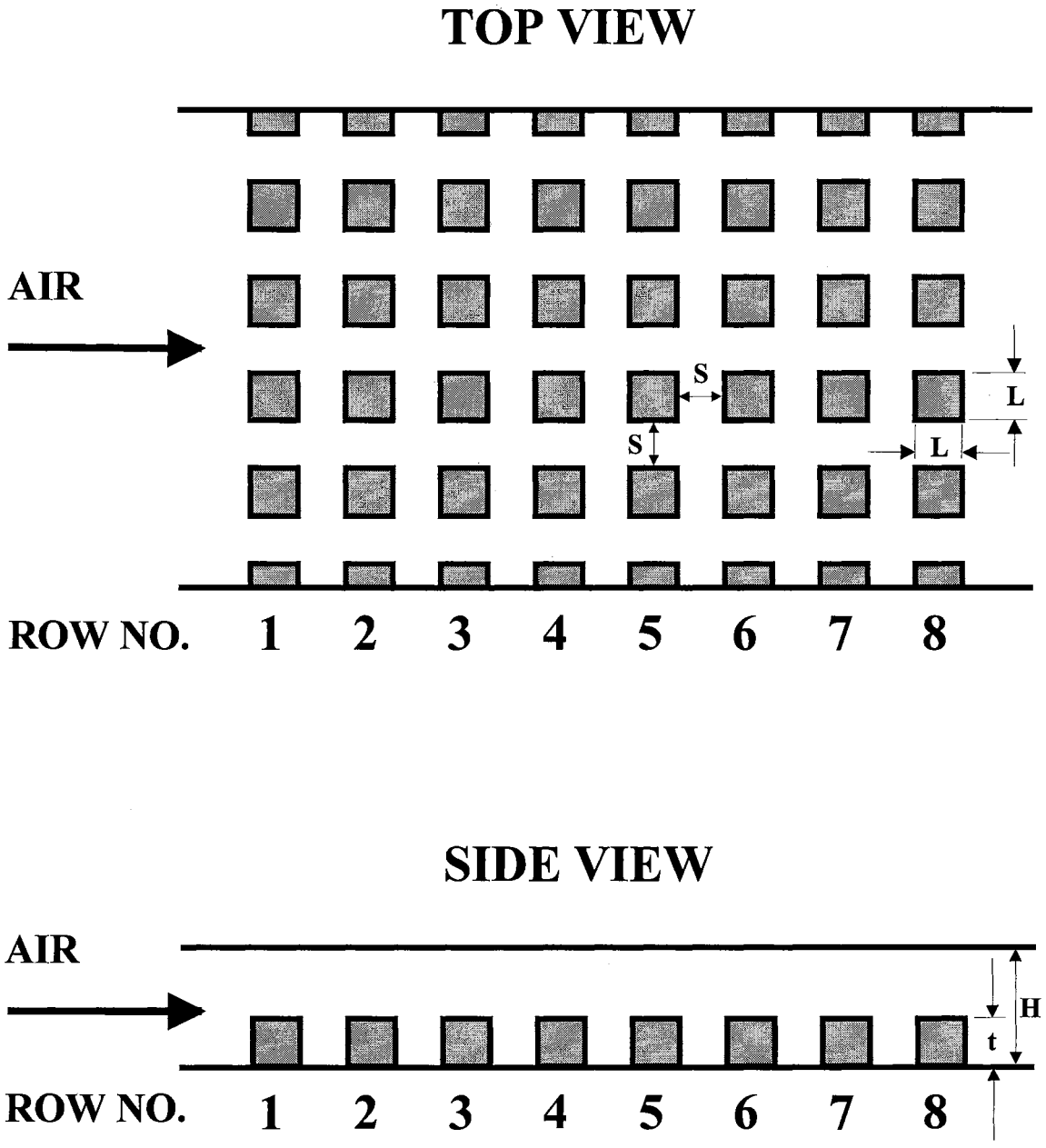

Fig. 2.5 Schematics of the top and side views of the test section with an in-line array of cubic modules (on the adiabatic test board) used in the present study (S=L=2.54 cm, t=2.54 cm and H=7.62, 5.08 or 3.81 cm).

2.2.4 Modules

Electronic components and integrated circuit (IC) chips were modeled by cubic (2.54 × 2.54 × 2.54 cm with square plan-view as shown in Fig. 2.6) aluminum blocks with a thermal conductivity of 216.3 W/m °C (Kraus and Bar-Cohen, 1983). Each module were highly polished to reduce the radiation effects (Wirtz and Dykshoorn, 1984). There are four length dimensions which define the geometrical characteristics of the module array and its relationship to the flow passage. These include the component planform dimension L, the component height t, the inter-component space S and the channel height H of the flow passage. In this study, these four length dimensions are listed as follows:

L = 2.54 cm (1 in.),

t = 2.54 cm (1 in.),

S = 2.54 cm (1 in.),

H = 3.81, 5.08 and 7.62 cm (1.5, 2.0 and 3.0 in.).

The modules were heated by electric resistance. Each tested module is hollowed out to install two electric resistors (475 ohm ceramic resistor, RN60D-NA60, Mini-system, Inc.) or one 500 ohm resistor (SL3-500, Memcor-Truohm, Inc.). The cavity with a resistor inside the modules was filled with Omegabond 101 thermally conductive epoxy. This epoxy was chosen because it has a high thermal conductivity (2.304 W/m-K), a high electrical resistivity (10^{14} ohm-cm), and it is rated for continuous use at temperatures up to 130 °C. The electric leads of the resistor were wrapped with teflon material to avoid electrical contact with the aluminum and then soldered to stranded 22

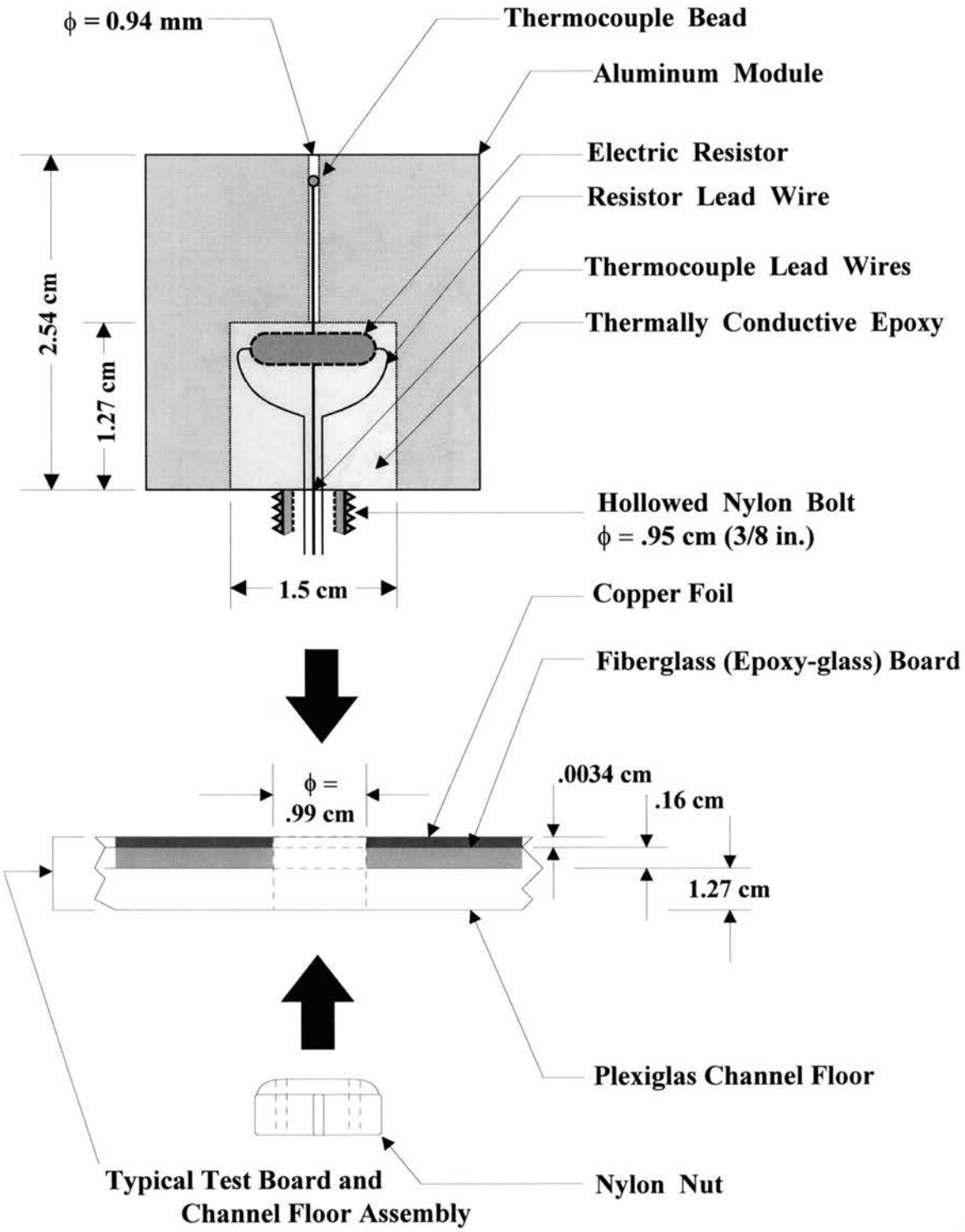

Fig. 2.6 Detailed plan-view of a full-size cubic aluminum module and a typical test section channel floor assembly.

AWG wires.

The power delivered to each module was manually controlled by using a DC power supply (Harrison Laboratories model 890A, 0-0.6 amps). The power was constantly monitored and measured by two multimeters so that if an adjustment of power supplied is necessary to keep the power to the desired value (10W or 20W), it could be done accordingly. The HP 3466A digital multimeter was used to measure the actual voltage drop across the heat dissipating resistor and the Radio Shack 22-163 LCD auto range digital multimeter was used to measure the current of the power circuit.

2.2.5 Plenum

After traveling the length of the rectangular channel, the air is discharged into an acoustically absorbent relaxation plenum. The plenum is constructed of plywood and is 81 cm long, 76 cm wide and 28 cm high. The increased cross-sectional area decelerates the air flow as it enters from the rectangular channel. Additionally, a wooden plate (30.48 cm wide, 28 cm high, and 1.9 cm thick) is inserted vertically in the center of the plenum in order to limit the effect of jet flow coming out of the channel. The plenum is permanently sealed with a clear silicone sealant.

2.2.6 Blower

A New York Blower compact G. I. Fan, size 106 was chosen to draw ambient air to past the test components, plenum and a section of circular duct. The air is then exhausted outside of the laboratory through sections of circular ducts. The blower has 2 horsepower driver electric motor operating at 3600 rpm and a maximum capacity of 600

cfm. To limit excessive acoustic noise, the blower was mounted inside an insulated plywood housing. Fiberglass lines the inside wall surfaces of the housing. A single vane damper at the exit of the blower can be used to control the volume of air drawn by the blower. An adjustable wooden damper plate (see Fig. 2.7) was placed in front of the blower and on one wall of the plywood housing. This allowed for a better control of the volume of air drawn especially at lower channel flow rates (i.e. lower velocities).

2.2.7 Thermocouples

To measure the surface temperature of each module, 36 AWG T-type copper/constantan thermocouple (0.127 mm wire diameter by Omega Company) was used. The thermocouple for each module was cemented flush with the module's top surface using Omegabond 100 epoxy, having a thermal conductivity of 1.038 W/m-K and a electrical insulation volume resistivity of 10^{12} ohm-cm. A hole of 0.94 mm diameter was drilled at the center of each module in order to route the thermocouple wire through it. Thermocouple wires and the leads of the resistor were then routed through a threaded, hollow nylon bolt, which was used to hold the module to the test section floor with a nylon fastener nut. The thermocouples were calibrated in a constant temperature bath. The result of the calibration showed an accuracy of $\pm 0.5^{\circ}C$ when compared with a platinum temperature probe. More details of the thermocouple calibration can be found in section 2.3.2.

2.2.8 Data Acquisition and Control System

For adequate control and data acquisition during the experiments, interactive

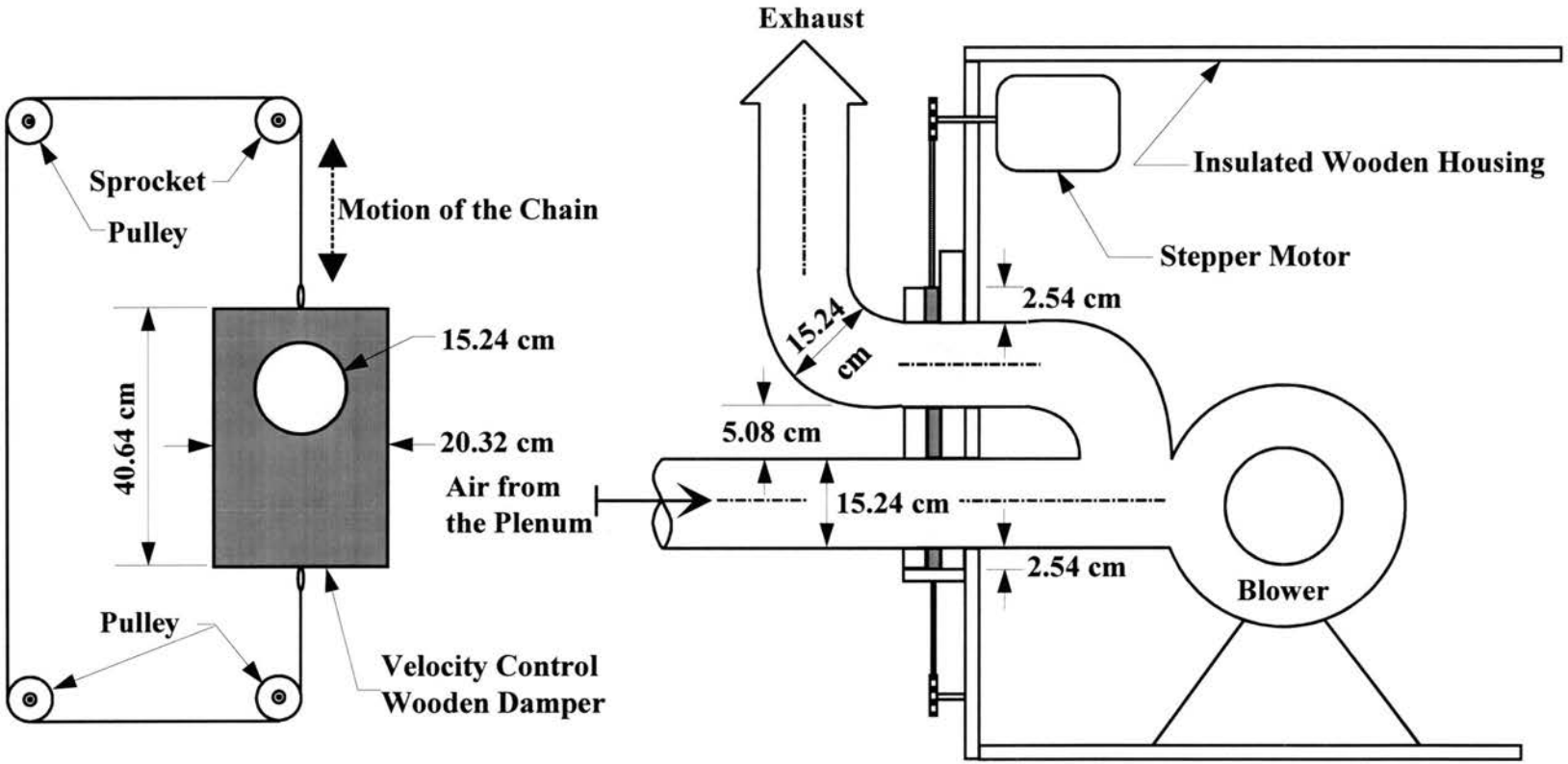

a. Front view of the damper movement

b. Side view of the velocity control damper and stepper motor along with other facilities attached to the wooden houseing

Fig. 2.7 Schematic of the adjustable wooden damper and the arrangement for controlling the rectangular channel centerline velocity.

computer programs were used to determine and control the channel velocity, monitor and acquire the module temperatures. A DC power supply provided the current needed to heat the modules. The array modules were heated by taking a DC voltage drop across the electric resistors (two 475 ohm ceramic resistors in parallel or one 500 ohm). Two different multimeters were used to measure the power supplied. The total power was computed as a product of the current and the measured voltage drop across the ceramic resistor(s). The primary controller was an IBM 386 compatible personal computer with a 40MB hard disk, two floppy drives and 2MB of memory. There were two data acquisition and control boards installed in the PC. They were an RS-232 board and a Metrabyte DAS-8 analog-to-digital (A/D) conversion board.

2.2.9 Thermocouple Data Logger

An Electronics Controls Design (ECD) model 5100 digital data logger with forty channel capacity was used to monitor and record the temperature readings. Using PC-PLUS, a communication software, the model 5100 data logger can interface with the personal computer through a shielded cable to a second RS-232 port. The model 5100 data logger has a resolution of 0.06 °C, over a temperature range of -106 to 400 °C and a +0.06 °C conformity error over a range of -76 to 204 °C. The different features of ECD-5100 include a built-in 24 column thermal printer, an alphanumerical keyboard, a 16-digit vacuum florescent display, a real time clock and an RS-232 port. It also includes a data cache memory which provides temporary storage of the logged data for reviewing before printing or downloading to the computer. The data logger was initially calibrated with a reading accuracy of ±0.05 °C. The data cache memory of the data logger can be

transferred to the PC through PC-PLUS. An interactive data reduction computer program, RED40, read data from the file created by PC-PLUS. The program was written in MS-FORTRAN and outputs the averages, maximum and minimum temperatures of the specified number of data logger channels (every channel was connected to one thermocouple) for a given number of data sets over a certain period of time. More information about RED40 can be found in Rajagopalan (1991).

2.2.10 Air Flow Control

To control and monitor the air velocity in the channel, the air velocity was measured at a location 6 cm (2.4 in) upstream of the first row of modules. A pitot static probe was placed in the center of the rectangular cross section. This probe was connected to a differential pressure transducer which was, in turn, connected to the computer via the analog to digital conversion board. This transducer enabled the computer to measure the pressure drop (from the probe). The air velocity was then calculated from the pressure drop using Bernoulli's equation. The velocity was taken at the beginning of the run, but as data was taken over several hours for a given run, the channel (center-line) velocity was taken again right before the last module was tested. For some cases, longer running hours were needed to conduct the experiments, one or two more velocities were take intermediately. The averages of the velocities, Reynolds numbers and ambient temperatures were always used as the velocity, Reynolds number and ambient temperature for that specific run. A computer program VELAIR was written in C language by Rajagopalan (1991) to control the velocity by changing the damper's position. The wooden damper plate (40.6 cm high and 20.3 cm wide) can be lowered or

raised vertically by a plastic chain attached to a stepper motor controlled by the computer program. This stepper motor was from Superior Electronic Company (model number SS50-1009) and with a specification of 5.5 volts DC, 1.3 amps, 60Hz and 50 oz-in torque at 200 step/revolution. The motor was controlled through a Metrabyte DAS-8 analog-to-digital board. VELAIR also reads the output digital signals from the A/D conversion board, which converts analog voltage from the pressure transducer, to calculate the corresponding channel center-line air velocity. The program actually reads the signals at a user defined number of samples and delay (in millisecond) between each sampling. The delay determines the sampling rate (number of samples per second). Fig. 2.8 shows the apparatus for measuring and setting the centerline velocity in the rectangular channel.

2.2.11 Rectangular Channel Velocity Profile

Direct local velocity measurements were made by Arabzadeh (1993). The measurements were made upstream of the test section (68.6 cm from the entrance of the rectangular channel) at three locations across the span-wise direction of the channel (at channel centerline and about 6 cm from the wall on either side of the channel). At each of these three span-wise locations, the local velocity measurements were taken at up to thirteen locations (depending on the channel height) traversing the height of the channel. The normalized velocity (V_{local}/V_{max}) profiles for low (2 m/s), medium (6 m/s) and high (10 m/s) velocities were presented in Arabzadeh (1993). The normalized velocity profiles at three span-wise locations at the same velocity were consistently close (almost overlapped) to each other. These profiles also showed the essential feature of turbulent flow, a more or less uniform velocity distribution (a nearly flat core section of the

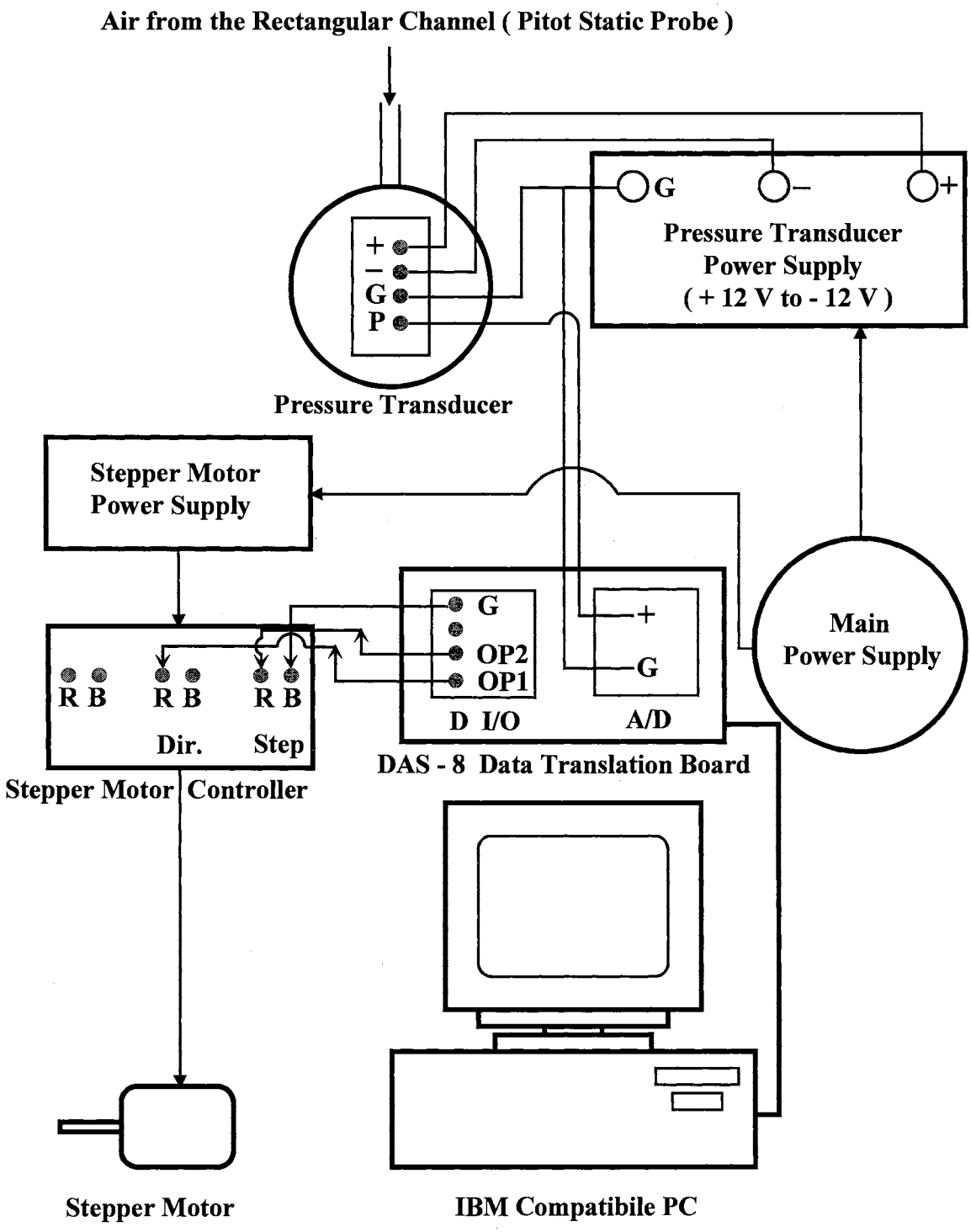

Fig. 2.8 Schematic of the appratus for monitoring and setting the rectangular channel centerline velocity.

profile). The reader is referred to Arabzadeh (1993) for more details concerning velocity profile measurements for the wind tunnel. Local velocities were also taken from time to time while this study was going on. A set of typical data for three channel heights and four channel centerline velocities at three vertical locations on the center plane (span-wise) are presented and discussed in Appendix B.

2.2.12 Pressure Transducer

An MKS model 223BD differential pressure transducer was employed to relay the pressure drop measured by the pitot probe at the rectangular test section to the PC. It is connected to a Metrabyte DAS-8 analog-to-digital (A/D) conversion board installed in the IBM 386 compatible computer. This board has 8 A/D channels each with a 12 bit resolution, 3 channels of digital input, and 4 digital output. This transducer can register a maximum of 0.5 in. of water (approximately 14.5 m/s channel air velocity) and has an output range of -5 to +5 volts. It can be powered by a -12 to +12 volts power supply The accuracy of this differential pressure transducer is within ±0.3% (MKS, manufacturor).

2.2.13 DC Voltmeter

An HP 3466A digital multimeter was used to measure the actual voltage drop across the heat dissipating resistor. The range for voltage measurement was ±200 volt within an accuracy of ±0.03% of the reading.

2.2.14 DC Ammeter

The current passing through the heat dissipating resistor was measured with a Radio Shack 22-163 LCD auto range digital multimeter placed in series with the resistor.

The range for current measurement was within an accuracy of ±1.5% of the reading.

2.3 Calibration Processes

In the setup used, three key pieces of equipment needed to be calibrated. They were (1) ECD 5100 data logger, (2) thermocouples and (3) pressure transducer. The calibration processes of the equipment will be presented here.

2.3.1 Calibration of ECD 5100 Data Logger

The model 5100 data logger required a calibration procedure outlined in the operation manual to ensure correct readings from the thermocouples. To perform the calibration a standard DC voltage was required. To begin the calibration, it was required to perform the setup procedure as described in the manual. With the datalogger held on channel number one, a 2.0000 volt ±10 microvolts standard voltage was applied to the channel. On the accessory card, the R32 unit in the datalogger was adjusted until the mainframe display indicated exactly 2.0000 volts.

2.3.2 Calibration of Thermocouples

The thermocouples used in the study were calibrated by means of a constant temperature bath (Maxi-Cool Recirculator with Heater, RC100LT, FTS System, Inc.). The recirculator with a Deluxe Digital Controller has an operating temperature range from -40 to 75 °C and a stability of ±0.1°C. A platinum temperature probe connected to a digital process indicator with a resolution of 0.1 °C (Model DP-86R, Omega Engineering, Inc.) was use to read the reservoir temperature. Seven sets of data were taken from 15 to 75 °C at 10 °C intervals. For every set of data, when a steady state condition was

accomplished (when platinum probe temperature readings varied within ±0.1°C), all thermocouples indicated a deviation within ±0.5 °C of the platinum probe temperature. Both the positive and negative maximum deviations of every temperature data set at 10 °C intervals from 15 to 75 °C are shown in Fig. 2.9.

2.3.3 Calibration of Pressure Transducer

To calibrate the pressure transducer, a volt-meter and an inclined manometer are required. A "T" tubing connector was used to connect the pressure transducer, the inclined manometer and a manual controlled pressurization end. The pressure readings from the manometer were recorded versus the voltage readings from the transducers as shown in Fig. 2.10. A linear equation was fitted to the pressure and the voltage readings. The correlation coefficient of the linear curve-fitted equation is 0.99.

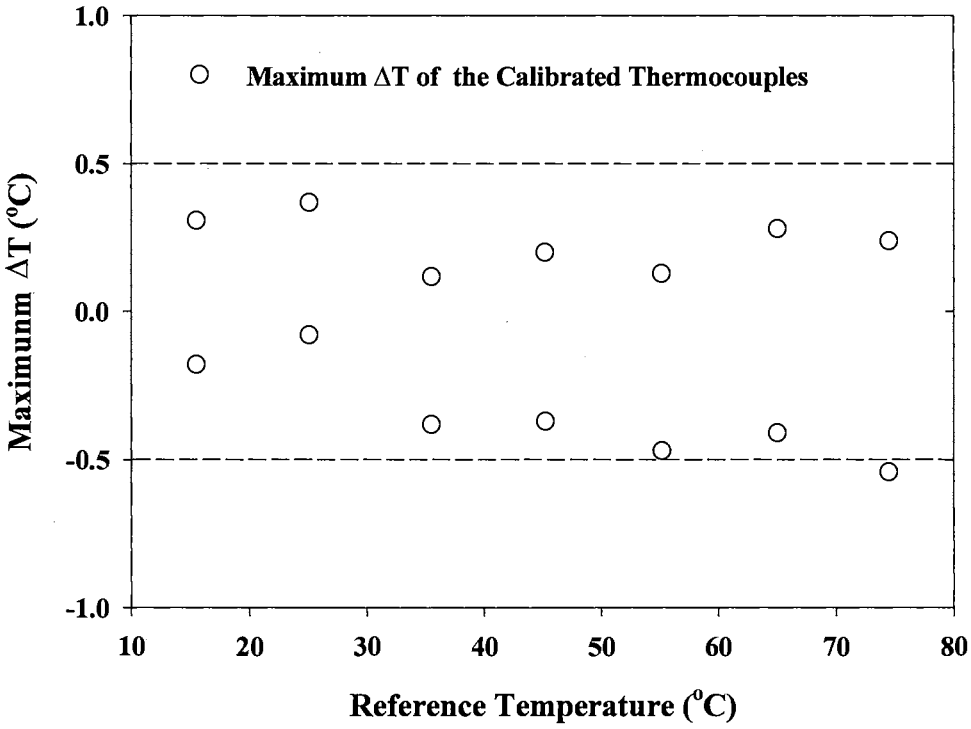

Fig. 2.9 Maximum temperature deviations between the thermocouple readings and reference temperatures (from 15 to 75°C).

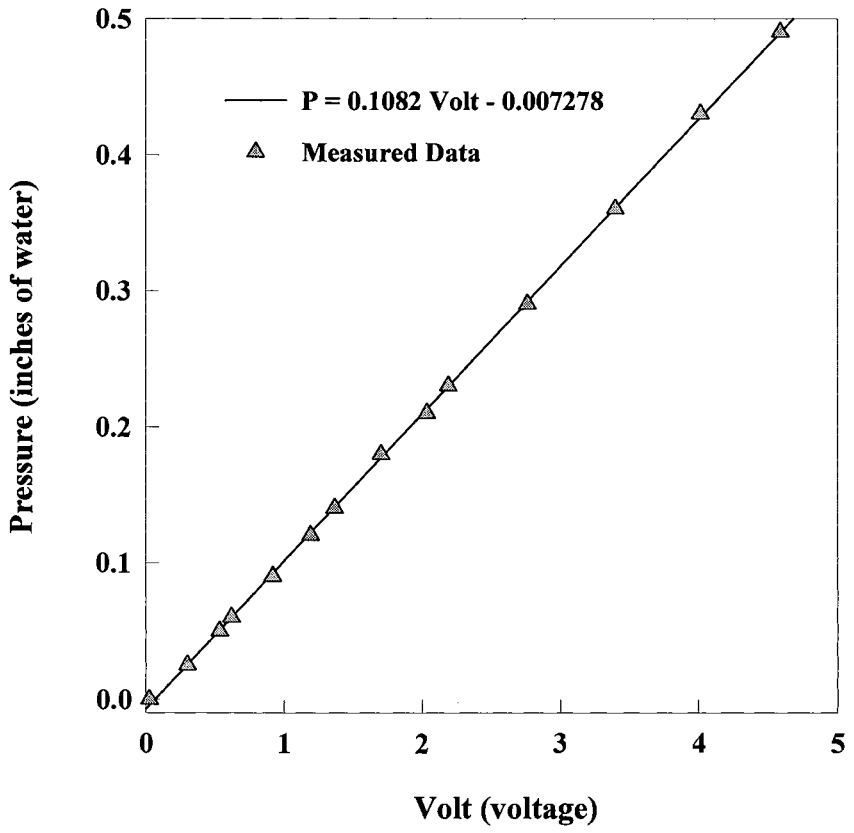

Fig. 2.10 Manometer pressure vs. monitored digital voltage for pressure transducer calibration.

2.4 Repeatability of the Experimental Data

2.4.1 Module Temperature

All twenty-four thermocouples applied to measure every test module were checked for consistency often. The thermocouples were checked either before the experiment was conducted or after finishing the regular routine of the experiment. During the checking, all the test modules were in passive states (none of the modules was given power) with the blower running at the specified desired velocity. All the thermocouples were monitored until the temperature of every module varied within ±0.1°C, the temperatures of every module monitored by the data logger were recorded. Three cycles (every cycle begins with the first module and ends with the last module) of data were taken and the averages were used as the final recorded temperature for every module. For all the runs, the difference between the highest and lowest recorded module temperature was always within 1°C (the thermocouples have an accuracy of ±0.5°C). The average difference between the highest and lowest module temperatures for thirty-five times of checking over a time period more than three months was 0.67 °C.

2.4.2 Channel Centerline Velocity

As described in the Air Flow Control section, centerline velocity measurements were taken at least twice during a specific experimental run, usually about six hours in between. For some cases, longer running hours were needed to conduct the experiments, one or two more velocities were take intermediately. The averages of these measurements were used as the velocity for that specific experimental run. Therefore, the consistency of

the channel centerline velocity measurement was checked for every run of experiment routinely. The average percent difference between all the centerline velocity measurements taken during every experimental run was found to be 0.7%.

2.4.3 Convection Heat Transfer Coefficient

The 2.54 cm band conductive board was tested two times with more than three months in between running the same experiments. Due to practical limitations, exact same experimental state (ambient air temperature, atmospheric pressure and centerline velocity... etc.) could not be achieved but similar conditions were established. Still all the heat transfer coefficients were compared with each other at every corresponding state between the two sets of data. The results showed that the average percent deviation of the heat transfer coefficient between the different runs was 3.5%.

2.5 Experimental Procedures and Data Reduction

The following steps were taken to conduct an experiment:

1. Install the desired test board on the channel floor of the test section, connect the power supply leads to the power supply unit and the thermocouple wires to the data logger.
2. Adjust the wind tunnel to the required channel height, tighten every screw to secure every piece of the setup in place.
3. Put the ceiling of the test section in place, seal it with adhesive tape and use caulk to seal the channel floor for any possible leak.

4. Turn on the data logger, the personal computer, the blower, the step motor, and pressure transducer power supply.

5. Control the channel air velocity through VELAIR to the desired value and then measure the velocity again through VELAIR to get the velocity reading for the experiment. Usually, before the last testing module's temperature is taken, another measurement of the channel air velocity is made and the average of the two measurements is used for the Reynolds number.

6. Monitor the module temperature every five minutes until the steady state condition is reached (when the temperature variation of any monitored module is within ± 0.5°C).

7. Download the temperature data from the data logger and use RED40 to calculate the steady state temperatures of the monitored modules and print it out as data sheet for the experiment.

This experiment is a forced convection heat transfer problem and therefore the vertical conduction heat losses through the board (channel floor) are small relative to the convection heat transfer. The radiation heat losses were estimated using a simple basic model. A steady state energy balance on the control volume surrounding a module yields the convective heat release as:

$$Q_m = Q_t - Q_k - Q_r \tag{2.1}$$

where

Q_m = the equivalent (lumped) convection heat transfer rate of the heat dissipating

module in Watts.

Q_t = the input power to the active (heat dissipating) module in Watts.

Q_k = the estimated vertical conduction heat loss in Watts.

Q_r = the estimated radiation heat loss in Watts.

Since the test boards which are fiber glass (or epoxy-glass) boards with copper foils on it were used in the experiments of this study, the plexiglas channel floor beneath it would behave almost like an adiabatic floor. The thermal conductivity of each material are listed in Table 2.1.

TABLE 2.1
Thermal Conductivities of the Materials for Test Boards and Rectangular Channel Floor.

Material	Thermal Conductivity (W/ m - ^oC)	
Copper	401	(Incropera and DeWitt, 1990)
Epoxy-glass	0.293	(Polypenco, Inc., 1991)
Plexiglas (Plexiglass)	0.193	(Polypenco, Inc., 1991)

With a thermal conductivity ratio of copper (foil) to plexiglas greater than 2000, it can be seen that the test boards were virtually insulated vertically, thus lateral conduction in the copper foil dominates the conduction heat transfer of a heat dissipating module. Heat conduction in vertical direction in the copper foil plays a very minimum role in conduction of this conjugate heat transfer process. A one-dimensional conduction model was applied to estimate the vertical conduction heat loss from a heat dissipating module

through the channel floor.

$$Q_k = (T_m - T_\infty) / R_w \tag{2.2}$$

where T_m (in °C) is the heat dissipating module temperature, T_∞ (in °C) is the approaching air temperature measured upstream of the test section with a T-type thermocouple connected to the ECD-5100 digital data logger. Neglecting contact resistance, R_w (in °C/W) is the thermal resistance of the floor right under the heat dissipating module. The floor is a composite board of three different layers of different materials. The first layer right under the module is a copper foil then a layer of fiber glass, finally a layer of plexiglas. Therefore, R_w is calculated by

$$R_w = \frac{1}{A_k}\left(\frac{t_1}{k_1} + \frac{t_2}{k_2} + \frac{t_3}{k_3}\right) \tag{2.3}$$

where

$A_k = (0.0254)^2$ m^2 is the module contact surface area with the test board.

$t_1 = 3.43 \times 10^{-5}$ m is the thickness of the copper foil (1 oz.).

$k_1 = 401$ W / m - °C is the thermal conductivity of pure copper (Incropera and DeWitt, 1990).

$t_2 = 0.0016$ m is the thickness of the fiber glass circuit board.

$k_2 = 0.293$ W / m - °C is the thermal conductivity of the fiberglass (Polypenco, Inc., 1991).

$t_3 = 0.0127$ m is the thickness of the commercial plexiglas bottom board

(wind tunnel floor).

$k_3 = 0.193$ W / m - °C is the thermal conductivity of the commercial plexiglas (Polypenco, Inc., 1991).

For the estimated vertical conduction heat loss through the channel floor, separate experiments with different board material with different thermal conductivities, were performed on the same experimental setup (see Arabzadeh, 1993; and Arabzadeh et al., 1993). These experiments demonstrated that a board composed of plexiglas and fiberglass can be considered as a non-conductive board, and one-dimensional conduction calculation would be sufficient (in vertical direction, a layer of copper foil on top of the fiberglass board would not change the conclusion).

The lateral conduction heat spread through the copper foil from the heat dissipating module eventually finds its way to the cooling air flow. After subtracting the estimated vertical conduction heat loss through the channel floor and radiation heat loss from the input power to the heated module, Q_m is used to calculate the convection heat transfer coefficient. In other words, in this study, the lateral conduction heat spread from a heat dissipating module is lumped together with the convection heat transfer from the exposed surfaces of the module to calculate an equivalent heat transfer coefficient and the corresponding Nusselt number. The estimated radiation heat loss from the heat dissipating module to the surroundings is calculated by

$$Q_r = \sigma \varepsilon A_m (T_m^4 - T_\infty^4) \tag{2.4}$$

where

$\sigma = 5.729 \times 10^{-8}$ W/ m^2 - K^4 is the Stefan-Boltzmann constant.

$\varepsilon = 0.06$ is the emissivity of polished aluminum (Kraus and Bar-Cohen, 1983).

$A_m = 5\ (0.0254)^2\ m^2$ is the exposed surface area of the heat dissipating module.

After knowing the heat dissipating module temperature (T_m) and approaching air temperature (T_∞), the estimated vertical conduction heat loss (Q_k) through the channel floor and radiation heat loss (Q_r) to the surroundings can be calculated. For a given input power (Q_t) to a heat dissipating module, the equivalent convection heat transfer rate (Q_m) then can be found by equation (2.1). Thus, the equivalent convection heat transfer coefficient (h) of the heat dissipating module can be calculated by

$$h = \frac{Q_m}{A_m(T_m - T_\infty)} \tag{2.5}$$

and the corresponding Nusselt number (Nu) is found by

$$Nu = \frac{ht}{k} \tag{2.6}$$

where

t = 0.0254 m is the defined characteristic length of the experiments, the height of the module.

k = the thermal conductivity of the cooling air flow. It is determined based on the average approaching air temperature (T_∞) for a specific experimental run.

Some selected data from the experiments are presented in Table 2.2. All the

TABLE 2.2
Selected Cases of the Heat Transfer Experimental Measurements and Results of Data Reduction.

Row No.	T_m (°C)	T_∞ (°C)	Q_t (W)	Q_k (W)	Q_r (W)	Q_m (W)	Q_k/Q_m %	Q_r/Q_m %	h (W/m^2 °C)	Nu
Adiabatic Board, Channel Height **H = 7.62 cm**, Velocity **V = 5 m/s**										
1	67.75	28.52	10	0.3552	0.0579	9.587	3.7 %	0.6 %	75.8	73.2
7	78.75	30.25	10	0.4391	0.0761	9.485	4.6 %	0.8 %	60.6	58.6
3*	123.34	29.55	20	0.8491	0.1809	18.97	4.5 %	1.0 %	62.7	60.6
2 oz, 2.54 cm Band Width Board, Channel Height **H = 3.81 cm**, Velocity **V = 11 m/s**										
1	44.39	25.21	10	0.1736	0.0249	9.801	1.8 %	0.3 %	158.4	154.9
7	45.24	24.13	10	0.1911	0.0273	9.782	2.0 %	0.3 %	143.6	140.5
3*	71.36	24.75	20	0.4220	0.0689	19.51	2.2 %	0.4 %	129.8	126.9
1 oz, 1.27 cm Band Width Board, Channel Height **H = 5.08 cm**, Velocity **V = 7 m/s**										
1	54.27	23.94	10	0.2746	0.0411	9.684	2.8 %	0.4 %	99.0	96.8
7	58.31	25.32	10	0.2987	0.0458	9.656	3.1 %	0.5 %	90.7	88.7
3*	91.63	24.25	20	0.6100	0.1096	19.28	3.2 %	0.6 %	88.7	86.8
1 oz, 0.318 cm Band Width Board, Channel Height **H = 3.81cm**, Velocity **V = 9 m/s**										
1	47.61	22.20	10	0.2300	0.0330	9.737	2.4 %	0.3 %	150.3	147.8
7	50.61	23.63	10	0.2443	0.0358	9.720	2.5 %	0.4 %	111.7	109.8
3*	79.24	22.69	20	0.5120	0.0860	19.40	2.6 %	0.4 %	106.4	104.6

tabulated information is either the experimental measurements of the present study or calculated results from the equations mentioned in this segment (equations 2.1 to 2.6). The additional information of Q_k/Q_m (the ratio of the estimated vertical conduction loss to the heat transfer rate of the heat dissipating module) and Q_r/Q_m (the ratio of the estimated radiation heat loss to the heat transfer rate of the heat dissipating module) are also provided in the table. For the tabulated data, rows 1 and 7 were heated with 10 Watts of input power and row 3 which is designated with an "*", was heated with 20 Watts of input power.

Table 2.2 basically presents the ranges and variations of the experimental heat transfer measurements (T_m, T_∞, V, H, Board Band Width) and results (calculated from equations 2.1 to 2.6) for the present study by tabulating some selected cases of the experiments. The ratios Q_k/Q_m and Q_r/Q_m provide additional insight as to the percentage energy loss by the heat dissipating module due to conduction and radiation. For example, as shown in Table 2.2, the maximum ratio of Q_k/Q_m was 4.6%, and the maximum ratio of Q_r/Q_m was 1.0%. Both happened on the adiabatic test board and at the lowest channel centerline velocity of 5 m/s and highest channel height of 7.62 cm. The complete results of the present study will be presented and discussed in the following chapter.

CHAPTER III

RESULTS AND DISCUSSION

This chapter presents the heat transfer results for forced convection in a rectangular channel containing an in-line array of aluminum cubes on three conductive boards and one baseline adiabatic board. For these conductive boards, three different copper foil band widths (exposed copper foil surface area) and two different copper foil thicknesses were investigated. A total of six conductive boards were tested. Half of the boards had a 1 oz (0.0034 cm) thickness with three different band widths and the other half had a 2 oz (0.0068 cm) thickness with the same three band widths as the 1 oz boards. The copper foil distribution pattern was exactly the same for all the conductive boards. Each conductive board was designed to have the same thirty-two square copper surface area of 2.54^2 cm^2 (1 in^2) which every aluminum module (2.54 cm cube) was mounted on. These square copper covered areas were connected to the neighboring modules with uniform width copper bands. Sixteen half modules, copper areas and the corresponding copper bands were used for the left and right boundaries of a conductive board. An experimental run in this study is defined as a certain period of time (usually 9 to 10 hours) which all the necessary measurements were taken at a specific channel centerline velocity and a specific channel height. The modified Reynolds number is defined as

$$Re = \frac{V^* t}{\nu} \tag{3.1}$$

where ν is the kinematic viscosity of the air evaluated at T_∞, t is the characteristic length of the study (the module height, 2.54 cm) and V* is the modified centerline velocity which is defined as

$$V^* = \frac{V\ A_{cross}}{\left(A_{cross} - A_{blocked}\right)} \tag{3.2}$$

where V is the channel centerline velocity, A_{cross} is the cross sectional area of the rectangular channel and $A_{blocked}$ is the cross sectional area of the channel blocked by the aluminum modules (5×2.54^2 cm^2). The range of the modified Reynolds numbers was between 9100 to 26300 in the present study. Accordingly, the flow regime for the entire experiments conducted in the present study was turbulent. The characteristic length was chosen as the height of the module (t) in the study. The other possible choices, channel height (H) and the spacing that the free stream passes (H-t), were not chosen because using either one of them would result in undesirable trend of the Reynolds number. For example, as the channel height increased, the Reynolds number would also increase if the channel height (H) or the free stream pass spacing (H-t) was used as the characteristic length. However, the experimental data indicated clearly that the Nusselt number actually decreased if the channel height increased. In order to avoid these two contradictory trends in the study, the characteristic length was chosen to be the module height (t). It remained the same for the three different channel heights. To accommodate the effects of channel height variations, the modified centerline velocity (V*) was used in the definition of Reynolds number for this study.

The first section of this chapter describes the general trend of heat transfer coefficient for three different conductive boards and a baseline adiabatic board. The influences of the exposed copper surface area and the thickness of copper foil will be presented in the second and third sections respectively. The fourth section discusses the influence of input power variation on convection heat transfer coefficient of a heat dissipating module in the in-line array. The module temperature rises due to a single heat dissipating module will be discussed in the fifth section. In the last section a heat transfer correlation will be introduced.

3.1 Heat Transfer Coefficient Results

As defined earlier, the convection heat transfer coefficient is given as:

$$h = \frac{Q_m}{A_m(T_m - T_\infty)} \tag{2.5}$$

where Q_m is the equivalent convection heat transfer rate, T_m is the heat dissipating module temperature, T_∞ is the approaching air temperature and A_m is the exposed surface area of the heat dissipating module. The corresponding Nusselt number (Nu) is found by

$$Nu = \frac{ht}{k} \tag{2.6}$$

where t is the defined characteristic length of the experiments (the height of the module) and k is the thermal conductivity of the cooling air flow.

On six conductive boards (1oz and 2 oz, band width = 2.54, 1.27 and 0.318 cm) and the baseline adiabatic board , heat transfer coefficients were measured at channel

heights of H = 3.81, 5.08 and 7.62 cm (1.5, 2.0 and 3.0 in.), for centerline velocities of V = 5.0, 7.0, 9.0 and 11.0 m/s on the first seven of eight rows of the array. The results for each channel height are shown in Figs 3.1 to 3.6. Each figure consists of four sub figures for the four test boards. A schematic of the top view of the in-line array of modules on a test board is also included in each figure to help demonstrate the experimental data. The schematic also shows the copper bands of a typical conductive test board connecting all the modules. The schematic of the adiabatic test board was not included because of the limited space. The only difference between the two types (adiabatic and conductive) of test boards is that the conductive boards have conductive paths (copper bands) connecting every module in the array, while the adiabatic board has none. In the top view schematic, the darkened column of modules in the air flow direction represents the column of modules that was heated. From row 1 to row 7, one module was heated at a time and the Nusselt number of each heat dissipating module was calculated from the experimental measurements. Figs. 3.1 through 3.6 show the convection heat transfer coefficient was greatest on the first row and then dropped to a fully developed value by the third row. This so called "fully developed" Nusselt number value which started at the third row was not a constant value for every experimental run. Due to the uncertainties of the experimental measurements, the Nusselt numbers from the third row on would fall in the vicinity of the fully developed value instead of falling exactly on a horizontal line. However, they were within the uncertainty of the experiments (±3.8%). Nevertheless, some significant deviations (maximum 13% higher than row 5) can be observed for the sixth module (row 6) for some experimental runs. It was especially so for the 2.54

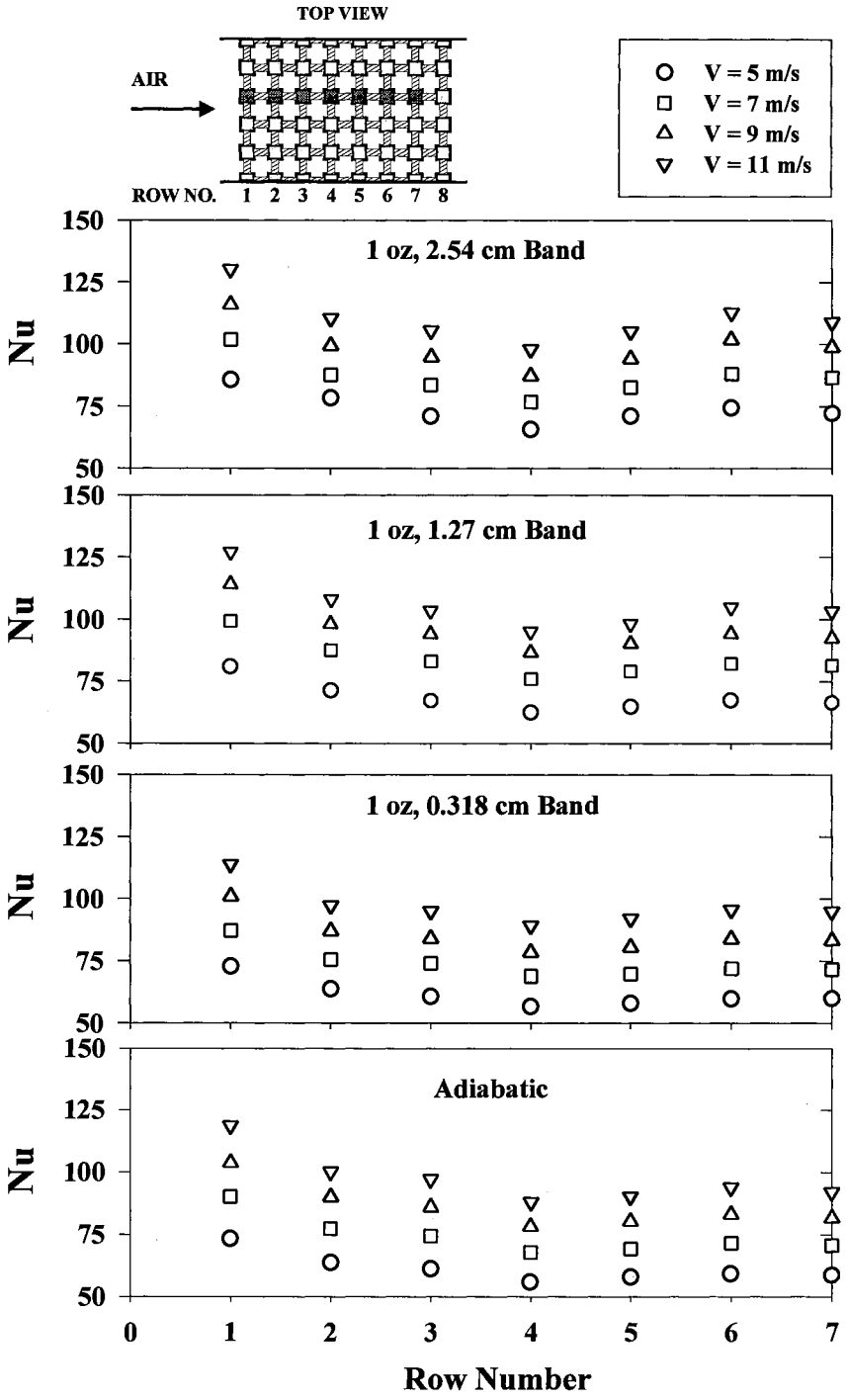

Fig. 3.1 Nusselt number of three 1 oz conductive and the adiabatic test boards at four different velocities and a fixed channel height (H = 7.62 cm).

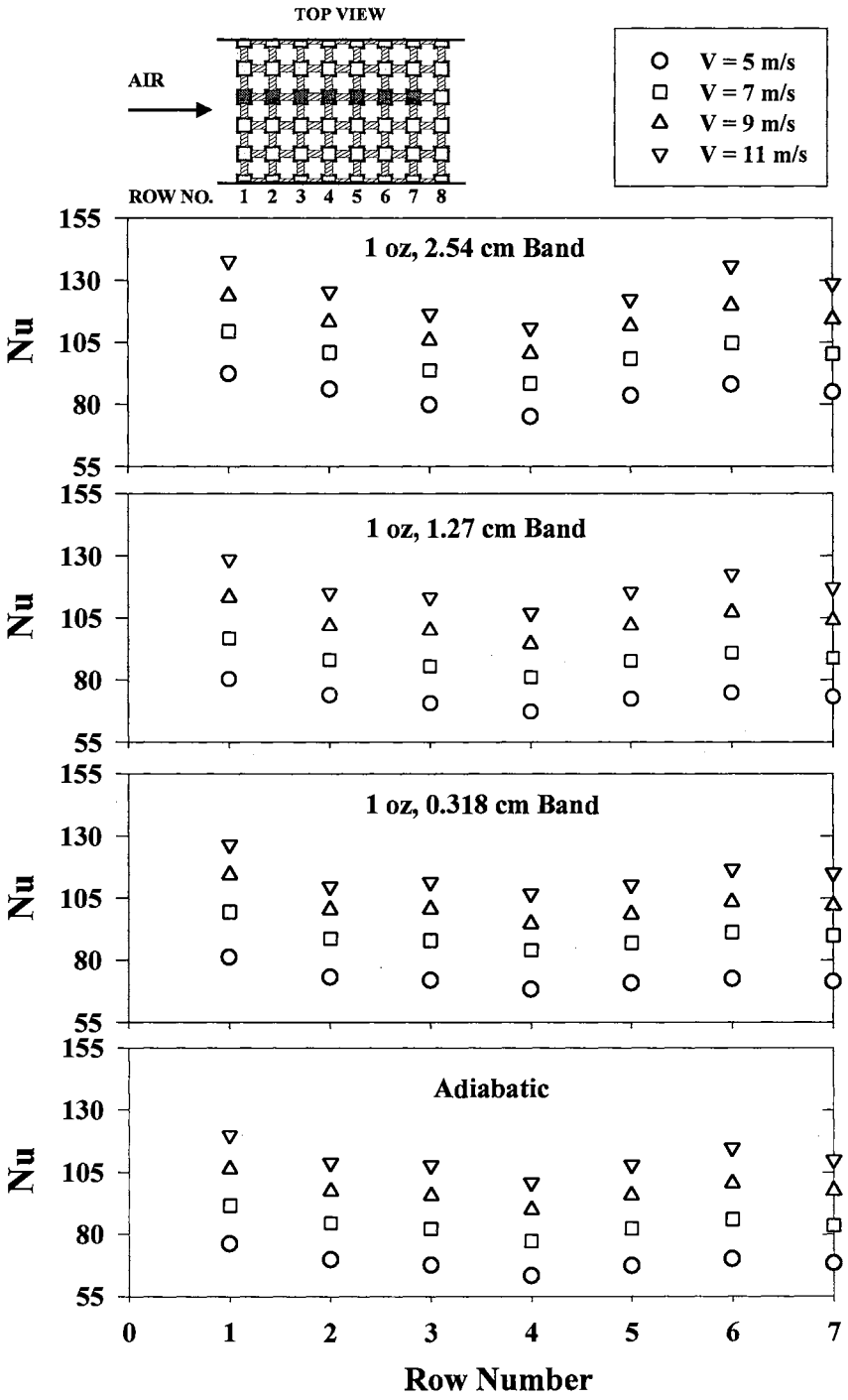

Fig. 3.2 Nusselt number of three 1 oz conductive and the adiabatic test boards at four different velocities and a fixed channel height (H = 5.08 cm).

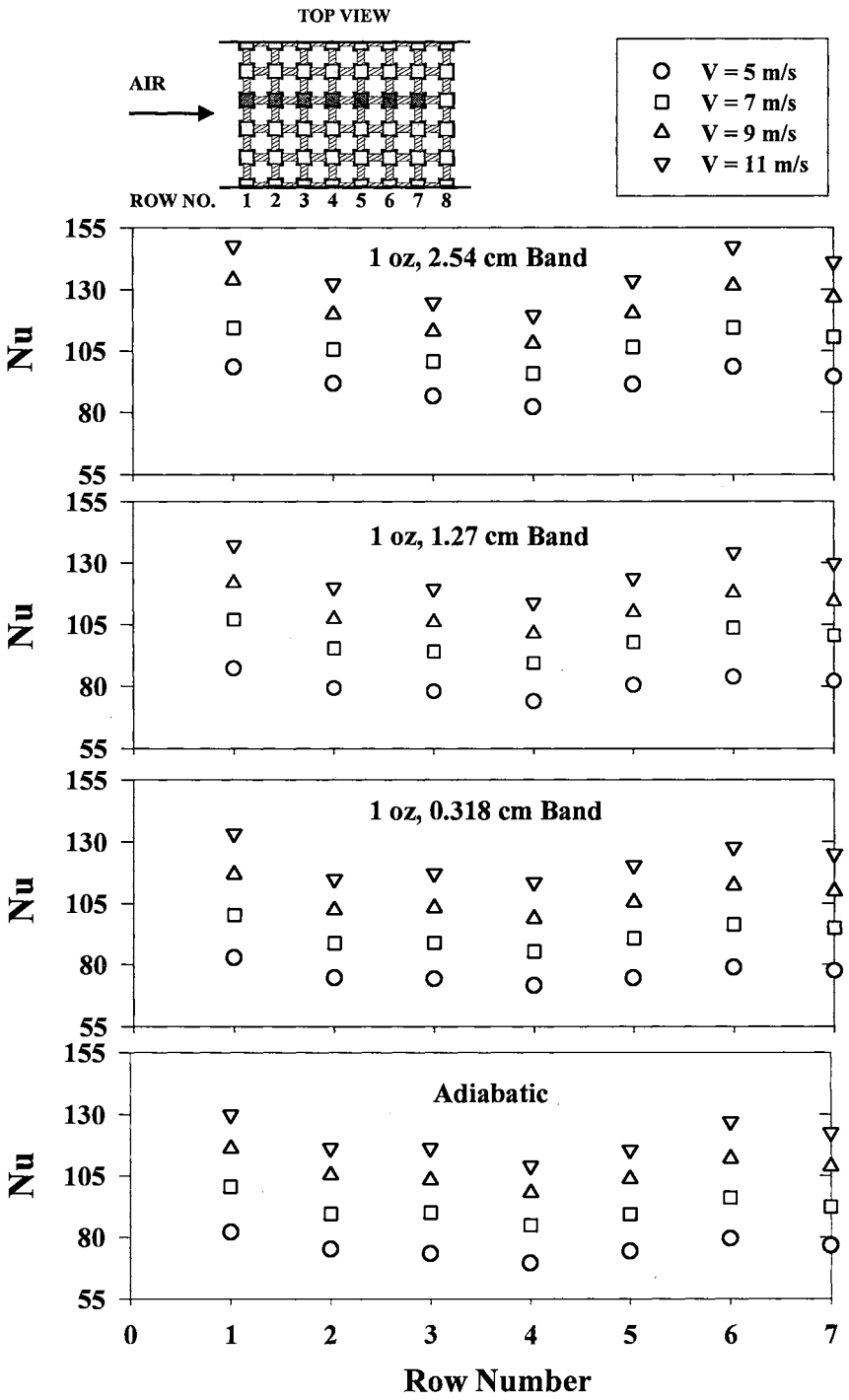

Fig. 3.3 Nusselt number of three 1 oz conductive and the adiabatic test boards at four different velocities and a fixed channel height (H = 3.81 cm).

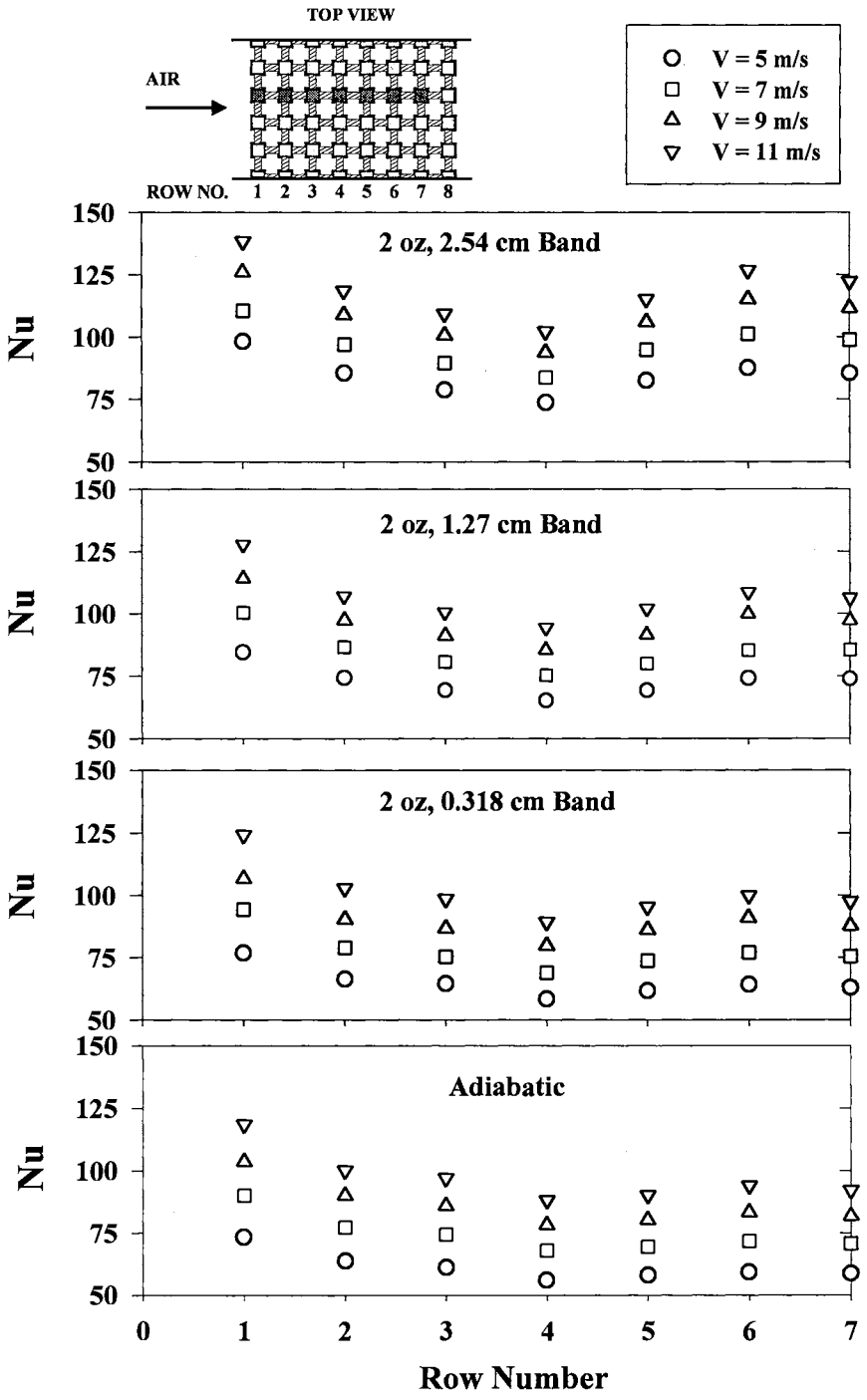

Fig. 3.4 Nusselt number of three 2 oz conductive and the adiabatic test boards at four different velocities and a fixed channel height (H = 7.62 cm).

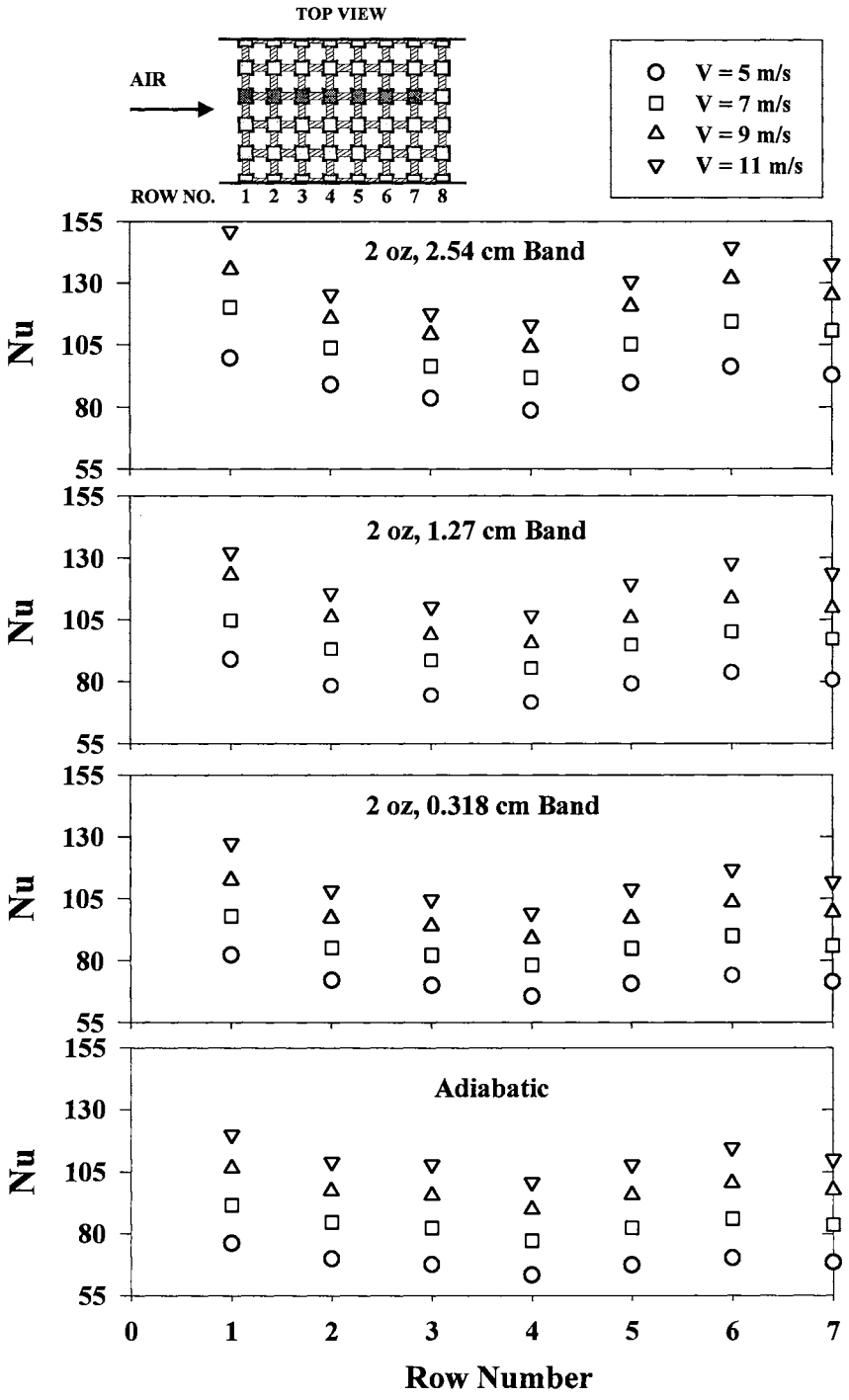

Fig. 3.5 Nusselt number of three 2 oz conductive and the adiabatic test boards at four different velocities and a fixed channel height (H = 5.08 cm).

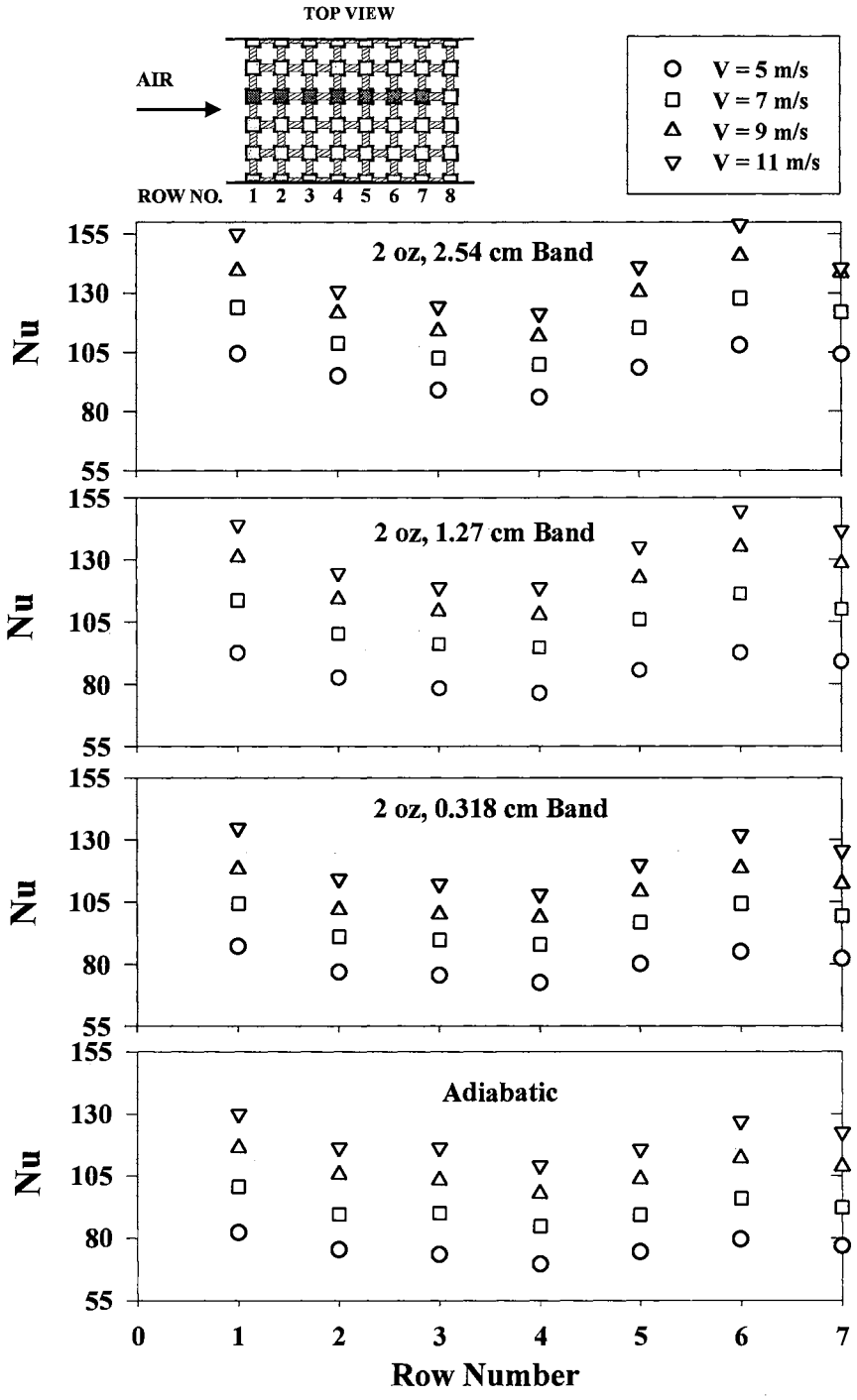

Fig. 3.6 Nusselt number of three 2 oz conductive and the adiabatic test boards at four different velocities and a fixed channel height (H = 3.81 cm).

cm conductive test board at the highest channel centerline velocity of 11 m/s which always had the most significant deviations for all three channel heights. There are two possible factors for this phenomenon : (1) the uncertainty of the thermocouple embedded in the sixth module (±0.5°C) and (2) the bottom surface of the sixth module which is the contact surface of the module to the conductive copper foil. The bottom surface of the sixth module may have a better contact with the copper foil than the rest of the modules thus dissipating more heat through the copper foil.

Exploratory experiments were conducted to check the deviations of the heat transfer coefficients of the sixth row by switching the fifth and sixth modules. This was accomplished by taking measurements with the present sixth module and then switching the sixth module with the fifth module and comparing the results. For three channel heights at four velocities, the difference between Nusselt number of fifth module and Nusselt number of fifth module switched to the sixth row were always less than 3% (the average, 1.2%). The data indicated that indeed the two factors mentioned above were the most likely explanations for the significant deviations of Nusselt number observed for the sixth module and possibly all the significant deviations among all other test modules.

From the figures, it can be deduced that the value of heat transfer coefficient is the highest in the first row and decreases with row number. This trend was also reported for modules of cubes by Moffat et al. (1985) and modules of flatpacks by Wirtz and Dykshoorn (1984) for adiabatic cases.

As shown in the figures, the Nusselt numbers increased with increasing centerline velocity V for a fixed channel height H. This trend can be consistently observed for all

seven test boards in all six figures (3.1 to 3.6). Therefore, it can be concluded that in turbulent flow regime, forced convection heat transfer is still the dominant mechanism of this conjugate heat transfer process. The same conclusion has been documented by both Moffat et al. (1985) and Wirtz and Dykshoorn (1984) for adiabatic cases. To compliment Figs. 3.1 to 3.6, some numerical examples for two selected modules are tabulated in Tables 3.1 and. 3.2.

The Nusselt number values of the selected modules (first and seventh) and the percent variation of the Nusselt numbers with respect to velocity are listed in Table 3.1 for seven test boards at a fixed channel height of 7.62 cm.

The opposite trend to what was shown in Table 3.1 could be observed for decreasing channel height and a fixed centerline velocity. With decreasing channel height H, the Nusselt numbers increased for a fixed centerline velocity V. This trend was also reported by Moffat et al. (1985) for cubic modules and adiabatic cases. Again, to demonstrate this trend numerically, some examples of two selected modules are given in Table 3.2 for two selected velocities (5 and 11 m/s) and three test boards (1 oz, 2 oz 2.54 cm band and adiabatic).

Results shown in Figs. 3.1 to 3.6 and Tables 3.1 and 3.2 lead to the conclusion that both channel centerline velocity and the channel height are two essential parameters in the present study (in turbulent flow regime). The effects of both parameters were consistent without any exception for all the experiments. For any of the seven test boards, conductive or adiabatic, the increase of centerline velocity would always result in higher

TABLE 3.1

Nusselt Number Variation with Respect to Centerline Velocity for Two Selected Modules and All Seven Test Boards at a Channel Height of 7.62 cm.

First Module (Row No.1)			Seventh Module (Row No.7)		
Velocity (m/s)	Nusselt No.	% increase of Nu from 5 m/s	Velocity (m/s)	Nusselt No.	% increase of Nu from 5 m/s
1 oz, 2.54 cm Band Width, Channel Height H = 7.62 cm					
5	85.7	0	5	72.3	0
7	101.7	19 %	7	86.6	20 %
9	115.7	35 %	9	98.7	36 %
11	130.2	52 %	11	109.0	51 %
2 oz, 2.54 cm Band Width, Channel Height H = 7.62 cm					
5	98.2	0	5	85.4	0
7	110.6	13 %	7	98.8	16 %
9	125.9	28 %	9	111.5	31 %
11	138.3	41 %	11	122.4	43 %
1 oz, 1.27 cm Band Width, Channel Height H = 7.62 cm					
5	81.0	0	5	66.4	0
7	99.3	23 %	7	81.5	23 %
9	113.9	41 %	9	92.4	39 %
11	127.0	57 %	11	103.2	55 %
2 oz, 1.27 cm Band Width, Channel Height H = 7.62 cm					
5	84.6	0	5	73.8	0
7	100.5	19 %	7	85.5	16 %
9	114.1	35 %	9	97.2	32 %
11	127.9	51 %	11	106.2	44 %
1 oz, 0.318 cm Band Width, Channel Height H = 7.62 cm					
5	72.8	0	5	59.9	0
7	87.2	20 %	7	71.6	19 %
9	100.9	39 %	9	83.2	39 %
11	113.8	56 %	11	94.9	58 %
2 oz, 0.318 cm Band Width, Channel Height H = 7.62 cm					
5	76.8	0	5	62.8	0
7	94.3	23 %	7	75.5	20 %
9	106.7	39 %	9	87.7	40 %
11	124.3	62 %	11	97.6	55 %
Adiabatic Board, Channel Height H = 7.62 cm					
5	73.2	0	5	58.6	0
7	90.2	23 %	7	70.6	21 %
9	103.5	41 %	9	81.6	39 %
11	118.4	62 %	11	92.1	57 %

TABLE 3.2

Nusselt Number Variation with Respect to Channel Height for Two Selected Modules and Three Test Boards at Two Different Centerline Velocities.

First Module (Row No.1)			Seventh Module (Row No.7)		
Channel Height (cm)	Nusselt No.	% increase of Nu from H = 7.62 cm	Channel Height (cm)	Nusselt No.	% increase of Nu from H = 7.62 cm
1 oz, 2.54 cm Band Width, Channel Air Velocity V = **5** m/s					
7.62	85.7	0	7.62	72.3	0
5.08	92.4	8 %	5.08	84.9	17 %
3.81	98.5	15 %	3.81	94.6	31 %
2 oz, 2.54 cm Band Width, Channel Air Velocity V = **5** m/s					
7.62	98.2	0	7.62	85.4	0
5.08	99.5	1 %	5.08	92.9	9 %
3.81	104.6	7 %	3.81	104.2	22 %
1 oz, 2.54 cm Band Width, Channel Air Velocity V = **11** m/s					
7.62	130.2	0	7.62	109.0	0
5.08	137.7	8 %	5.08	128.7	17 %
3.81	147.8	15 %	3.81	141.3	31 %
2 oz, 2.54 cm Band Width, Channel Air Velocity V = **11** m/s					
7.62	138.3	0	7.62	122.4	0
5.08	151.1	9 %	5.08	137.7	13 %
3.81	154.9	12 %	3.81	140.5	15 %
Adiabatic Board, Channel Air Velocity V = **5** m/s					
7.62	73.2	0	7.62	58.6	0
5.08	76.1	4 %	5.08	68.3	17 %
3.81	82.2	12 %	3.81	76.7	31 %
Adiabatic Board, Channel Air Velocity V = **11** m/s					
7.62	118.4	0	7.62	92.1	0
5.08	119.7	1 %	5.08	109.9	19 %
3.81	130.0	10 %	3.81	122.5	33 %

Nusselt number of the heat dissipating module at a fixed channel height. Also, for any test board, the decrease of channel height would always result in higher Nusselt number of the heat dissipating module at a fixed centerline velocity. It should also be pointed out that both the increase of the centerline velocity and the decrease of channel height would increase the modified Reynolds numbers of the experiments.

3.2 The Effects of Exposed Copper Foil Surface Area on the Convection Heat Transfer Coefficient

When a module was heated, part of the heat would be dissipated through the bottom surface (2.54^2 cm^2) of the module to the copper foil by conduction and then find its way to the cooling air flow. Most of that heat was conducted vertically through the bottom surface of the heated module to the copper foil then, would be distributed laterally to the four copper bands connecting the neighboring unheated modules. In the process, convection heat transfer would then take over to play the major role of dissipating that heat. The purpose of this configuration was to measure the effect of "exposed" copper foil covered surface area on the heat transfer of the in-line array modules. A parameter was proposed to reflect this effect.

The exposed area ratio A* is defined as:

$$A^* = \frac{\text{Total exposed copper surface area}}{\text{Total exposed area on the board}} \tag{3.3}$$

where total exposed copper surface area is the sum of all the copper band covered area. The contact surfaces were concealed by the mounted cube modules and were not included. The total exposed area on the board is the surface area of the board minus the

sum of all the surface areas occupied by the surface mounted modules. The adiabatic board is a "bare" 1.6 mm (1/16 in.) thick fiber glass board. The corresponding A* values for the three different copper foil distribution patterns were:

2.54 cm (1 in.) band width, A* = 0.682

1.27 cm (0.5in.) band width, A* = 0.341

0.318 cm (0.125 in.) band width, A* = 0.085

These three patterns with three A* ratios were generated on two sets (two different copper foil thicknesses) of conductive test boards. Figures 3.7 to 3.12 show the Nusselt numbers of all six conductive test boards normalized on the adiabatic board values versus row number, and parametric in velocity for channel heights H = 7.62, 5.08 and 3.81 cm. A schematic of the top view of the in-line array of modules on a test board was also included in each figure. The darker column of modules in the air flow direction represents the column of modules that were heated. The schematic also shows the copper bands of a typical conductive test board connecting all the modules.

The maximum increase was found to be 43% when compared with the Nusselt number of the base-line adiabatic test board at the corresponding conditions (the same channel centerline velocity and channel height). The maximum was for the fifth module of the heated column on the 2 oz, 2.54 cm band width conductive test board at the channel centerline velocity of 5 m/s for the channel height of 7.62 cm. The increases in the heat transfer coefficients on the average for each conductive board were 15.1 % on the 1 oz, 2.54 cm band width board; 22.4 % on the 2 oz, 2.54 cm band width board; 7.2 % on the 1 oz, 1.27 cm band width board; 10.9% on the 2 oz, 1.27 cm band width board; 1.8%

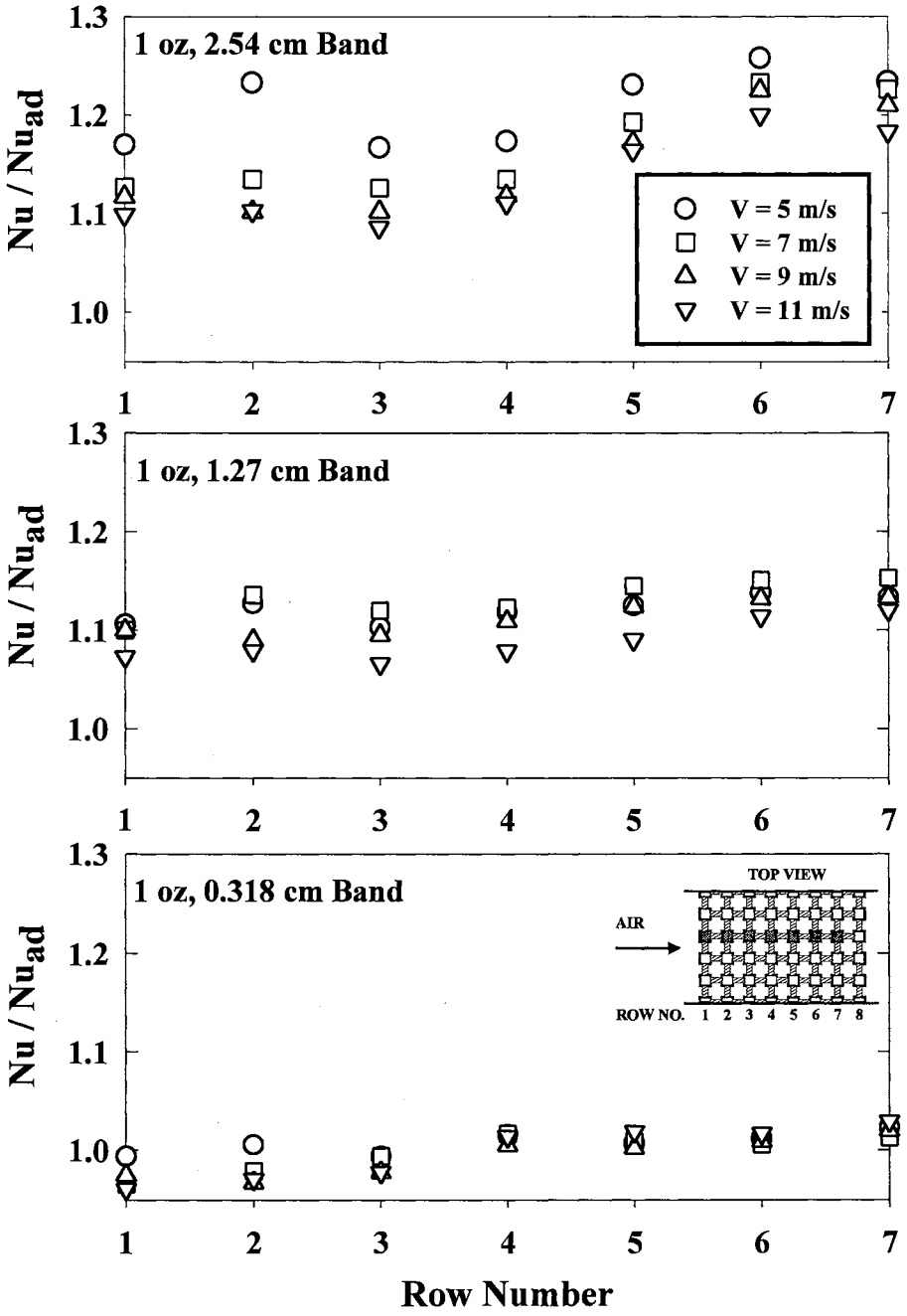

Fig. 3.7 Nusselt number of three 1 oz conductive test boards normalized with the adiabatic test board values at four different velocities and a fixed channel height of H = 7.62 cm.

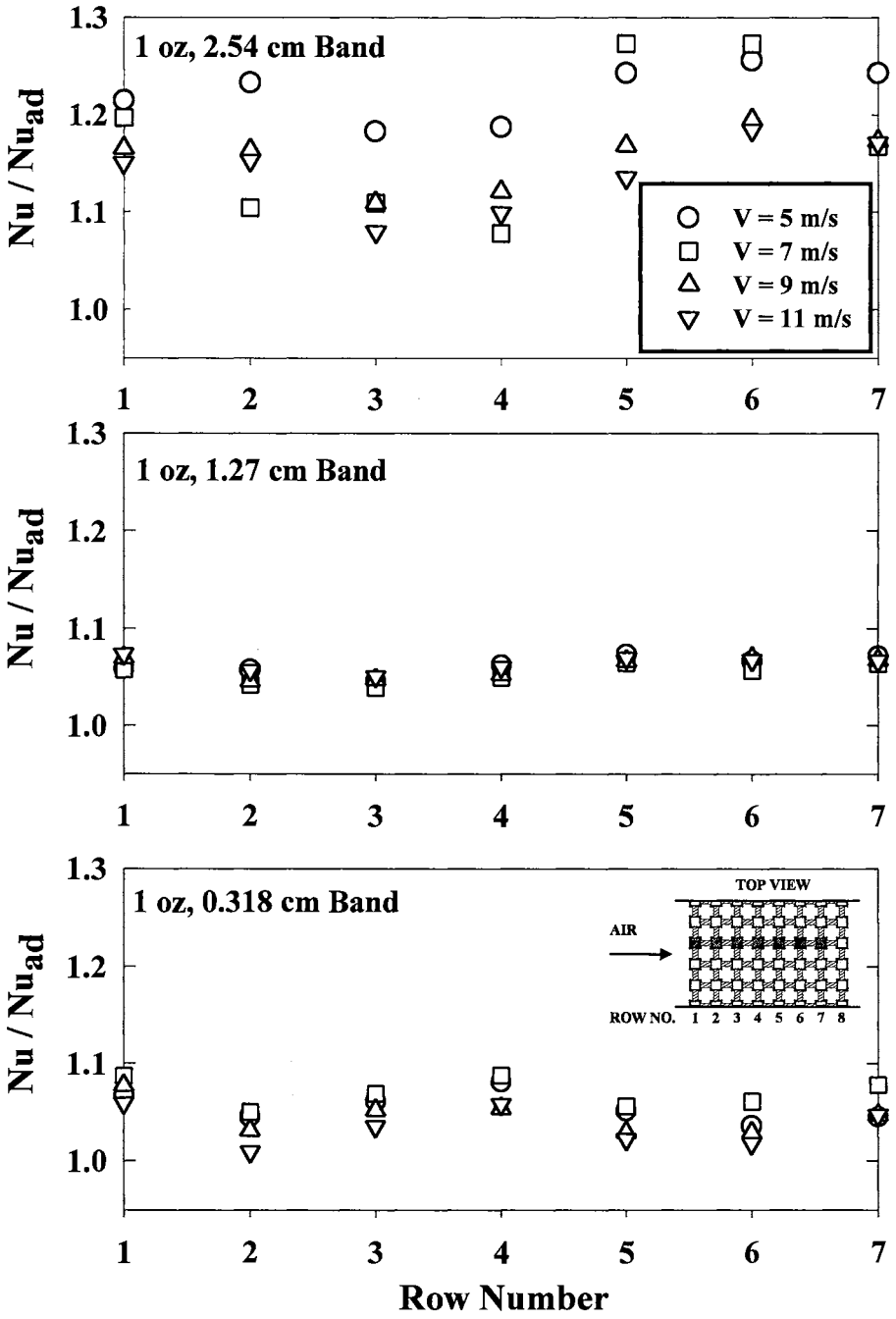

Fig. 3.8 Nusselt number of three 1 oz conductive test boards normalized with the adiabatic test board values at four different velocities and a fixed channel height of H = 5.08 cm.

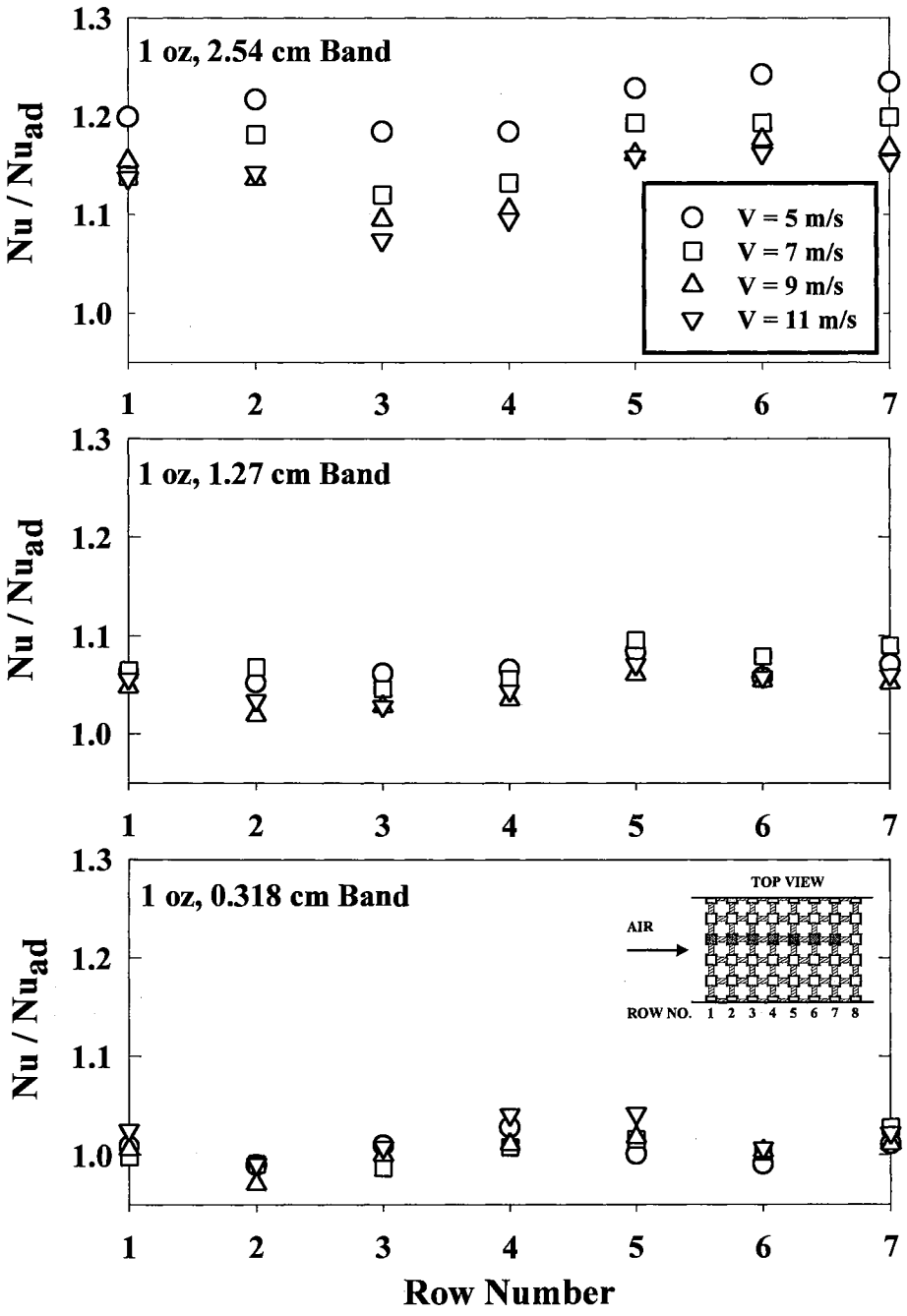

Fig. 3.9 Nusselt number of three 1 oz conductive test boards normalized with the adiabatic test board values at four different velocities and a fixed channel height of H = 3.81 cm.

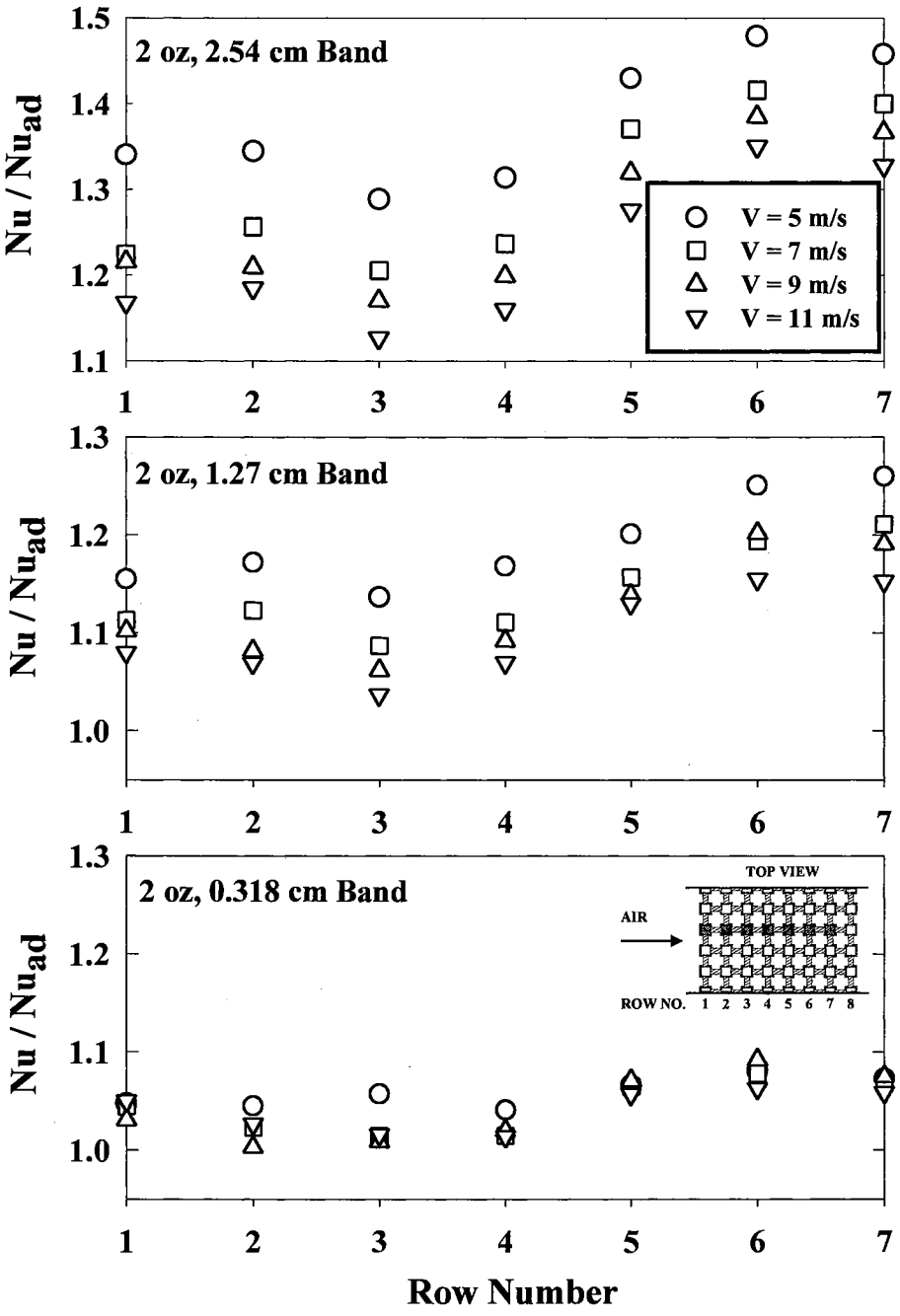

Fig. 3.10 Nusselt number of three 2 oz conductive test boards normalized with the adiabatic test board values at four different velocities and a fixed channel height of H = 7.62 cm.

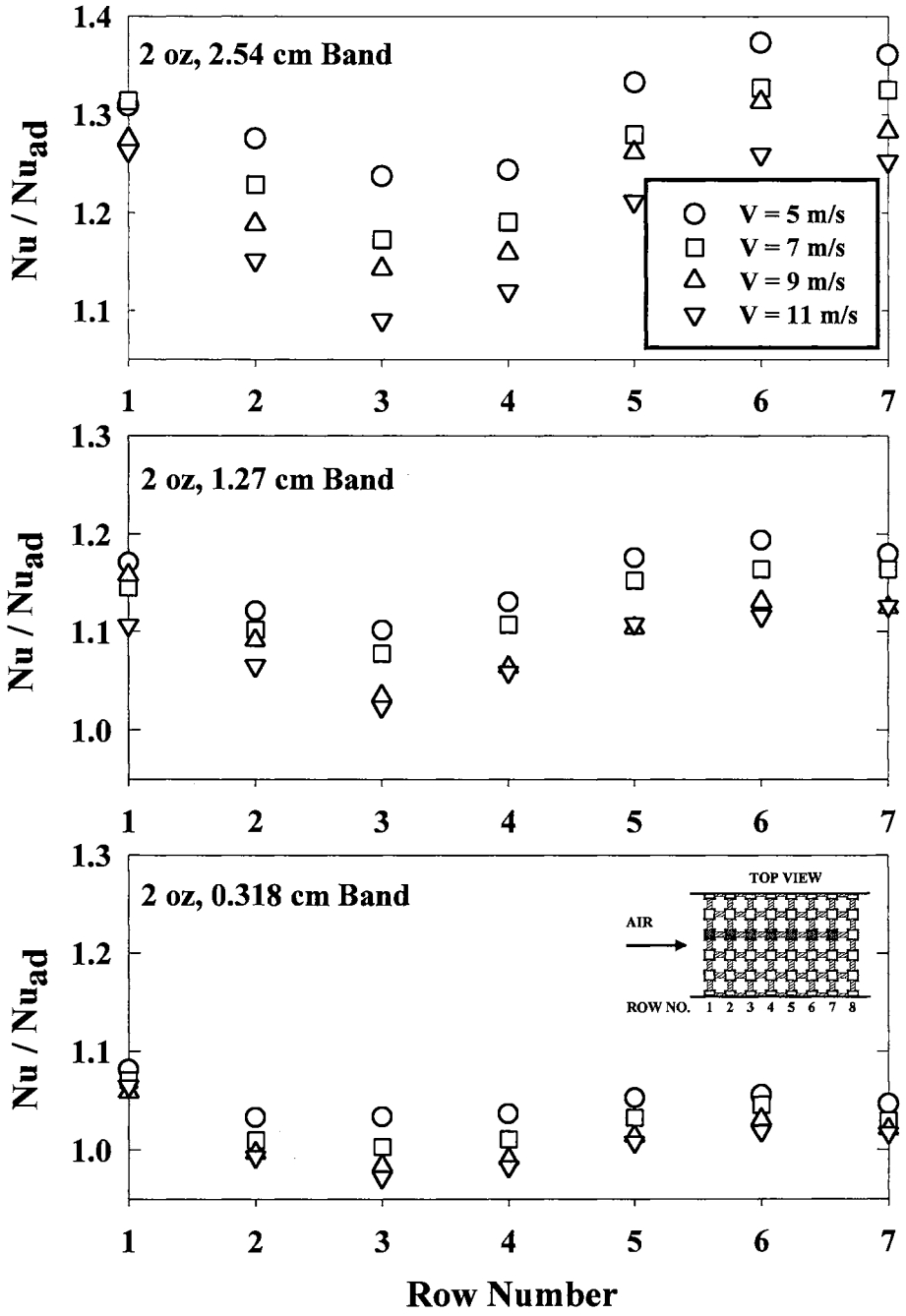

Fig. 3.11 Nusselt number of three 2 oz conductive test boards normalized with the adiabatic test board values at four different velocities and a fixed channel height of H = 5.08 cm.

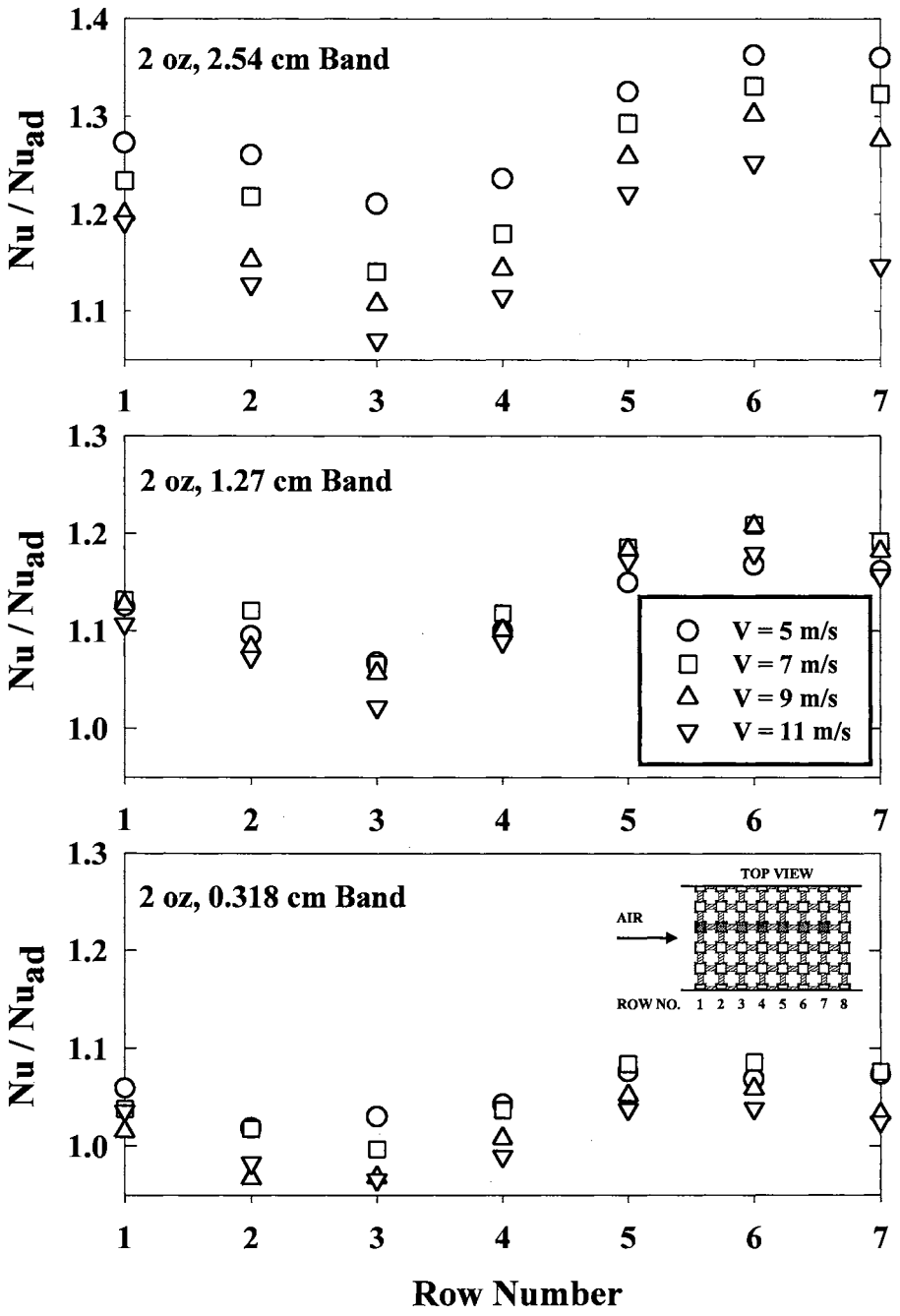

Fig. 3.12 Nusselt number of three 2 oz conductive test boards normalized with the adiabatic test board values at four different velocities and a fixed channel height of H = 3.81 cm.

on the 1 oz, 0.318 cm band width board and 2.6% on the 2 oz, 0.318 cm band width board. The ratios of normalized Nusselt numbers increased with increasing copper band width for a fixed channel height H. The highest and lowest normalized Nusselt numbers and the average of all the normalized Nusselt numbers of four centerline velocities for each conductive test board are given in Table 3.3 for each of the three channel heights (7.62, 5.08 and 3.81 cm). The comparison between the 1 oz, 0.318 cm band width board and the baseline adiabatic board gave mixed results. Eighteen out of eighty-four data points (21.4%) showed that the conductive board with 0.318 cm band width had lower Nusselt numbers than the adiabatic board. It was especially so for the first three rows at 7.62 cm channel height (the highest). However, the rest of the data points (78.6%) gave higher values. For the 2 oz, 0.318 cm band width, there were twelve points (14.3%) that showed lower Nusselt numbers than adiabatic board. Not even one of the data points for the 2.54 and 1.27 cm band conductive boards for both copper foil thicknesses had lower Nusselt numbers than the adiabatic board (Nu/Nu_{ad} was always greater than unity) when compared at the same conditions (the same channel height and centerline velocity) with the adiabatic board. This indicated that the heat transfer behavior of the 0.318 cm band width ($A^* = 0.085$) conductive boards were more toward the adiabatic board while both 2.54 cm ($A^* = 0.682$) and 1.27 cm band width ($A^* = 0.391$) conductive boards showed a significant difference in heat transfer behavior when compared with the adiabatic board ($A^* = 0$). The 2 oz, 0.318 cm band width board did show some improvement when compared with the 1 oz, 0.318 cm band width board but the difference was small. The effects of copper foil thickness variation will be discussed in the following section (3.3).

In general, the substrate (copper foil) conduction effects would be greater (higher

Nu/Nu_{ad} ratio) if the channel centerline velocity was lower. This is especially so for the 2.54 cm band test board which has the greatest exposed copper foil area. As the exposed copper foil area decreased, this trend gradually diminished. For 0.318 cm band test boards (least exposed copper foil area between the three copper foil patterns), the trend was never consistent. These general observations can be found in all six normalized Nusselt number figures, Figs. 3.7 to 3.12. The ratios of Nu/Nu_{ad} and variations with respect to centerline velocity of two selected modules (first and seventh) are tabulated in Table 3.4 for a selected channel height (7.62 cm) and six conductive test boards.

Tables 3.3 and 3.4 provide an overall view for Figs 3.7 to 3.12 which contained 504 data points in total. As shown in Table 3.3, the highest, lowest, and average Nu/Nu_{ad} (of a conductive test board for a fixed channel height, i.e., a subfigure) ratios varied between each subfigures of Figs. 3.7 through 3.12. The trends are very consistent, the highest, lowest, and average ratios always increased when the copper band width (A*) increased regardless of channel height variation. On the other hand, Table 3.4 illustrated that the influence of channel centerline velocity on Nu/Nu_{ad} ratios was not very consistent. For a fixed channel height, the ratios always decreased when velocity was increased for 2.54 cm band test boards. This trend can also be observed for the 1.27 cm band test boards but with a few irregular values. However, for the 0.318 cm band test boards, no clear trend for variation Nu/Nu_{ad} ratios with respect to channel centerline velocity could be observed.

TABLE 3.3

The Variation of Nu/Nu_{ad} of Four Centerline Velocities with Respect to Copper Band Width (or A*) and Copper Foil Thickness (T*) for Two Selected Modules and Three Different Channel Heights.

Band Width (cm)	Highest Nu/Nu_{ad}	% increase from 0.318 cm band	Lowest Nu/Nu_{ad}	% increase from 0.318 cm band	Average of all data of the test board	% increase from 0.318 cm band
1 oz, Channel Height H = **7.62** cm						
0.318	1.029	0	0.961	0	0.999	0
1.27	1.153	12 %	1.066	11 %	1.114	11 %
2.54	1.258	22 %	1.086	13 %	1.166	17 %
2 oz, Channel Height H = **7.62** cm						
0.318	1.092	0	1.003	0	1.045	0
1.27	1.260	15 %	1.037	3 %	1.134	9 %
2.54	1.479	35 %	1.127	12 %	1.283	23 %
1 oz, Channel Height H = **5.08** cm						
0.318	1.088	0	1.009	0	1.052	0
1.27	1.074	-1 %	1.039	3 %	1.060	1 %
2.54	1.273	17 %	1.078	7 %	1.172	12 %
2 oz, Channel Height H = **5.08** cm						
0.318	1.082	0	0.972	0	1.024	0
1.27	1.194	10 %	1.024	5 %	1.113	9 %
2.54	1.373	27 %	1.091	12 %	1.239	21 %
1 oz, Channel Height H = **3.81** cm						
0.318	1.042	0	0.971	0	1.008	0
1.27	1.096	5 %	1.019	5 %	1.057	5 %
2.54	1.243	19 %	1.074	11 %	1.163	15 %
2 oz, Channel Height H = **3.81** cm						
0.318	1.086	0	0.966	0	1.029	0
1.27	1.209	11 %	1.022	6 %	1.124	9 %
2.54	1.363	26 %	1.070	11 %	1.217	18 %

TABLE 3.4

The Variation of Nu/Nu_{ad} with Respect to CenterLine Velocity for Two Selected Modules, Three Different Copper Band Widths (or A*) and Two Copper Foil Thicknesses (T*) at a Channel Height of 7.62 cm.

First Module (Row No.1)			Seventh Module (Row No.7)		
Velocity (m/s)	Nu/Nu_{ad}	% difference between 5 m/s	Velocity (m/s)	Nu/Nu_{ad}	% difference between 5 m/s
1 oz, 2.54 cm Band Width, Channel Height H = 7.62 cm					
5	1.170	0	5	1.234	0
7	1.127	-3.7 %	7	1.226	-0.7 %
9	1.117	-4.5 %	9	1.210	-2.0 %
11	1.099	-6.1 %	11	1.183	-4.1 %
2 oz, 2.54 cm Band Width, Channel Height H = 7.62 cm					
5	1.341	0	5	1.458	0
7	1.225	-8.7 %	7	1.400	-4.0 %
9	1.216	-9.3 %	9	1.367	-6.2 %
11	1.168	-12.9 %	11	1.328	-8.9 %
1 oz, 1.27 cm Band Width, Channel Height H = 7.62 cm					
5	1.106	0	5	1.133	0
7	1.100	-0.5 %	7	1.153	1.8 %
9	1.100	-0.5 %	9	1.133	0.0 %
11	1.073	-3.0 %	11	1.120	-1.2 %
2 oz, 1.27 cm Band Width, Channel Height H = 7.62 cm					
5	1.155	0	5	1.260	0
7	1.113	-3.6 %	7	1.211	-3.9 %
9	1.102	-4.6 %	9	1.191	-5.5 %
11	1.080	-6.5 %	11	1.153	-8.5 %
1 oz, 0.318 cm Band Width, Channel Height H = 7.62 cm					
5	0.994	0	5	1.023	0
7	0.966	-2.8 %	7	1.013	-0.9 %
9	0.975	-1.9 %	9	1.020	-0.3 %
11	0.961	-3.3 %	11	1.029	0.7 %
2 oz, 0.318 cm Band Width, Channel Height H = 7.62 cm					
5	1.048	0	5	1.073	0
7	1.045	-0.3 %	7	1.068	-0.5 %
9	1.031	-1.6 %	9	1.075	0.2 %
11	1.050	0.2 %	11	1.059	-1.3 %

3.3 The Effects of Copper Foil Thickness on the Convection Heat Transfer Coefficient

All the conductive test boards used in the study are basically the same. They consist of a thin layer of essentially pure copper laminated to an insulator substrate. Two sets of conductive test boards (1 oz and 2 oz FR-4 Glass Epoxy) with the same copper foil distribution patterns were used. One ounce (1 oz) copper equates to one ounce of copper per one square foot of laminate. In actuality, this means the copper is 0.0034 cm thick. Two ounce (2 oz) copper means the copper is 0.0068cm thick likewise. The copper foil thickness ratio T* is defined as:

$$T^* = \frac{\text{Copper weight per square foot of the test board}}{\text{Maximum copper weight per square foot (4 oz)}} \tag{3.4}$$

where maximum copper weight (4 oz) per square foot is the maximum copper weight per square foot (thickest copper foil), generally used for printed circuit boards. The corresponding T* values for the two different sets of conductive boards were:

1 oz conductive test boards, $T^* = 0.25$

2 oz conductive test boards, $T^* = 0.50$

In general, increasing the thickness of copper foil on a conductive test board improves the heat transfer of the conductive test board. For example, the maximum increase from the adiabatic test board was 25.8% for 1 oz, 2.54 cm band width and 47.9% for 2 oz, 2.54 cm band width conductive test board. However, the influence of the thickness of the copper foil was closely associated with the copper foil band width of a conductive test board. The wider the band width, the greater the influence. Secondly, the higher the channel centerline velocity, the less the influence of the thickness of the copper

foil. Fig. 3.13 shows the average percentage difference of Nusselt number of all seven test modules between 1 and 2 oz conductive test boards. The ranges of the percent differences were

2.2 to 13.6% for 2.54 cm band width,

0.8 to 8.2% for 1.27 cm band width,

-3.8 to 5.4% for 0.318 cm band width.

The range was the highest for the 2.54 cm band width and then dropped to the lowest for the 0.318 cm band width. The negative values of the 0.318 cm band width were due to the diminishing influence of the thicker copper foil compounded by the uncertainty of the experiments. The majority of the curves in Fig. 3.13 also show a downward trend of the influence of the thicker copper foil when the channel centerline velocity increases.

Another perspective to see the influence of copper foil thickness on heat transfer is displayed in Fig. 3.14. Percentage increase of the average Nusselt number of three channel heights from the adiabatic board value for two sets (different copper foil thicknesses) of conductive test boards are shown in Fig. 3.14. The downard trends of the increase in Nusselt number with respect to air velocity and copper foil band width can be consistently seen in Fig.3.14. The ratio of ($Nu_{2\ oz}$ - $Nu_{1\ oz}$) to ($Nu_{1\ oz}$ - Nu_{ad}) in percentage are shown in the figure, too. The averages of the ratios were 50%, 50% and 40% for 2.54, 1.27 and 0.318 cm band widths respectively. This was fairly consistent regardless of copper foil band width. In other words, the enhancement in term of Nusselt number because of thicker copper foil was closely associated with copper foil band width. However, ratio of the "differences" between Nusselt numbers on different test boards

offered a different point of view. The enhancement in heat transfer from 1 oz to 2 oz boards relative to the increase from the adiabatic to 1 oz test boards appeared to be fairly uniform among different copper foil band widths.

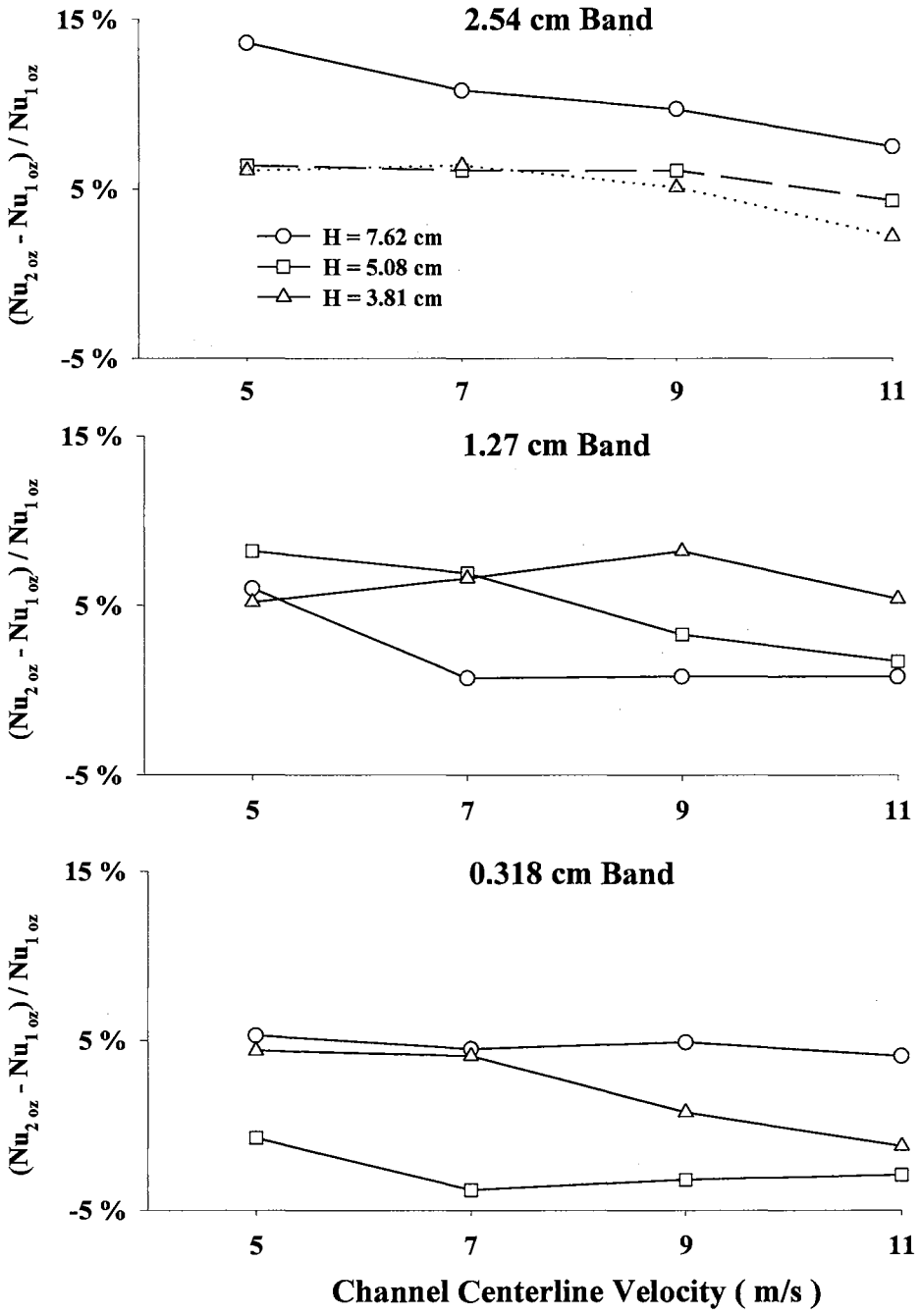

Fig. 3.13 Average percentage difference of Nusselt numbers between 1 and 2 oz conductive test boards for all seven modules at four different velocities and three channel heights.

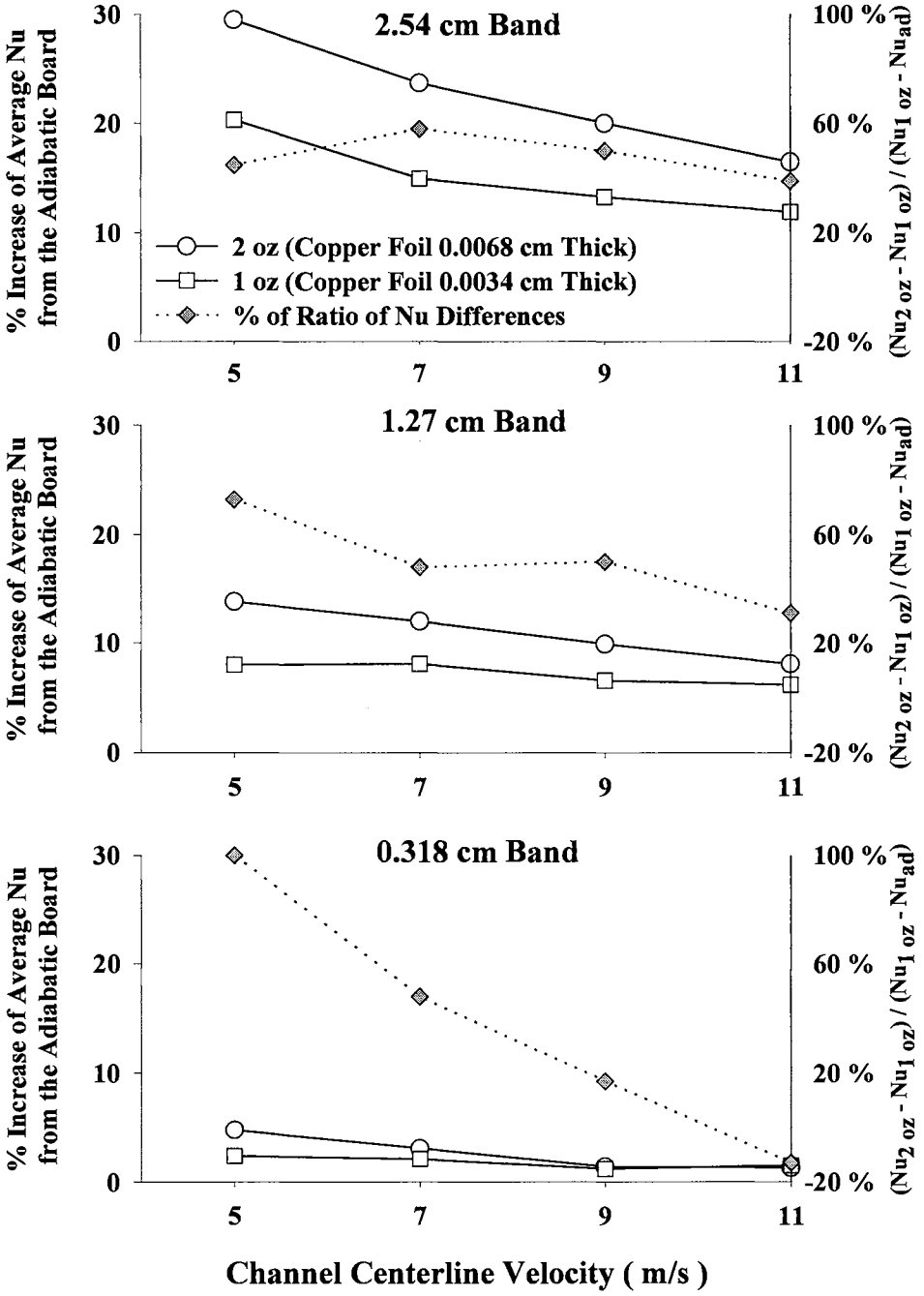

Fig. 3.14 Percentage increase of the average Nusselt number of three channel heights from the adiabatic board value, and the percentage of the difference of Nusselt number on different test boards.

3.4 The Effects of Input Power Variation on Convection Heat Transfer Coefficient

The third module of the center column was heated with two input power levels of 10 and 20W for every experimental run. Convection heat transfer coefficients were measured for both input power levels. Figs. 3.15 and 3.16 show the ratio of the convection heat transfer coefficient at 20W to the convection heat transfer coefficient at 10W versus the modified Reynolds number. There are two subfigures for each figure, Figs. 3.15a and 3.16a show the original heat transfer coefficient ratios versus modified Reynolds number, and Figs. 3.15b and 3.16b show the linear regression of the original data. As seen in Figs. 3.15a and 3.16a, the ratio of h_{20W}/h_{10W} versus the modified Reynolds number did not indicate a clear trend, thus linear regressions were performed on the original data. Non-linear quadratic regressions of the original data gave very similar results. Fig. 3.15b shows clearly that only at the highest board conductivity of this study (2.54 cm band) the slope of the linear regression distinguished itself from the rest of three test boards. Even so, the maximum ratio of h_{20W}/h_{10W} of the 1 oz board with 2.54 cm band was less than 1.02. The curves in Fig. 3.16b of 2 oz conductive test boards show a somewhat different pattern with the 0.318 cm band having the highest variation of h_{20W}/h_{10W} ratio. However, the slope of the curve of 2.54 cm band was still the largest. The maximum ratio of h_{20W}/h_{10W} of the 2 oz board with 0.318 cm band was about 1.03.The difference of the convection heat transfer coefficients between the two input power levels for all six conductive test boards within the range of modified Reynolds numbers from 9100 to 26300 were always less than 3%. In a practical sense, the input

power variation was hardly a factor in the conjugate heat transfer process of the present study.

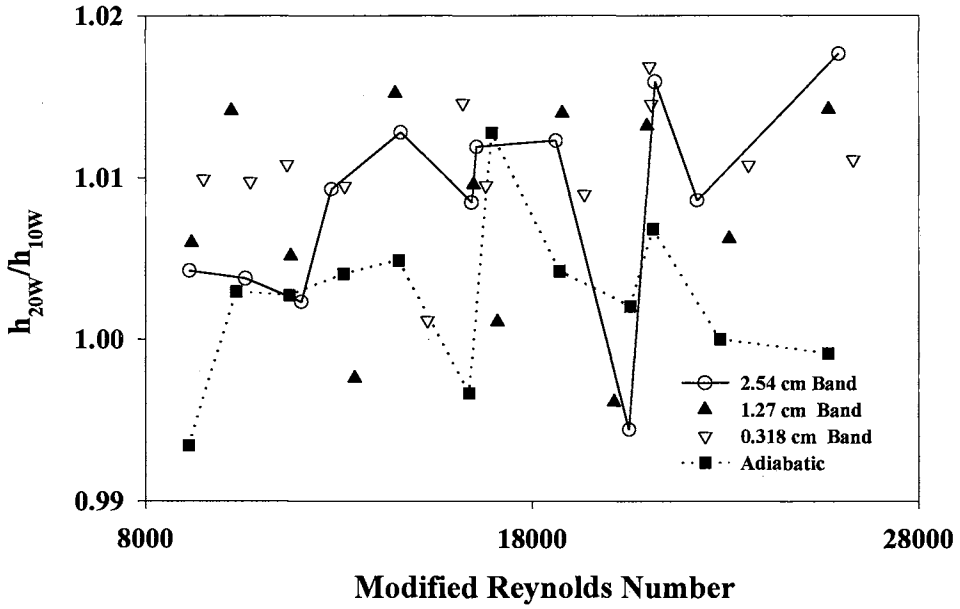

Fig. 3.15a Normalized heat transfer coefficient of 20W power dissipation with 10W power dissipation values for 1 oz conductive and adiabatic test boards.

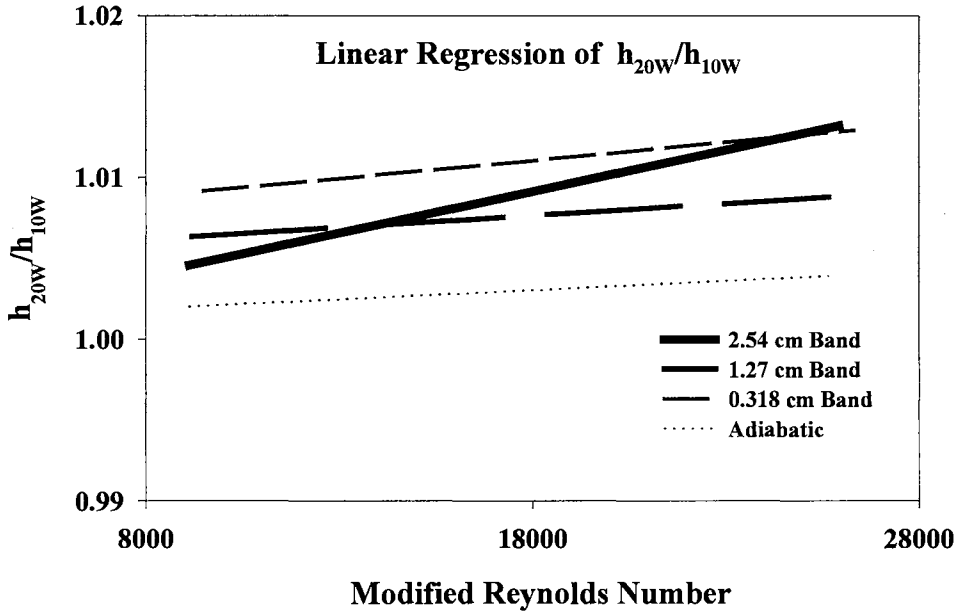

Fig. 3.15b Linear regression of the original data presented in Fig. 3.15a (h_{20W}/h_{10W} vs. modified Reynolds number).

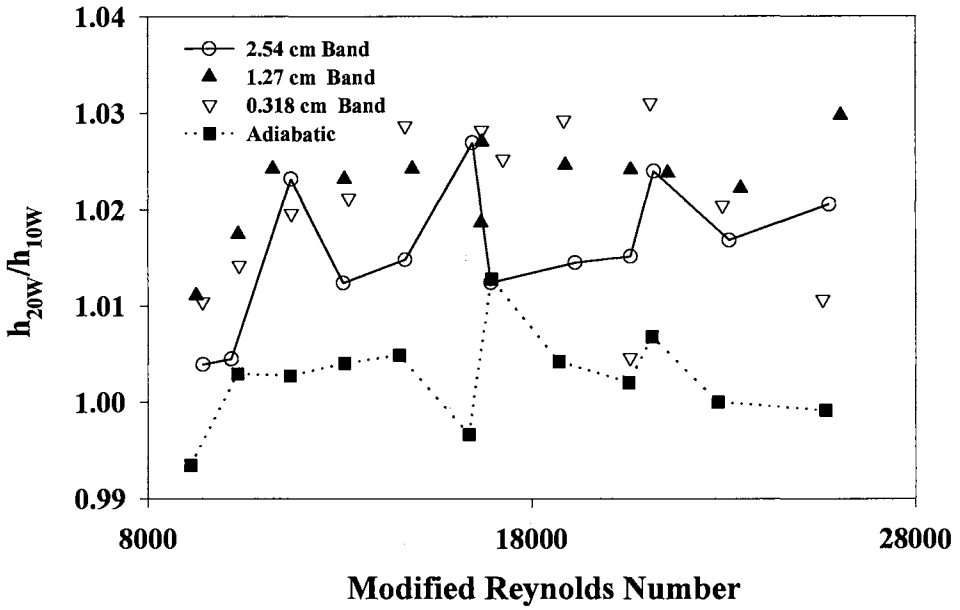

Fig. 3.16a Normalized heat transfer coefficient of 20W power dissipation with 10W power dissipation values for 2 oz conductive and adiabatic test boards.

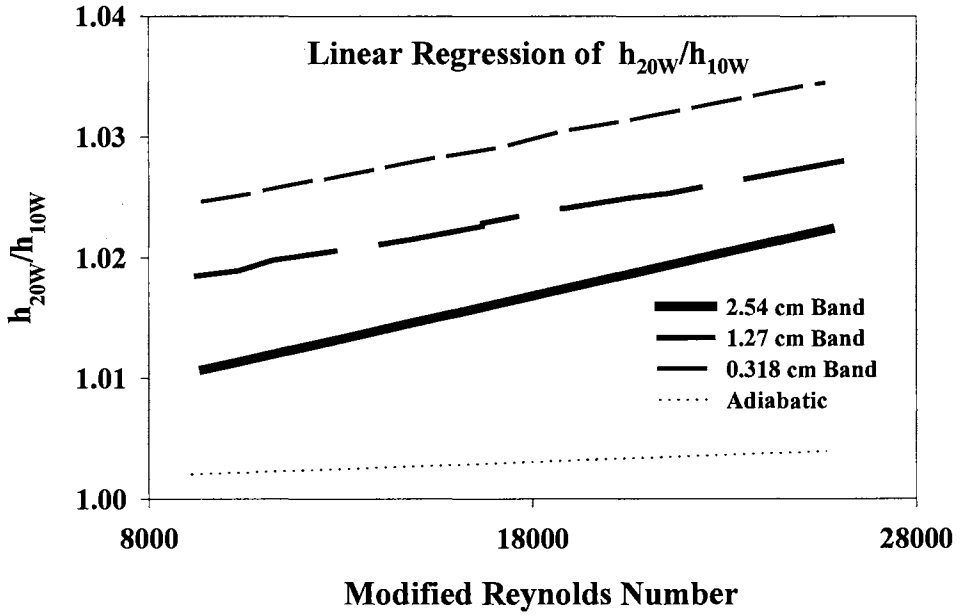

Fig. 3.16b Linear regression of the original data presented in Fig. 3.16a (h_{20W}/h_{10W} vs. modified Reynolds number).

3.5 Module Temperature Rise Distribution Results

The temperature rise (ΔT) of a monitored module was defined as the temperature difference between the temperatures of the monitored module after the third module of the center column was heated with twenty (20) Watts of input power and the temperature of the module when the third module was passive (not heated). The temperatures of all the monitored modules at the lowest ambient temperature when the third module was not heated was designated as the base-line. The temperature rise data for all cases were then generated by subtracting the base-line values of each monitored module from the temperature of each monitored module when the third module was heated. Thus, the temperature rise data would vary with the ambient temperature when each set of data was collected (after the third module was heated and steady state conditions were reached). Because of this, the temperature rise (ΔT) data presented in this section should only be used for comparison within each set of data between the modules under the same conditions. There were a total of twenty-four modules (three columns, eight rows) monitored at any experimental run for three 1 oz and the adiabatic test boards. Figures 3.17 to 3.32 show the temperature rises versus row number for 1 oz conductive test boards with copper band widths of 2.54, 1.27 and 0.318 cm and the adiabatic board at channel heights H = 7.62, 5.08 and 3.81cm and four different velocities (5, 7, 9, 11 m/s). A schematic of the top view of the in-line array of modules on a test board is included in each figure to give a better demonstration of the experimental data presented. The schematic also shows the copper bands of a typical conductive board connecting all the modules. For the adiabatic (bare) test board, the copper bands were absent. In the top

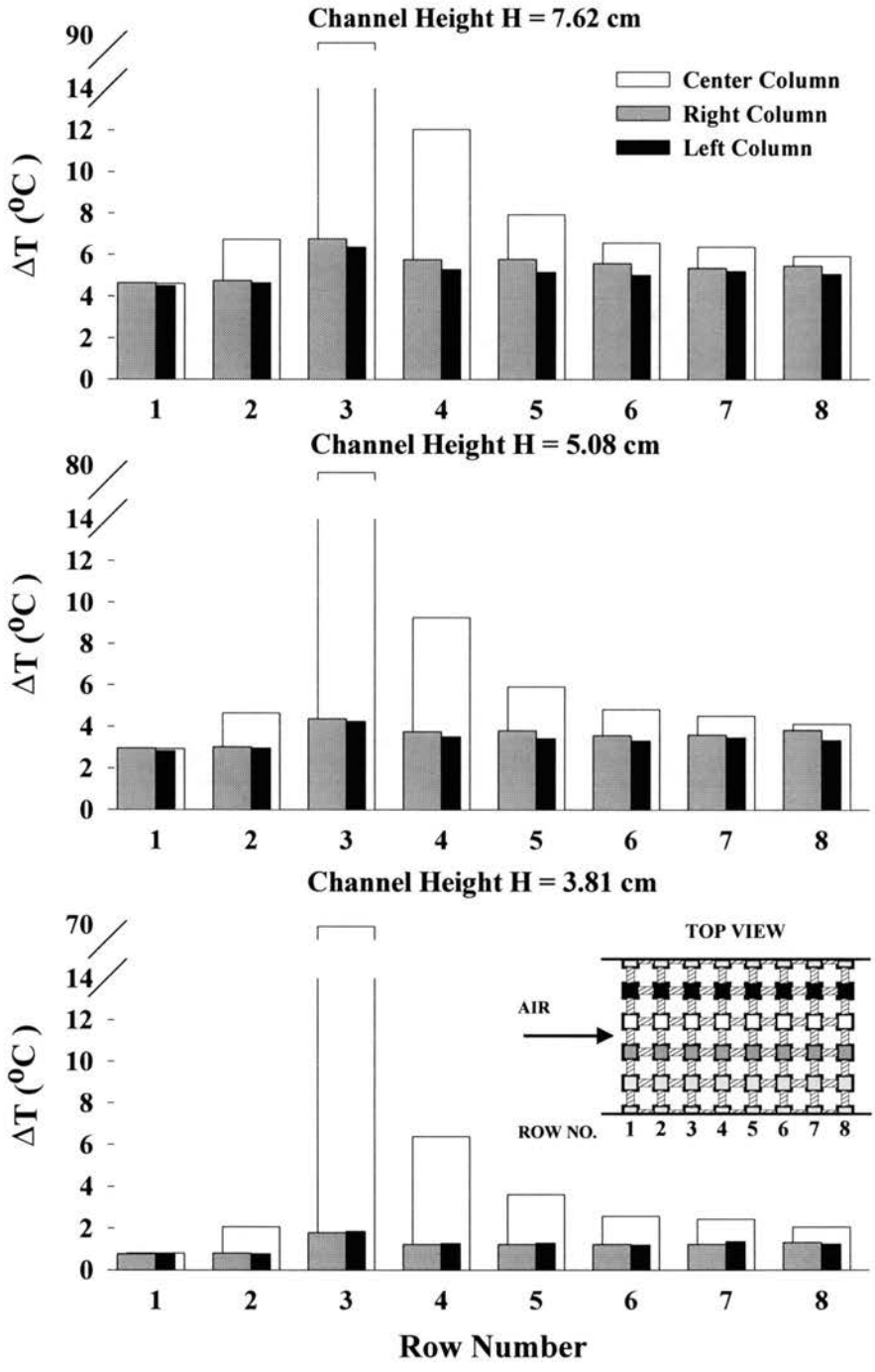

Fig. 3.17 Temperature increases when the third module of the center column was heated with 20 W on the 1 oz., 2.54 cm copper band board at three channel heights and a fixed channel centerline velocity of 5 m/s.

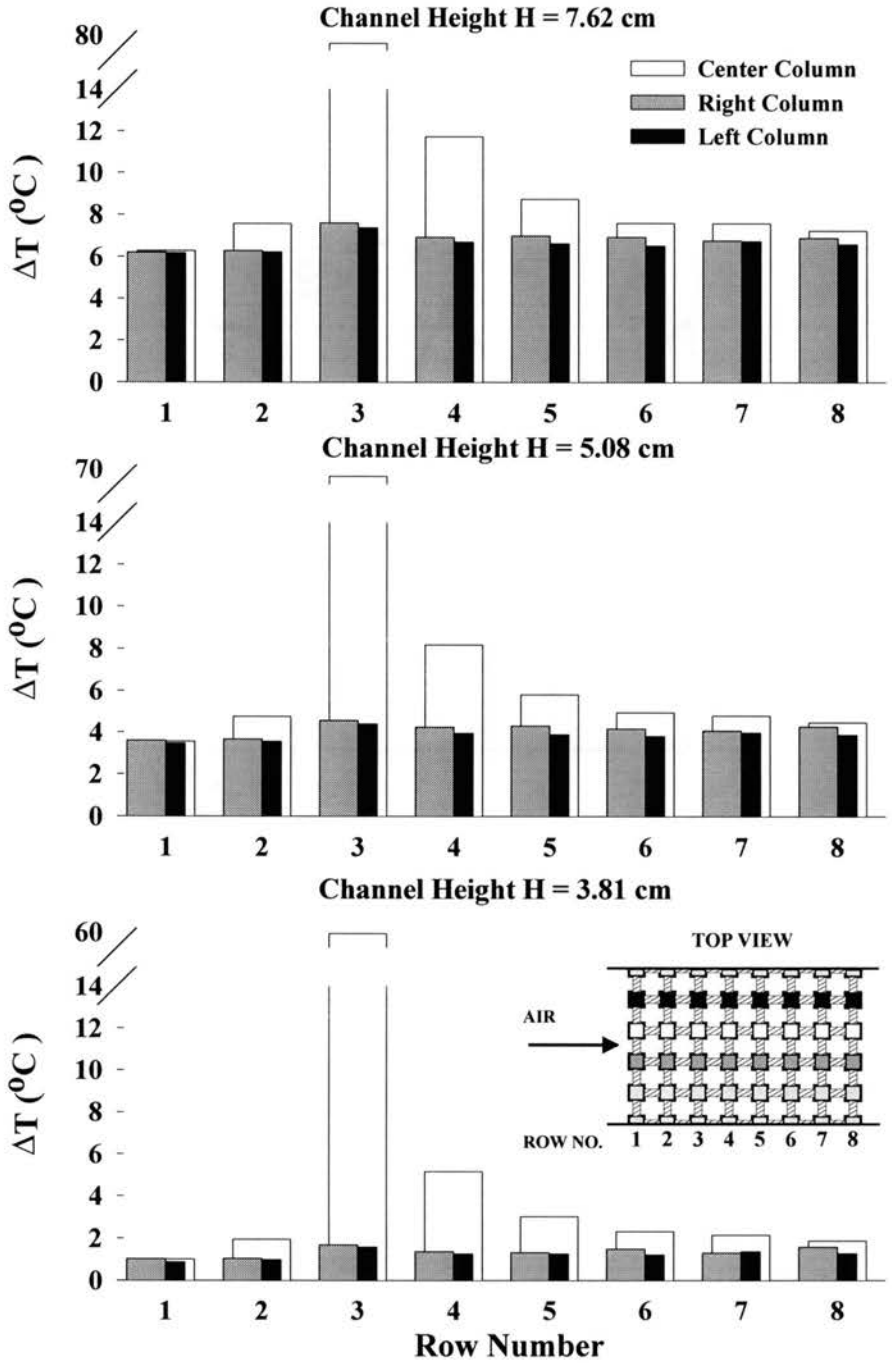

Fig. 3.18 Temperature increases when the third module of the center column was heated with 20 W on the 1 oz., 2.54 cm copper band board at three channel heights and a fixed channel centerline velocity of 7 m/s.

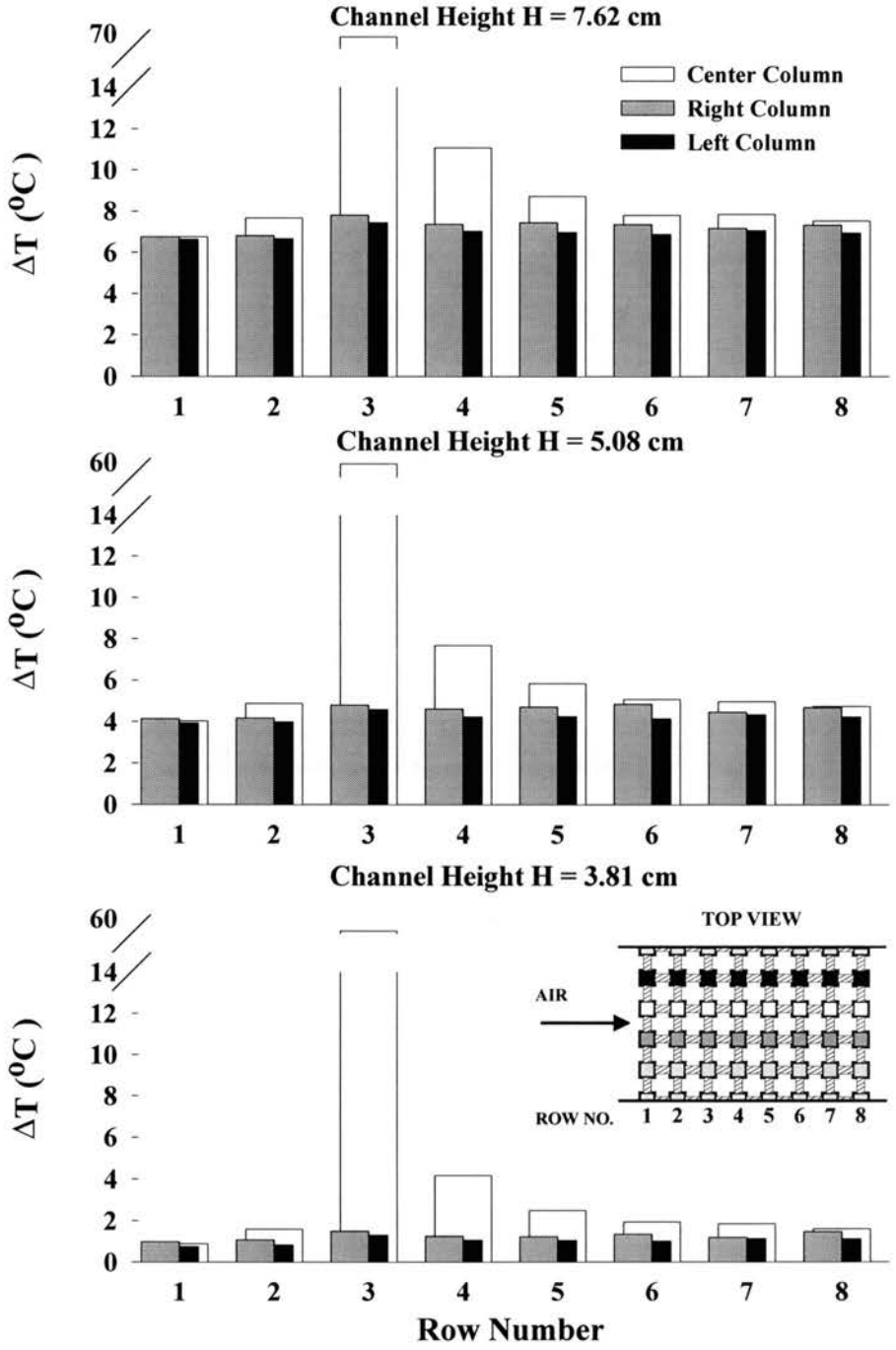

Fig. 3.19 Temperature increases when the third module of the center column was heated with 20 W on the 1 oz., 2.54 cm copper band board at three channel heights and a fixed channel centerline velocity of 9 m/s.

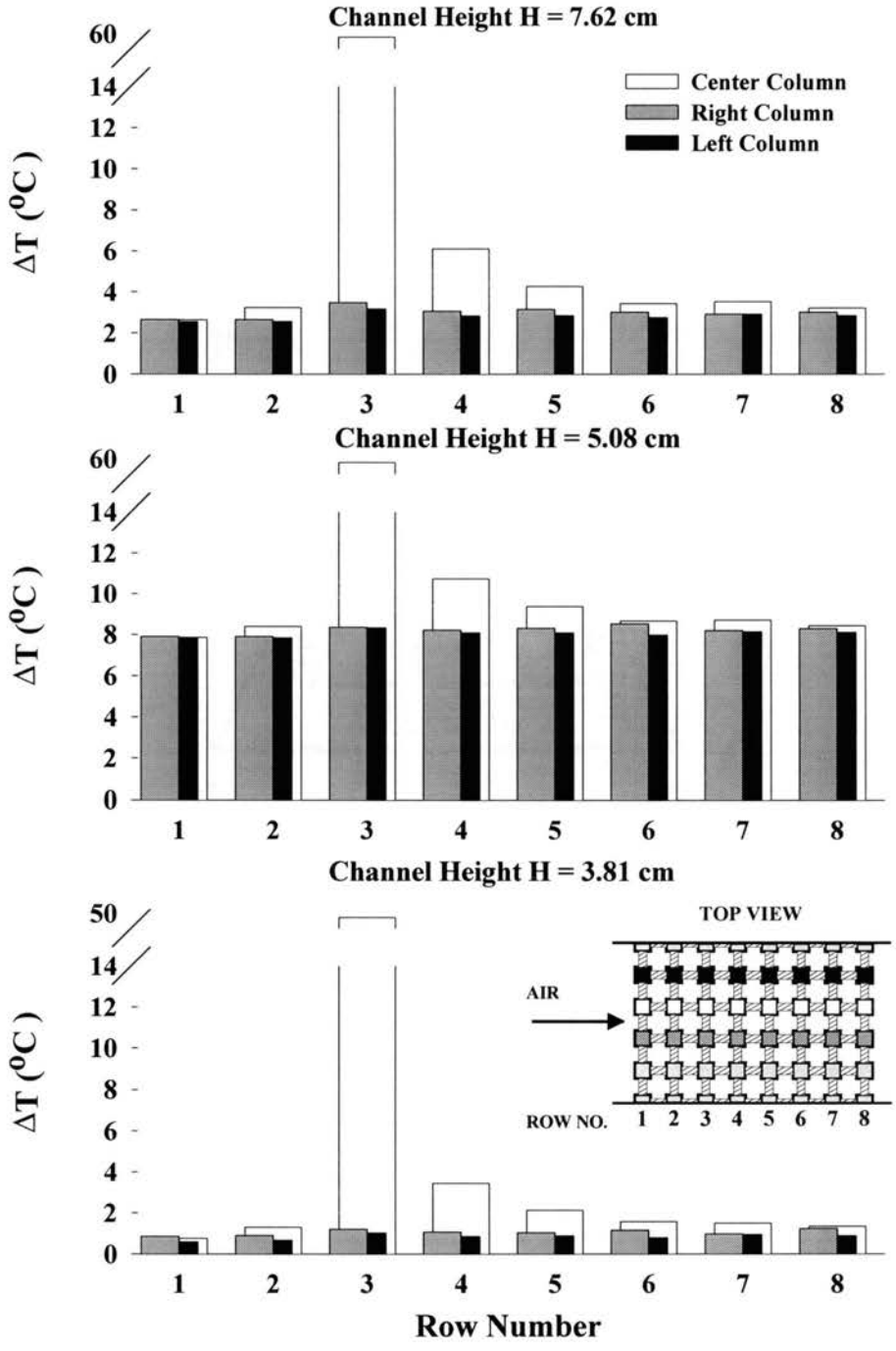

Fig. 3.20 Temperature increases when the third module of the center column was heated with 20 W on the 1 oz., 2.54 cm copper band board at different channel heights and a fixed channel centerline velocity of 11 m/s.

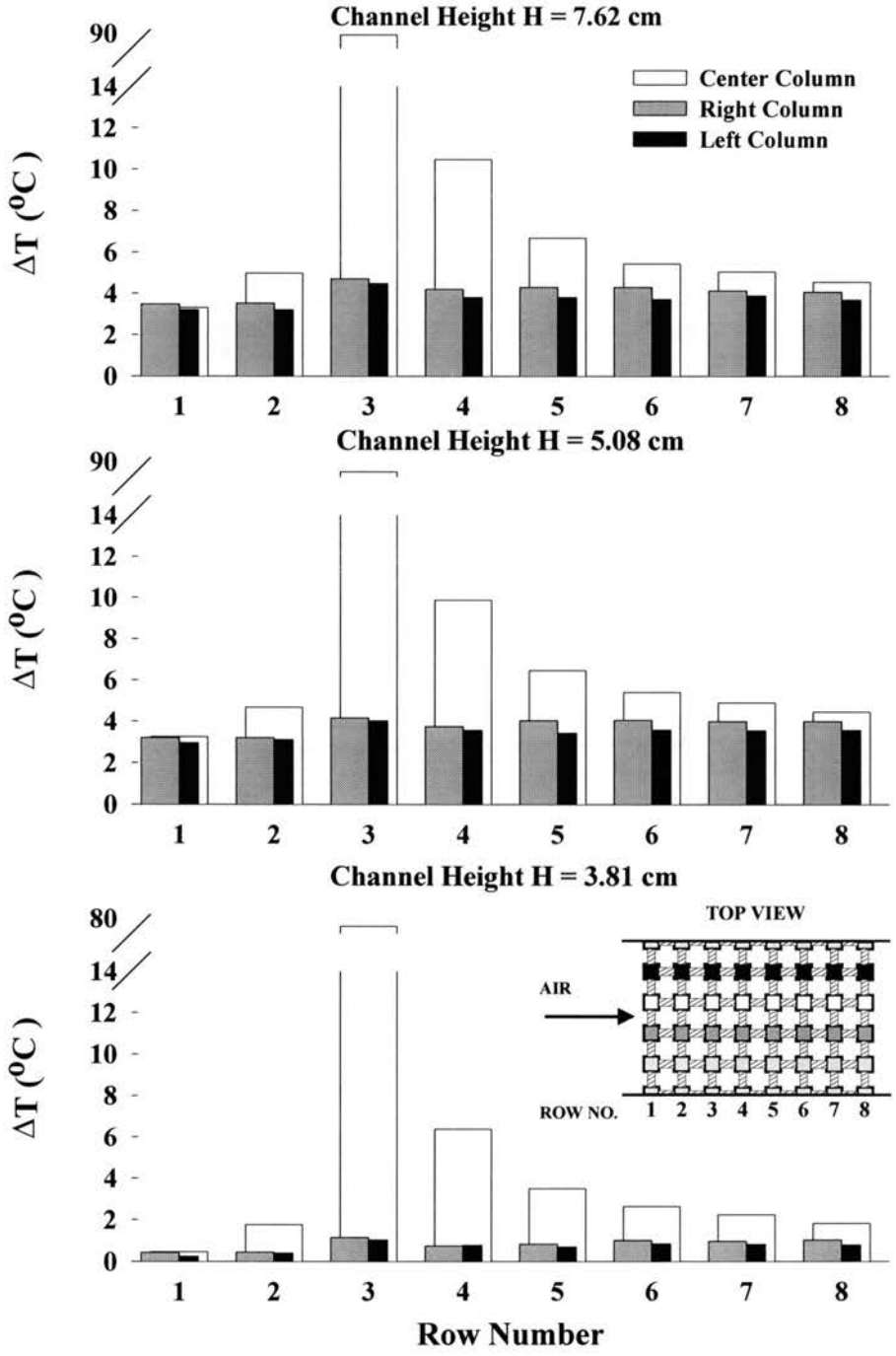

Fig. 3.21 Temperature increases when the third module of the center column was heated with 20 W on the 1 oz., 1.27 cm copper band board at three channel heights and a fixed channel centerline velocity of 5 m/s.

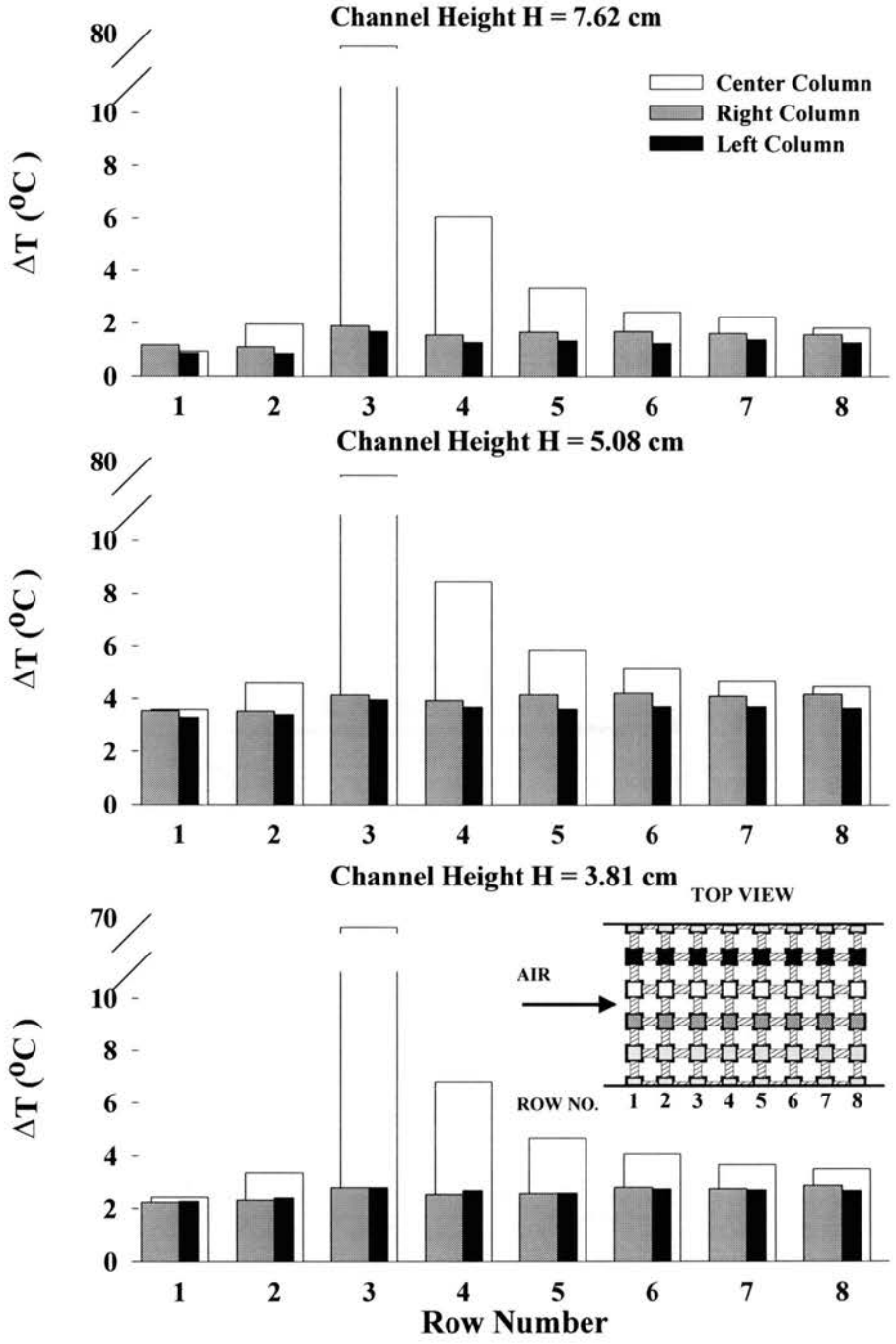

Fig. 3.22 Temperature increases when the third module of the center column was heated with 20 W on the 1 oz., 1.27 cm copper band board at three channel heights and a fixed channel centerline velocity of 7 m/s.

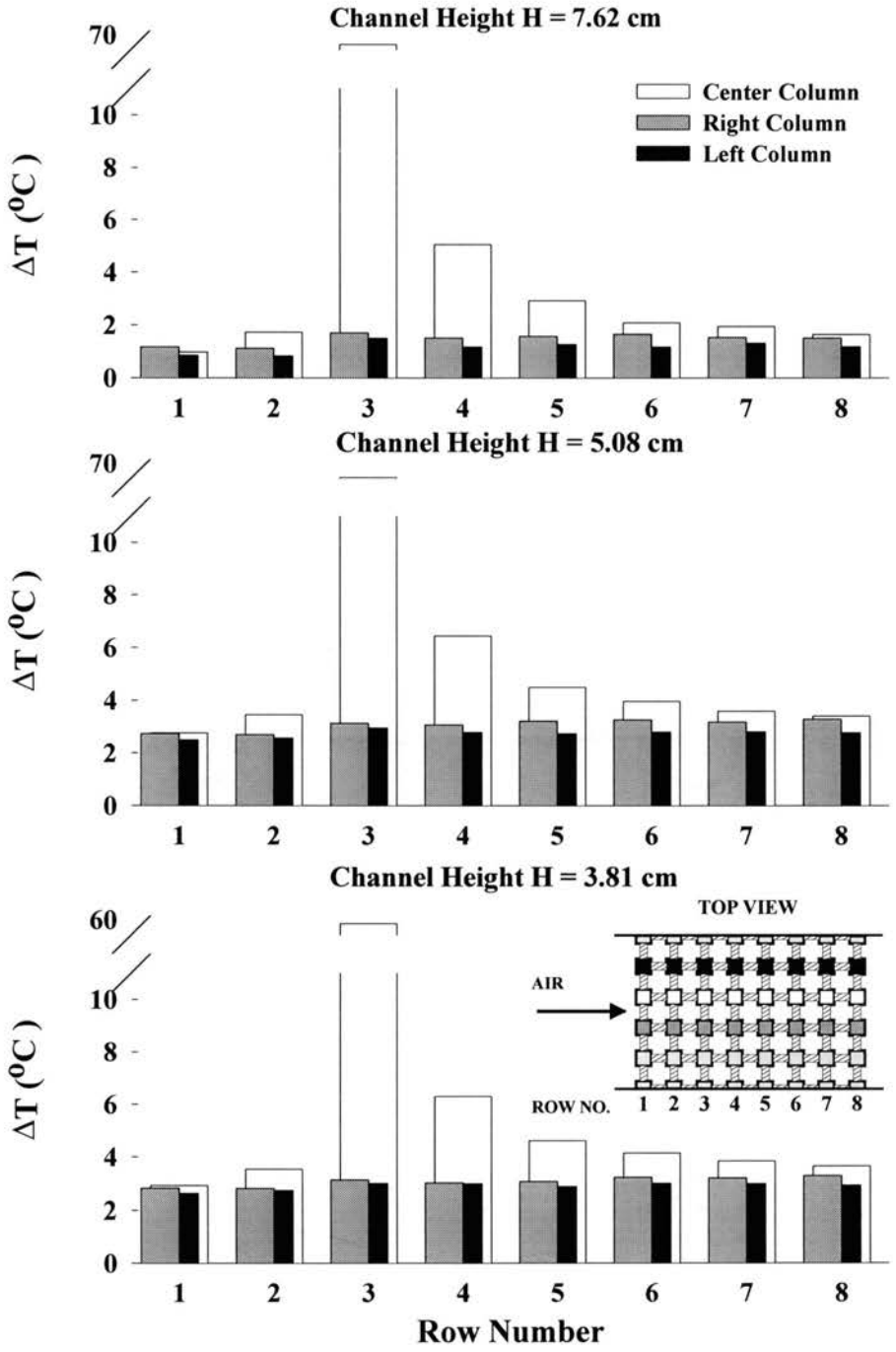

Fig. 3.23 Temperature increases when the third module of the center column was heated with 20 W on the 1 oz., 1.27 cm copper band board at three channel heights and a fixed channel centerline velocityof 9 m/s.

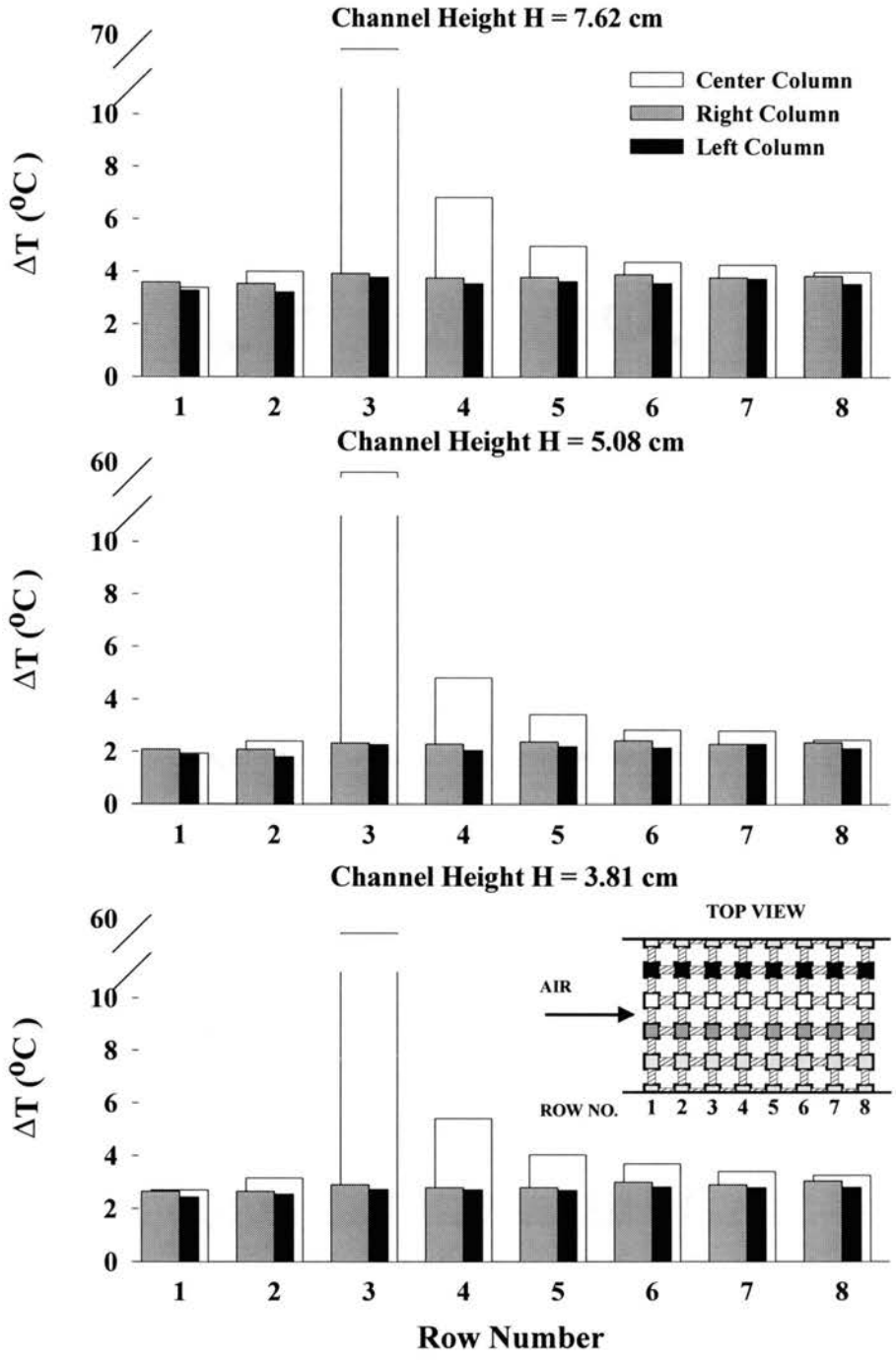

Fig. 3. 24 Temperature increases when the third module of the central column was heated with 20 W on the 1 oz., 1.27 cm copper band board at three channel heights and a fixed channel centerline velocity of 11 m/s.

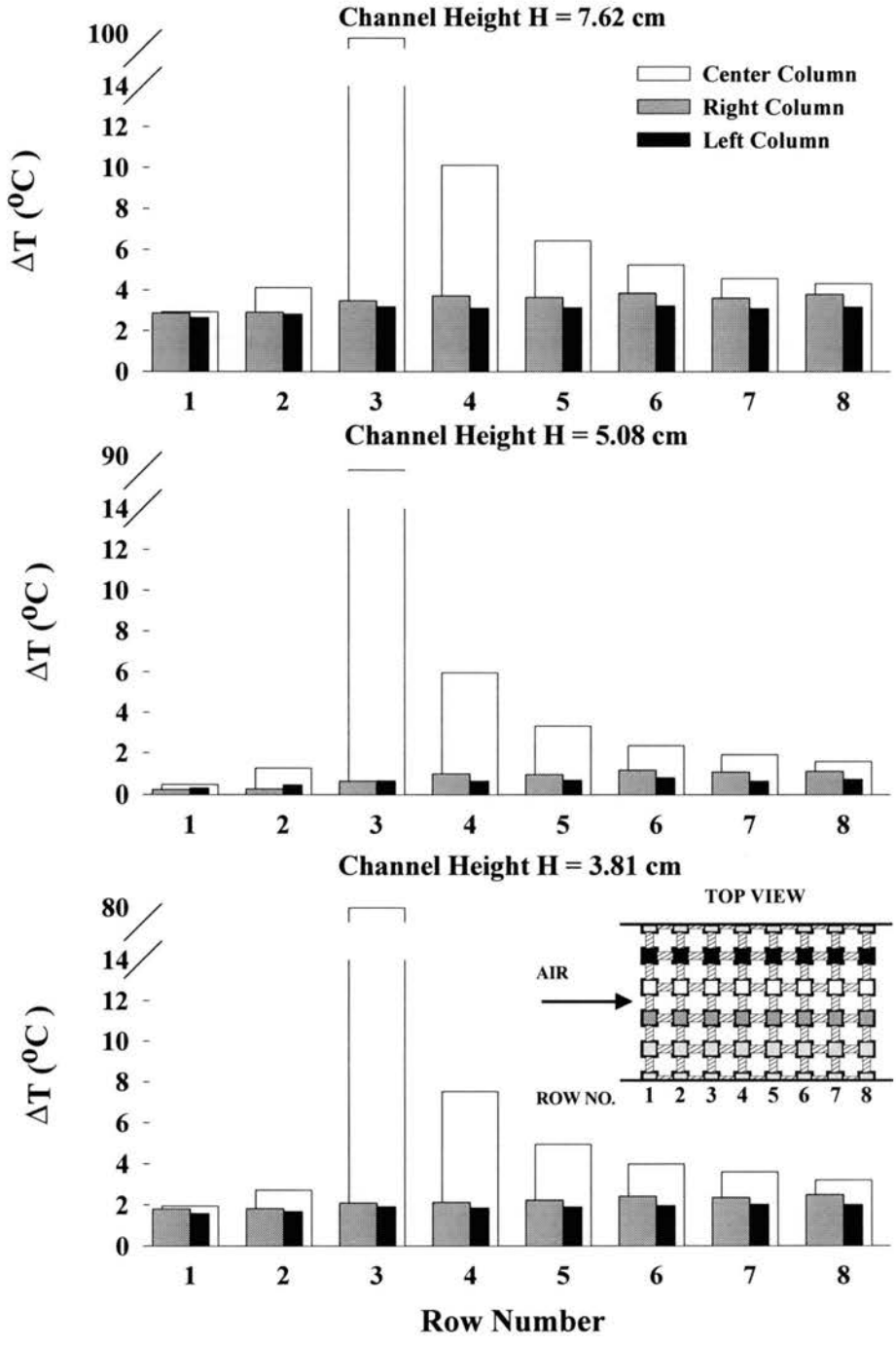

Fig. 3.25 Temperature increases when the third module of the center column was heated with 20 W on the 0.318 cm band board at three channel heights and a fixed channel centerline velocity of 5 m/s.

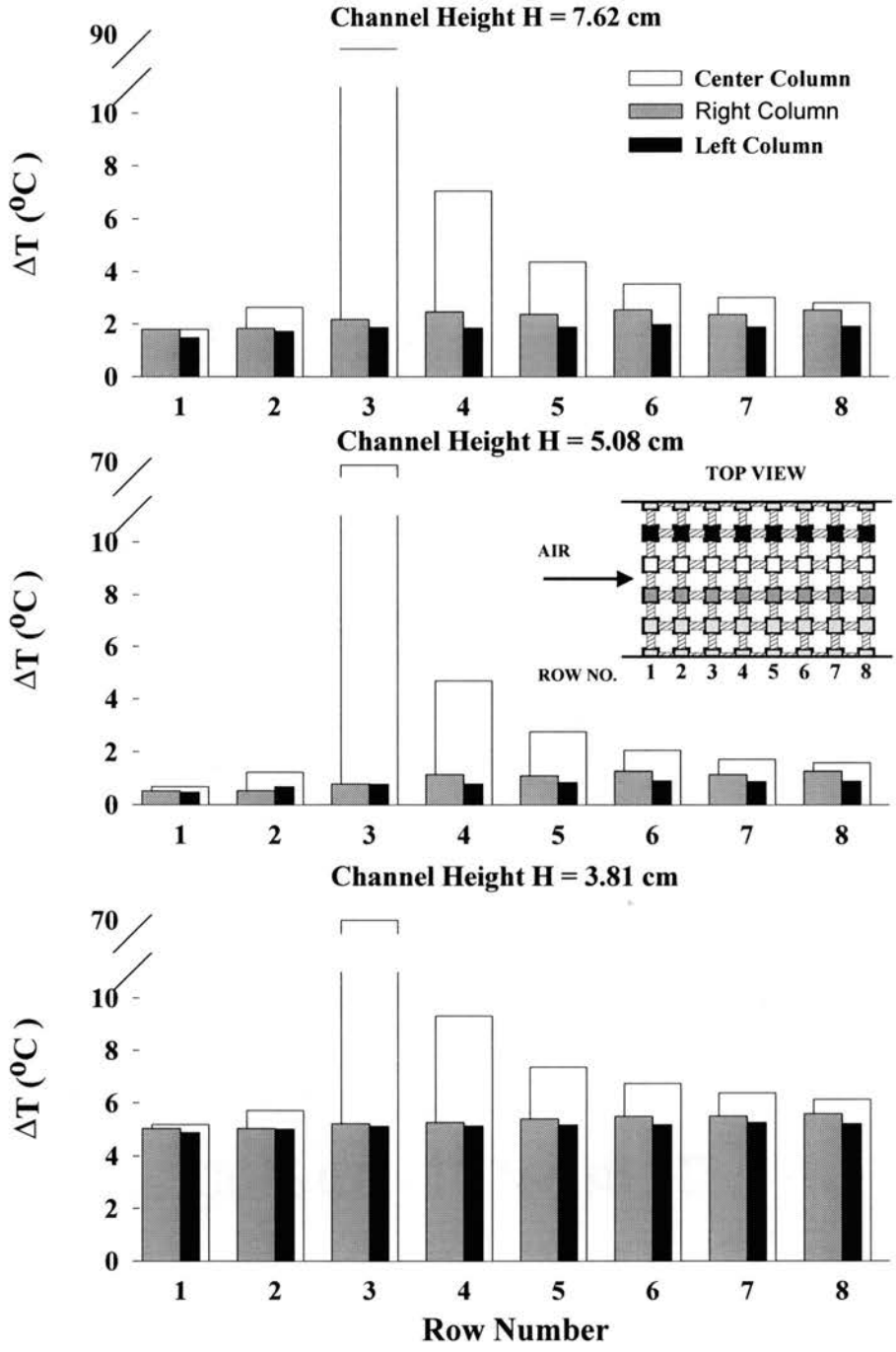

Fig. 3.26 Temperature increases when the third module of the center column was heated with 20 W on the 0.318 cm band board at three channel heights and a fixed channel centerline velocity of 7 m/s.

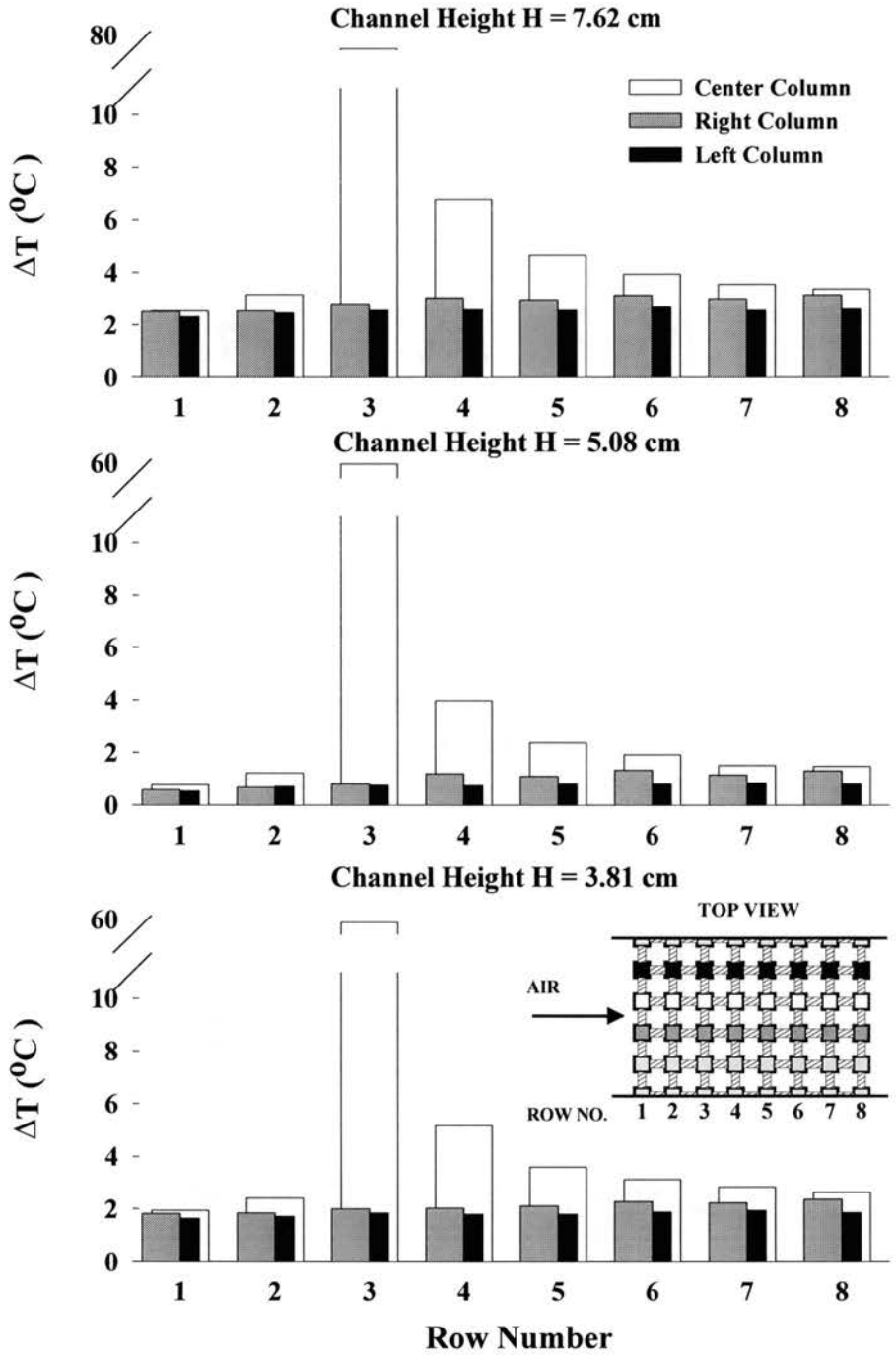

Fig. 3.27 Temperature increases when the third module of the center column was heated with 20 W on the 0.318 cm band board at three channel heights and a fixed channel centerline velocity of 9 m/s.

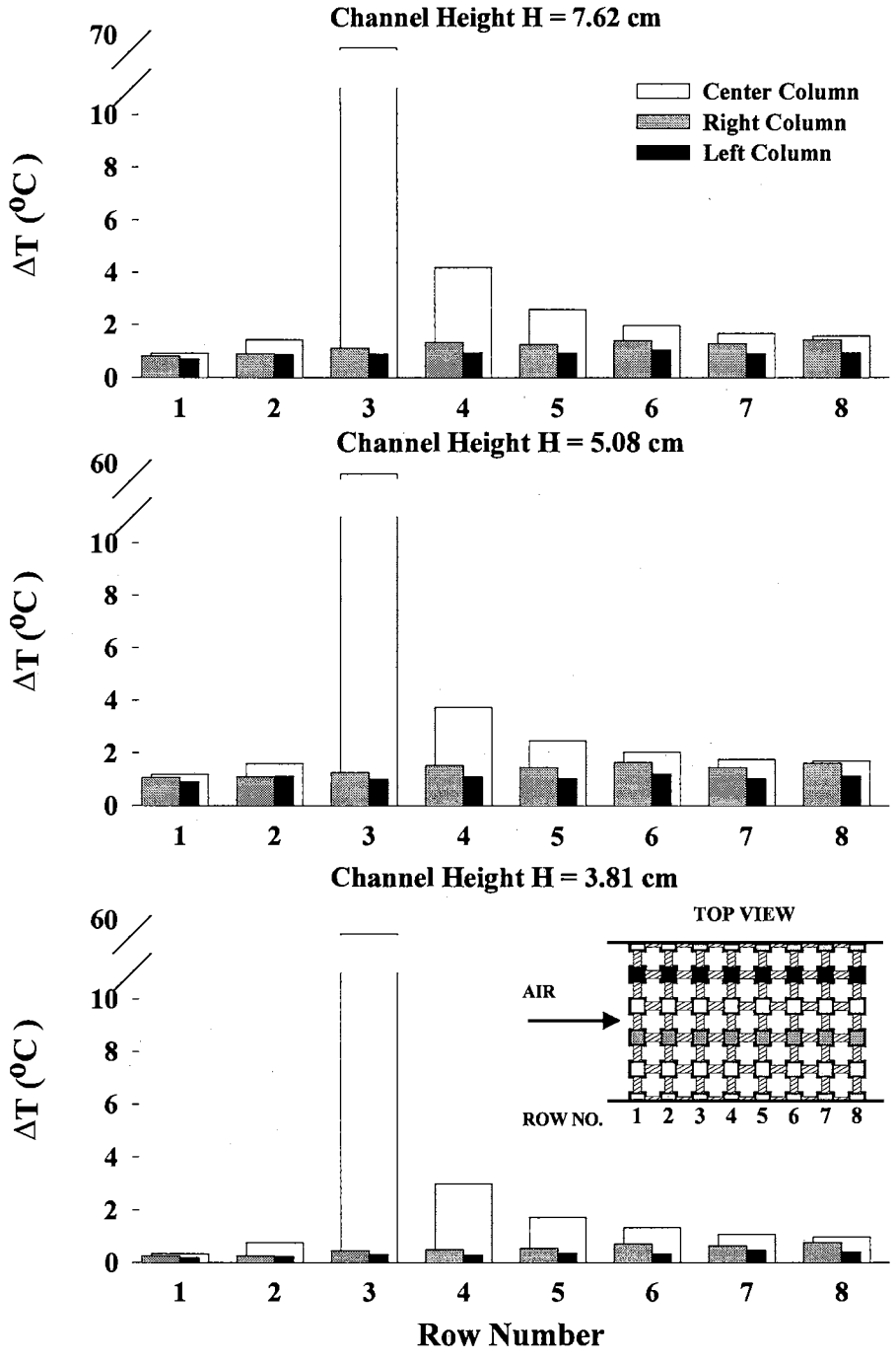

Fig. 3.28 Temperature increases when the third module of the center column was heated with 20 W on the 0.318 cm band board at three channel heights and a fixed channel centerline velocity of 11 m/s.

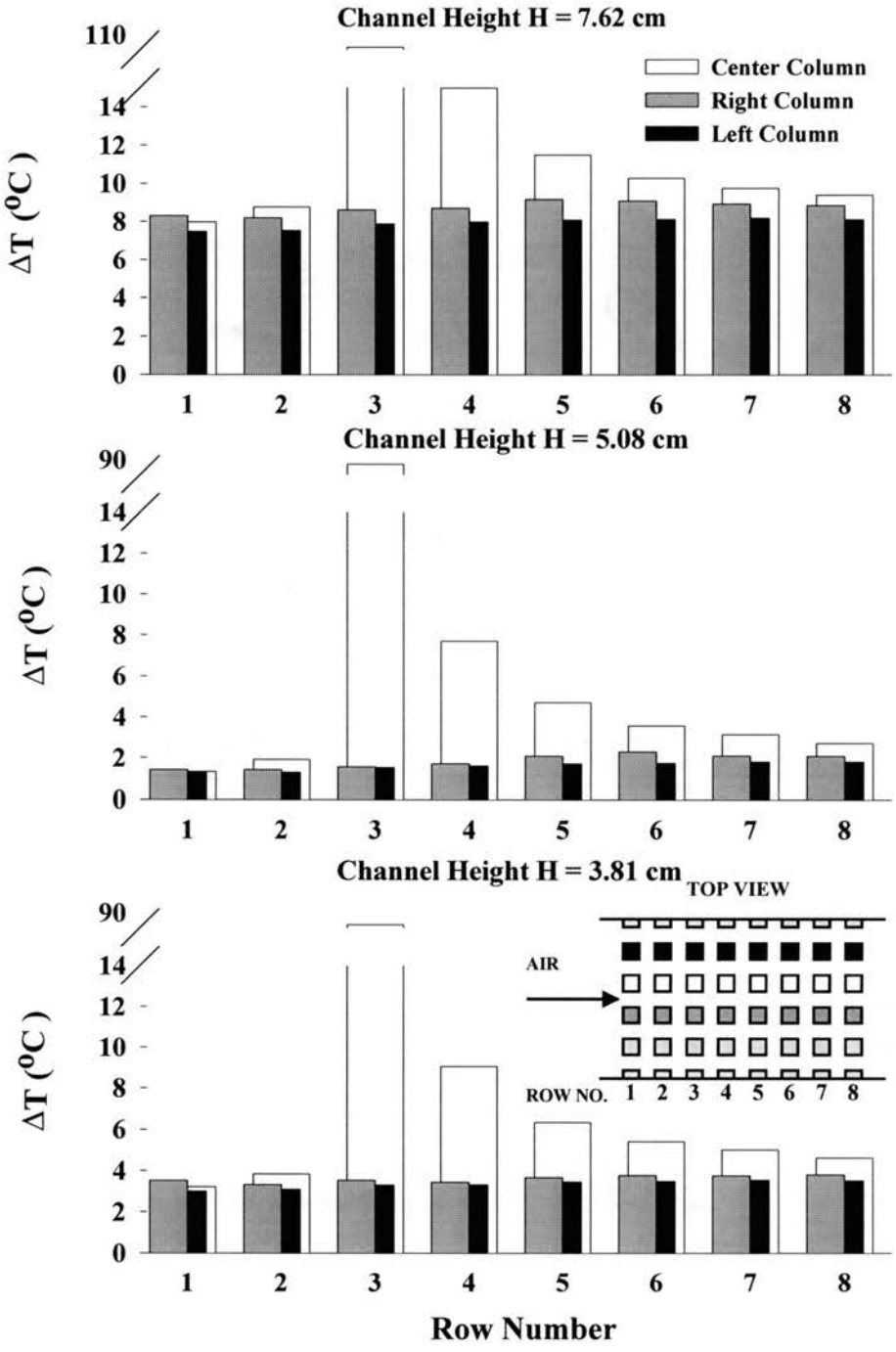

Fig. 3.29 Temperature increases when the third module of the center column was heated with 20 W on the adiabatic board at three channel heights and a fixed channel centerline velocity of 5 m/s.

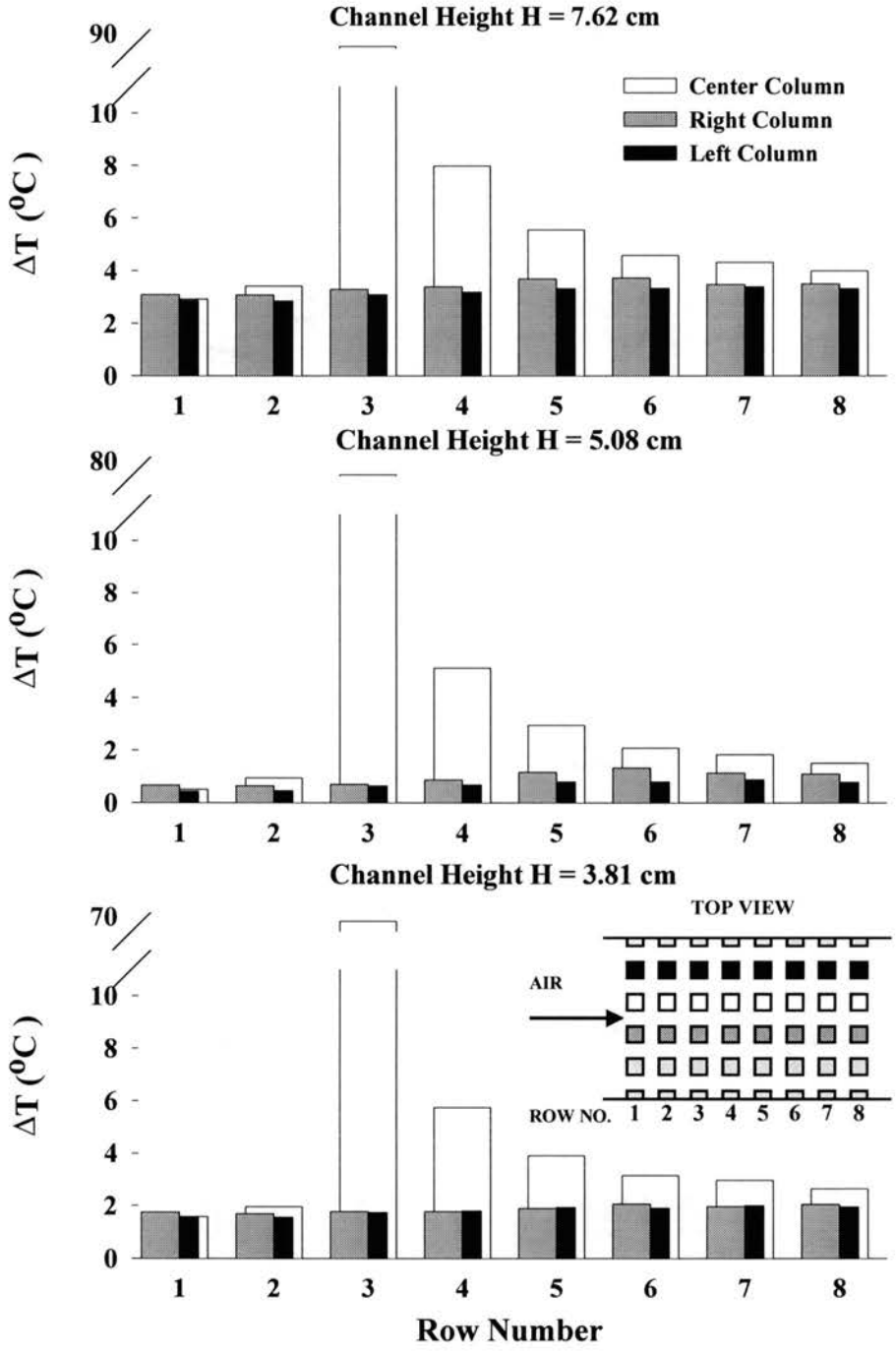

Fig. 3.30 Temperature increases when the third module of the center column was heated with 20 W on the adiabatic board at three channel heights and a fixed channel centerline velocity of 7 m/s.

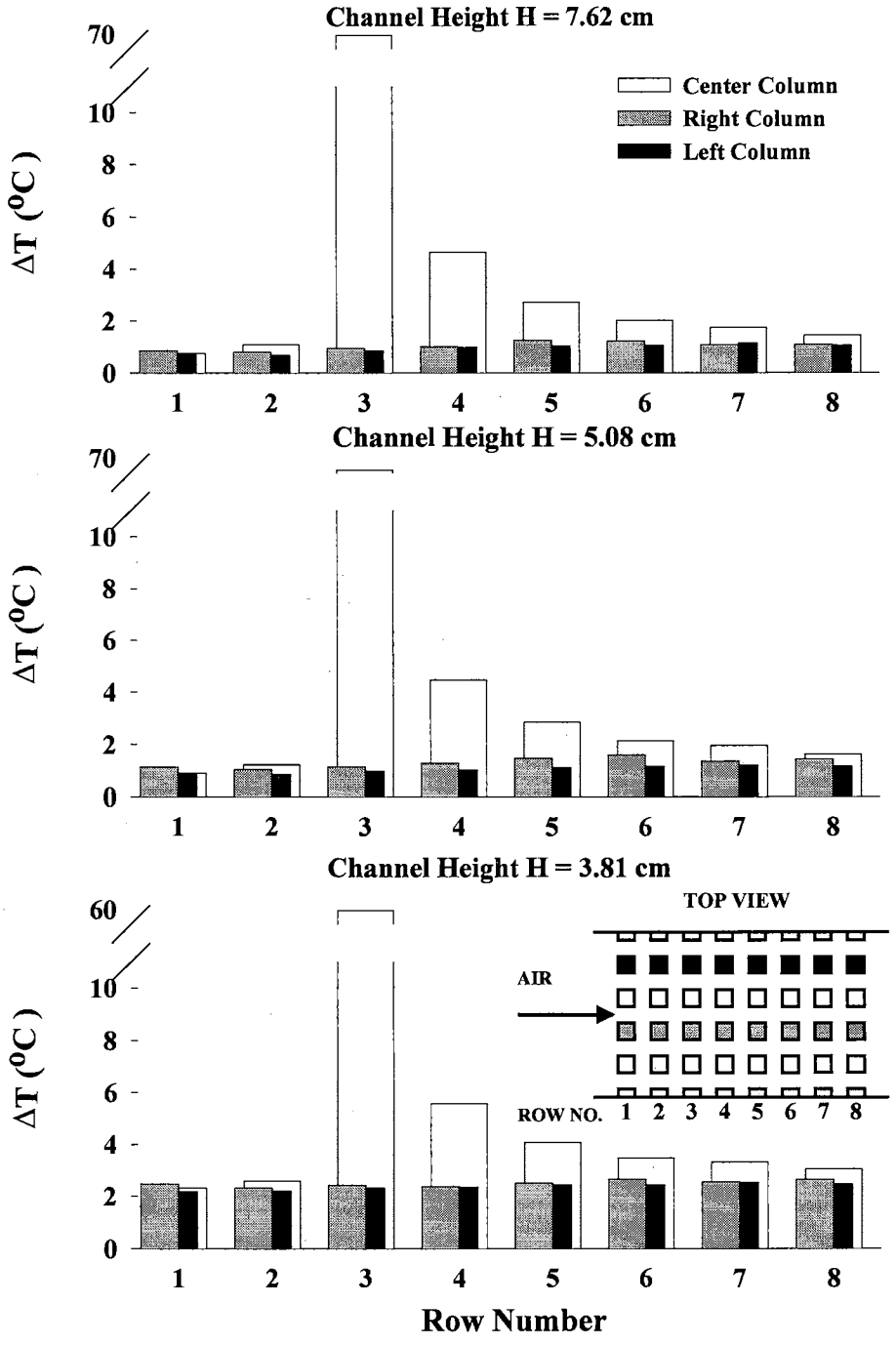

Fig. 3.31 Temperature increases when the third module of the center column was heated with 20 W on the adiabatic board at three channel heights and a fixed channel centerline velocity of 9 m/s.

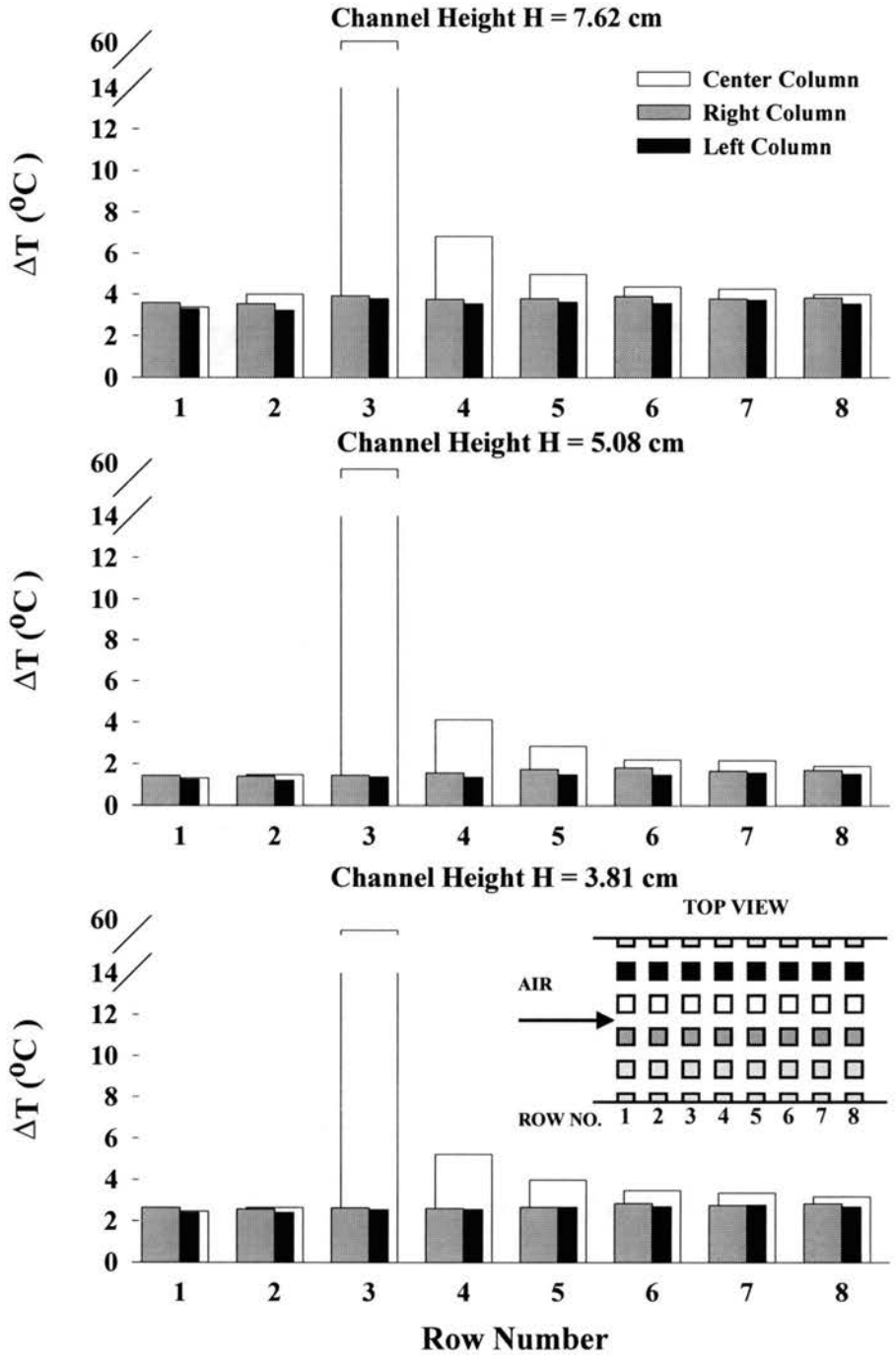

Fig. 3.32 Temperature increases when the third module of the center column was heated with 20 W on the adiabatic board at three channel heights and a fixed channel centerline velocity of 11 m/s.

view schematic, the non-shaded (white) column and the two darker (than the rest) columns of modules in different shades represent all the modules (twenty-four modules) that were monitored during the experiment. The third module of the non-shaded column (center column) was heated at 20W and the temperature measurements were taken for every monitored module after steady state conditions were reached. For the 2 oz conductive test boards, only nine modules (the heat dissipating and neighboring eight modules) were monitored at any experimental run. Consequently, figures similar to Figs. 17 to 32 were not produced for the three 2 oz test boards. However, the adjusted temperature rise ($\Delta T_{adjusted}$) data of the four neighboring modules for 2 oz boards will be presented and discussed later where similar data ($\Delta T_{adjusted}$) of 1 oz and the adiabatic boards are also presented.

On a conductive board, the forced convection was no longer the single dominant player. The conduction would also play a significant role in heat transfer on a conductive board. When a module had twice the energy to dissipate (from 10 to 20 W), it would reach a higher temperature and demonstrate the conduction effect even more clearly. The thermal wake effect alone was not sufficient to describe the heat transfer phenomenon under these conditions. At 7.62 cm channel height and centerline velocity of 5 m/s on the 2.54 cm band conductive board, the temperature rises (ΔTs in Figs. 3.17 to 3.32) of the upstream and lateral modules were at least 2 °C greater than the rest of the modules upstream of the heated module as shown in Fig. 3.17. Three similar trends can be seen in Figs. 3.17 to 3.32 :

1) The differences of the temperature rises decreased with increasing channel

centerline velocity for a uniform copper band width conductive board and a fixed channel height. This is consistent with the data from Biber and Sammakia (1986). Table 3.5 (for 2.54 cm band, V = 5, 7, 9 and 11m/s and channel height H = 7.62 cm) is provided as an example to illustrate the trend for all the temperature rise distribution results presented in Figs. 3.17 to 3.32.

As shown in Table 3.5, for the first row, the differences of temperature rises between three columns were not influenced by the channel centerline velocity. Because of the positions of the three first row modules, the thermal wake did not affect these modules upstream of the heat dissipating module (third module of the center column). Though the conductive substrate (copper foil) of the test board did influence the overall heat transfer process, again, the positions of the three first row modules were too far away from the heat dissipating module to pick up the conduction effect from the copper foil. The second module of the center column was the module upstream of the heat dissipating module and the best indicator of the copper foil conduction effect without the thermal wake effect mixing in. As shown in the table, the module temperature rise (ΔT) of the second module of the center column were consistently higher than the ΔTs of the second modules of the left and right columns. Both modules of the left and right columns were not directly connected to the heat dissipating module by copper bands. Thus, for these two modules, without copper foil conduction and thermal wake effect, the differences of ΔTs between these two modules and the second module of the center column were strictly copper foil conduction effect. This effect (differences of ΔTs of the second row) decreased when the velocity increased. The modules of the left and right columns of the third row (two lateral

TABLE 3.5

The Variation of the Difference of the Temperature Rises with Respect to Centerline Velocity for All the Monitored Modules and the 1 oz, 2.54 cm Band Test Board at a Channel Height of 7.62 cm.

Row Number	ΔT (°C) Center Column	ΔT (°C) Left Column	Difference of ΔT between Center Column	ΔT (°C) Right Column	Difference of ΔT between Center Column
V = **5** m/s, 1 oz, 2.54 cm Band Board, Channel Height H = 7.62 cm					
1	4.61	4.49	**0.1**	4.63	**0.0**
2	6.72	4.63	**2.1**	4.75	**2.0**
3	85.29	6.35	**78.9**	6.75	**78.5**
4	12.03	5.28	**6.8**	5.76	**6.3**
5	7.92	5.14	**2.8**	5.77	**2.2**
6	6.55	5.00	**1.6**	5.57	**1.0**
7	6.35	5.19	**1.2**	5.34	**1.0**
8	5.91	5.05	**0.9**	5.45	**0.5**
V = **7** m/s, 1 oz, 2.54 cm Band Board, Channel Height H = 7.62 cm					
1	6.27	6.17	**0.1**	6.19	**0.1**
2	7.56	6.21	**1.4**	6.28	**1.3**
3	75.08	7.36	**67.7**	7.59	**67.5**
4	11.72	6.69	**5.0**	6.92	**4.8**
5	8.72	6.62	**2.1**	6.99	**1.7**
6	7.58	6.51	**1.1**	6.92	**0.7**
7	7.57	6.72	**0.9**	6.76	**0.8**
8	7.21	6.56	**0.7**	6.87	**0.3**
V = **9** m/s, 1 oz, 2.54 cm Band Board, Channel Height H = 7.62 cm					
1	6.75	6.63	**0.1**	6.76	**0.0**
2	7.68	6.66	**1.0**	6.81	**0.9**
3	67.82	7.45	**60.4**	7.81	**60.0**
4	11.08	7.02	**4.1**	7.36	**3.7**
5	8.71	6.97	**1.7**	7.44	**1.3**
6	7.79	6.88	**0.9**	7.35	**0.4**
7	7.83	7.05	**0.8**	7.17	**0.7**
8	7.51	6.94	**0.6**	7.32	**0.2**
V = **11** m/s, 1 oz, 2.54 cm Band Board, Channel Height H = 7.62 cm					
1	2.63	2.55	**0.1**	2.66	**0.0**
2	3.24	2.56	**0.7**	2.66	**0.6**
3	57.84	3.17	**54.7**	3.48	**54.4**
4	6.10	2.83	**3.3**	3.06	**3.0**
5	4.26	2.85	**1.4**	3.16	**1.1**
6	3.43	2.76	**0.7**	3.02	**0.4**
7	3.53	2.93	**0.6**	2.93	**0.6**
8	3.22	2.85	**0.4**	3.03	**0.2**

modules of the active module) were subjected to the similar conditions of the second module of the center column (upstream of the active module), directly connected to the active module through copper band without the presence of thermal wake effect. Accordingly, the same trend of the copper conduction effect can be seen in the table. For all the monitored modules after the third row, thermal wake effect was present as was the copper foil conduction effect. Both mechanisms influenced the module temperature rise (ΔT) of each monitored module after the third row.

2) The differences of the temperature rises decreased with decreasing channel height for a uniform copper band width conductive board. Table 3.6 (for 2.54 cm band, H = 7.62, 5.08, and 3.81 cm and V = 5 m/s) is provided as an example to illustrate the trend for all the temperature rise distribution results presented in Figs. 3.17 to 3.32.

The conduction effect of the conductive substrate (copper foil) in the printed circuit boards with respect to channel height can be observed in Table 3.6. The trends are very similar to the previous segment because decreasing the channel height has the same effect of increasing the channel centerline velocity. In the study, a decrease in the channel height corresponded to an increase in the modified Reynolds number.

3) The differences of the temperature rises decreased with decreasing copper band width (or A*, the exposed area ratio) for a fixed channel height H. Table 3.7 (for channel height H = 7.62 cm, V = 5 m/s and four test boards) is provided as an example to illustrate the trend for all the temperature rise distribution results presented in Figs. 3.17 to 3.32.

TABLE 3.6

The Variation of the Difference of the Temperature Rises for All the Monitored Modules and the 1 oz, 2.54 cm Band Test Board at Three Different Channel Heights of 7.62, 5.08 and 3.81cm for a Fixed Centerline Velocity of 5 m/s.

Row Number	ΔT (°C) Center Column	ΔT (°C) Left Column	Difference of ΔT between Center Column	ΔT (°C) Right Column	Difference of ΔT between Center Column
Channel Height H = **7.62** cm, 1 oz, 2.54 cm Band Board, V = 5 m/s					
1	4.61	4.49	**0.1**	4.63	**0.0**
2	6.72	4.63	**2.1**	4.75	**2.0**
3	85.29	6.35	**78.9**	6.75	**78.5**
4	12.03	5.28	**6.8**	5.76	**6.3**
5	7.92	5.14	**2.8**	5.77	**2.2**
6	6.55	5.00	**1.6**	5.57	**1.0**
7	6.35	5.19	**1.2**	5.34	**1.0**
8	5.91	5.05	**0.9**	5.45	**0.5**
Channel Height H = **5.08** cm, 1 oz, 2.54 cm Band Board, V = 5 m/s					
1	2.93	2.83	**0.1**	2.96	**0.0**
2	4.66	2.96	**1.7**	3.03	**1.6**
3	75.72	4.26	**71.5**	4.38	**71.3**
4	9.26	3.51	**5.8**	3.76	**5.5**
5	5.92	3.42	**2.5**	3.81	**2.1**
6	4.82	3.32	**1.5**	3.58	**1.2**
7	4.52	3.48	**1.0**	3.61	**0.9**
8	4.13	3.35	**0.8**	3.84	**0.3**
Channel Height H = **3.81** cm, 1 oz, 2.54 cm Band Board, V = 5 m/s					
1	0.80	0.76	**0.0**	0.77	**0.0**
2	2.06	0.78	**1.3**	0.81	**1.3**
3	68.83	1.85	**67.0**	1.79	**67.0**
4	6.39	1.27	**5.1**	1.22	**5.2**
5	3.61	1.28	**2.3**	1.21	**2.4**
6	2.57	1.19	**1.4**	1.21	**1.4**
7	2.43	1.36	**1.1**	1.21	**1.2**
8	2.04	1.23	**0.8**	1.31	**0.7**

The same discussion of the previous segments for the modules of the first two rows can also be applied to Table 3.7. However, for the third row, the trend of the conduction effect (differences of ΔTs between the two lateral modules and the heat dissipating module) was opposite to the second row. The differences of ΔTs for the third row increased when the copper band width (A*) was decreased instead of decreasing. The reason is that the conduction effect of the copper foil for the third row was overcome by the forced convection effect in the two previous segments. The forced convection, as mentioned earlier, was the dominant heat transfer mechanism in the turbulent flow regime ($9100 < Re < 26300$) in the present study. For the two previous discussions, in both cases the modified Reynolds number increased. That is, in the first case the velocity was increased and in the second case the channel height was decreased while keeping the value of the rest of the parameters fixed for comparison purposes. For this case, the velocity was fixed at the lowest value of 5 m/s so the convection effect had the same degree of influence on the four test boards. On the other hand, the conduction effect was changed by decreasing the copper band width (A*). Consequently, the active (heat dissipating) module dispersed less heat to the surroundings and attained a higher temperature. The higher the active module temperature, the larger the difference of ΔT for the two lateral modules of the active module. Again, the module temperature rise (ΔT) of each monitored module after the third row was basically the result of both thermal wake and copper foil conduction effects.

To better demonstrate the conduction effect of the copper foil in the conductive test boards, the temperature rises of the four neighboring modules of the heat dissipating

Table 3.7
The Variation of the Difference of the Temperature Rises for All the Monitored Modules and Three 1 oz and the Adiabatic Test Boards at a Channel Height of 7.62 cm for a Fixed Centerline Velocity of 5 m/s.

Row Number	ΔT (°C) Center Column	ΔT (°C) Left Column	Difference of ΔT between Center Column	ΔT (°C) Right Column	Difference of ΔT between Center Column
1 oz, **2.54** cm Band Board, Channel Height H = 7.62 cm, V = 5 m/s					
1	4.61	4.49	**0.1**	4.63	**0.0**
2	6.72	4.63	**2.1**	4.75	**2.0**
3	85.29	6.35	**78.9**	6.75	**78.5**
4	12.03	5.28	**6.8**	5.76	**6.3**
5	7.92	5.14	**2.8**	5.77	**2.2**
6	6.55	5.00	**1.6**	5.57	**1.0**
7	6.35	5.19	**1.2**	5.34	**1.0**
8	5.91	5.05	**0.9**	5.45	**0.5**
1 oz, **1.27** cm Band Board, Channel Height H = 7.62 cm, V = 5 m/s					
1	3.31	3.21	**0.1**	3.48	**-0.2**
2	4.98	3.20	**1.8**	3.52	**1.5**
3	88.89	4.48	**84.4**	4.71	**84.2**
4	10.47	3.80	**6.7**	4.20	**6.3**
5	6.67	3.81	**2.9**	4.30	**2.4**
6	5.43	3.72	**1.7**	4.29	**1.1**
7	5.04	3.87	**1.2**	4.12	**0.9**
8	4.54	3.68	**0.9**	4.07	**0.5**
1 oz, **0.318** cm Band Board, Channel Height H = 7.62 cm, V = 5 m/s					
1	2.93	2.66	**0.3**	2.86	**0.1**
2	4.13	2.82	**1.3**	2.91	**1.2**
3	97.29	3.18	**94.1**	3.49	**93.8**
4	10.11	3.12	**7.0**	3.73	**6.4**
5	6.42	3.15	**3.3**	3.64	**2.8**
6	5.25	3.24	**2.0**	3.86	**1.4**
7	4.57	3.09	**1.5**	3.62	**1.0**
8	4.32	3.17	**1.2**	3.81	**0.5**
Adiabatic Board, Channel Height H = 7.62 cm, V = 5 m/s					
1	7.98	7.49	**0.5**	8.30	**-0.3**
2	8.77	7.53	**1.2**	8.19	**0.6**
3	102.47	7.88	**94.6**	8.62	**93.9**
4	14.96	7.98	**7.0**	8.70	**6.3**
5	11.47	8.07	**3.4**	9.16	**2.3**
6	10.26	8.11	**2.2**	9.07	**1.2**
7	9.74	8.18	**1.6**	8.91	**0.8**
8	9.37	8.09	**1.3**	8.83	**0.5**

module at the same conditions (the same run, the same T_∞ and Re) were further reduced (adjusted). The adjusted ΔTs were calculated by subtracting the temperature rise of a specific module (first module of the left column) at the same conditions from the temperature rises of the four neighboring modules. The first module of the left column was chosen because it always had the lowest temperature rise within the twenty-four monitored modules. The adjusted ΔT ($\Delta T_{adjusted}$) displayed in Figs. 3.33 to 3.40 can be seen as the comparison of the temperature rise between the neighboring passive modules at the same conditions. However, the original module temperature rise (ΔT in Figs. 3.17 to 3.32) was the comparison of a monitored module itself before and after the active module was heated. The adjusted ΔT data for 1 oz and the adiabatic boards were displayed in Figs. 3.33 to 3.36. Again, for Figs. 3.33 to 3.40, a schematic of the top view of the in-line array of modules on a test board is included in each figure to help demonstrate the experimental data presented. The schematic also shows the copper bands of a typical conductive test board connecting all the modules. Schematic of the adiabatic test board was not included because of the limited space. The only difference between the two types of boards (adiabatic and conductive) is that the conductive boards have conductive paths (copper bands) connecting every module in the array, while the adiabatic board has none. In the top view schematic, the heat dissipating module is shown with no shading (white). The module of interest is shown in the darkest shade in the schematic.

The results are more clear to depict the differences of the module temperature rises between the four neighboring modules of the heat dissipating module. Clear trends

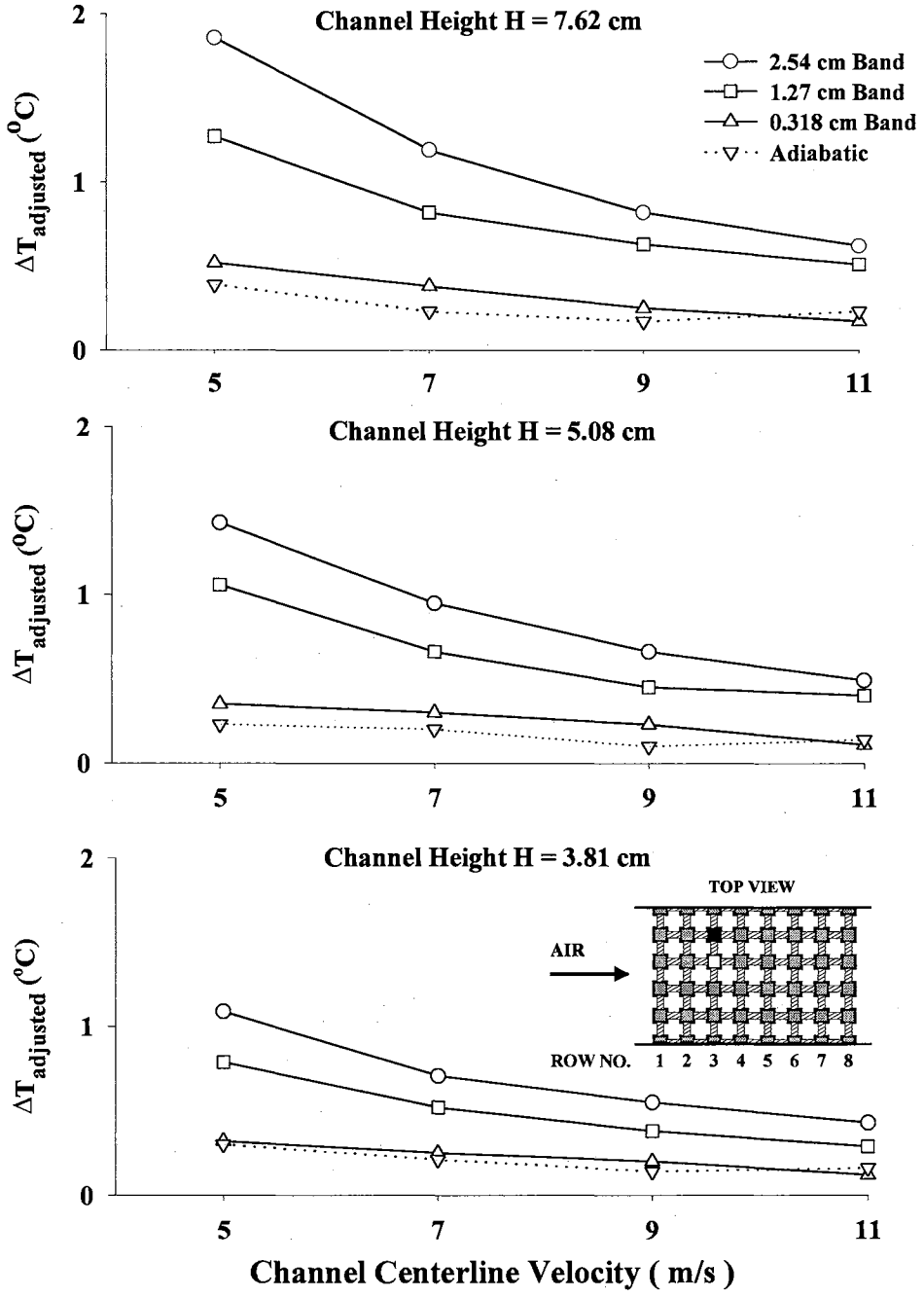

Fig. 3.33 Adjusted ΔT of the module to the left (in the flow direction) of the heat dissipating module when it was heated with 20 W for three 1 oz conductive and the adiabatic test boards.

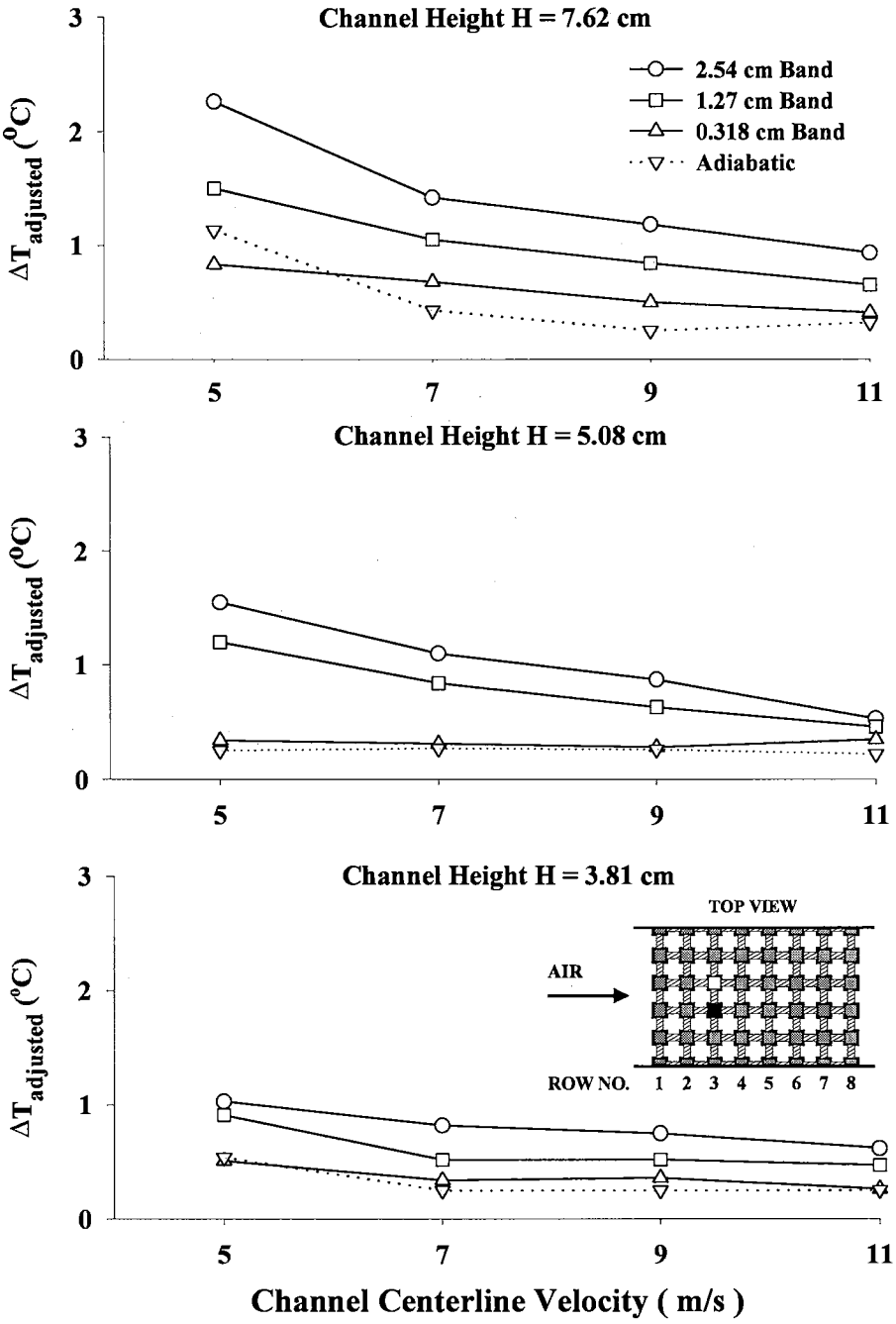

Fig. 3.34 Adjusted ΔT of the module to the right (in the flow direction) of the heat dissipating module when it was heated with 20 W for three 1 oz conductive and the adiabatic test boards.

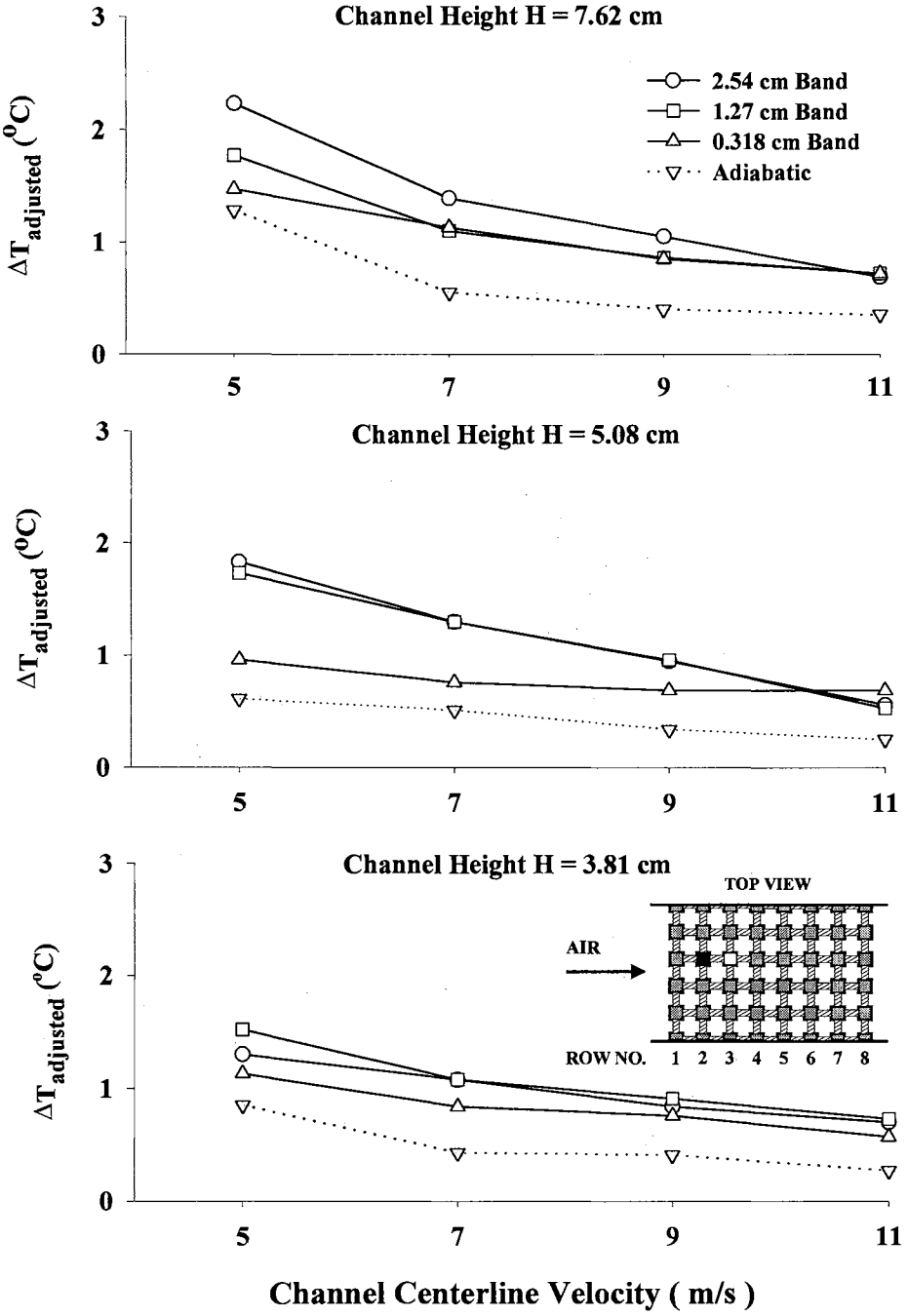

Fig. 3.35 Adjusted ΔT of the module upstream of the heat dissipating module when it was heated with 20 W for three 1 oz conductive and the adiabatic test boards.

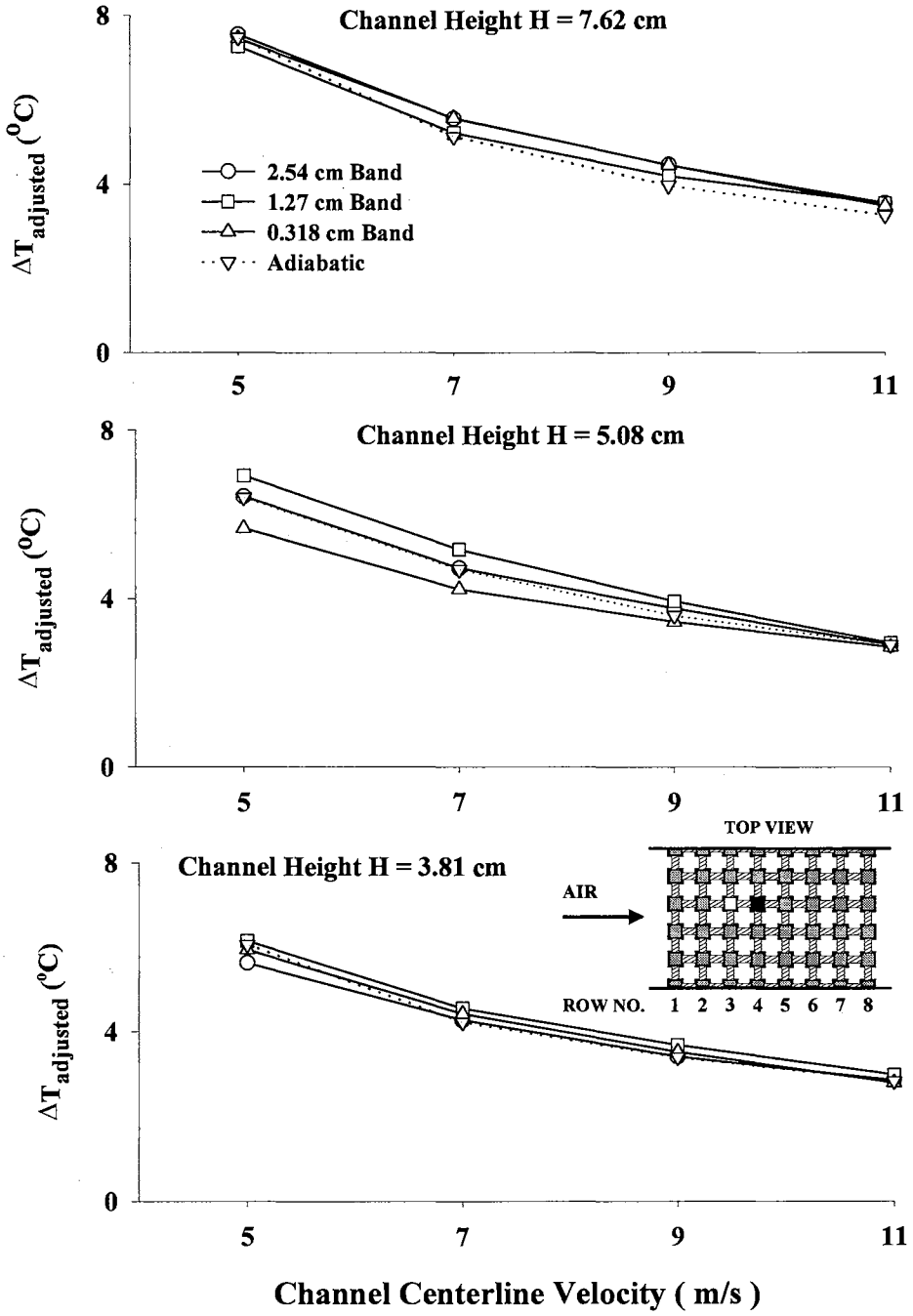

Fig. 3.36 Adjusted ΔT of the module downstream of the heat dissipating module when it was heated with 20 W for three 1 oz conductive and the adiabatic test boards.

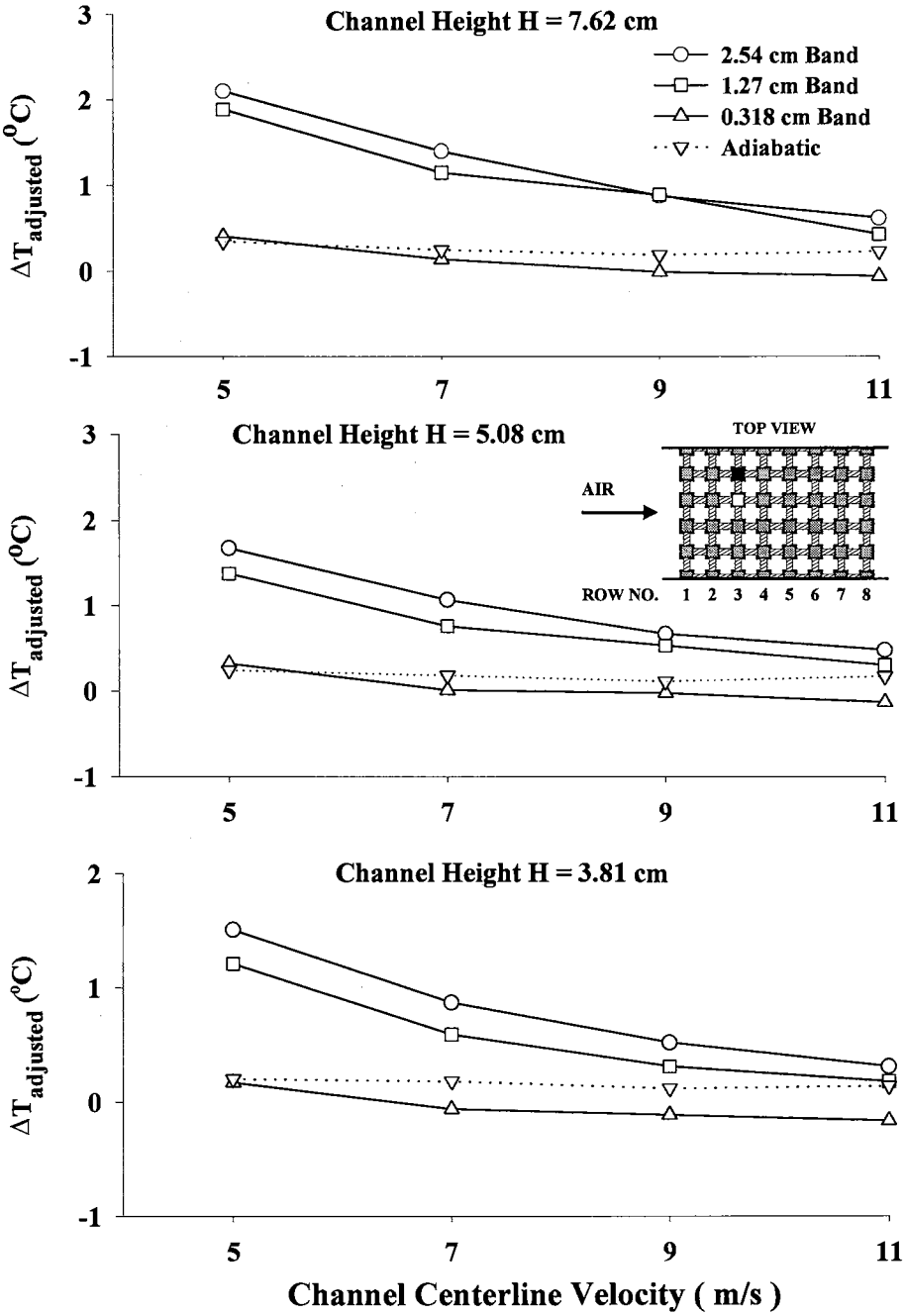

Fig. 3.37 Adjusted ΔT of the module to the left (in the flow direction) of the heat dissipating module when it was heated with 20 W for three 2 oz conductive nd the adiabatic test boards.

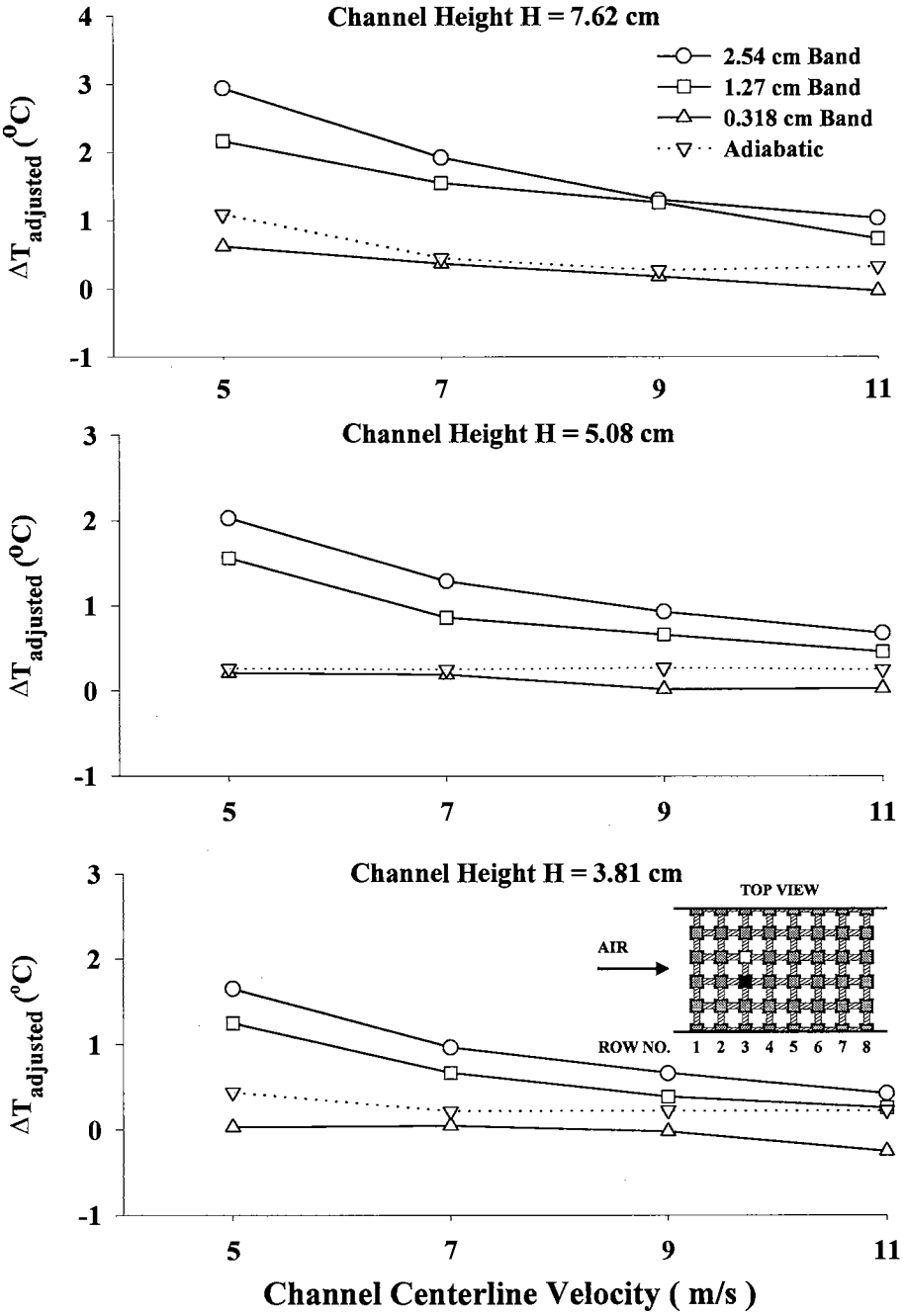

Fig. 3.38 Adjusted ΔT of the module to the right (in the flow direction) of the heat dissipating module when it was heated with 20 W for three conductive 2 oz and the adiabatic test boards.

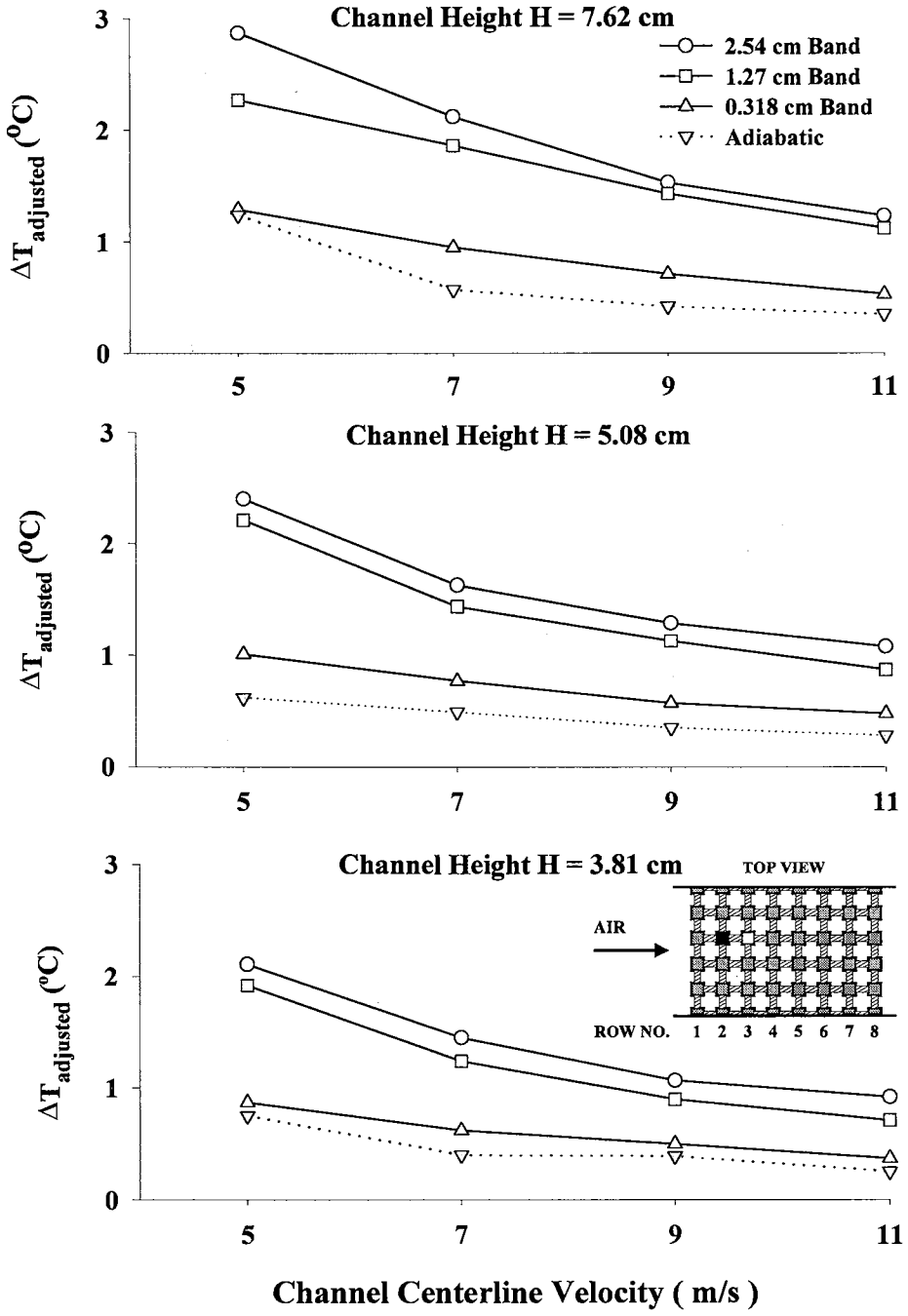

Fig. 3.39 Adjusted ΔT of the module upstream of the heat dissipating module when it was heated with 20 W for three 2 oz conductive and the adiabatic test boards.

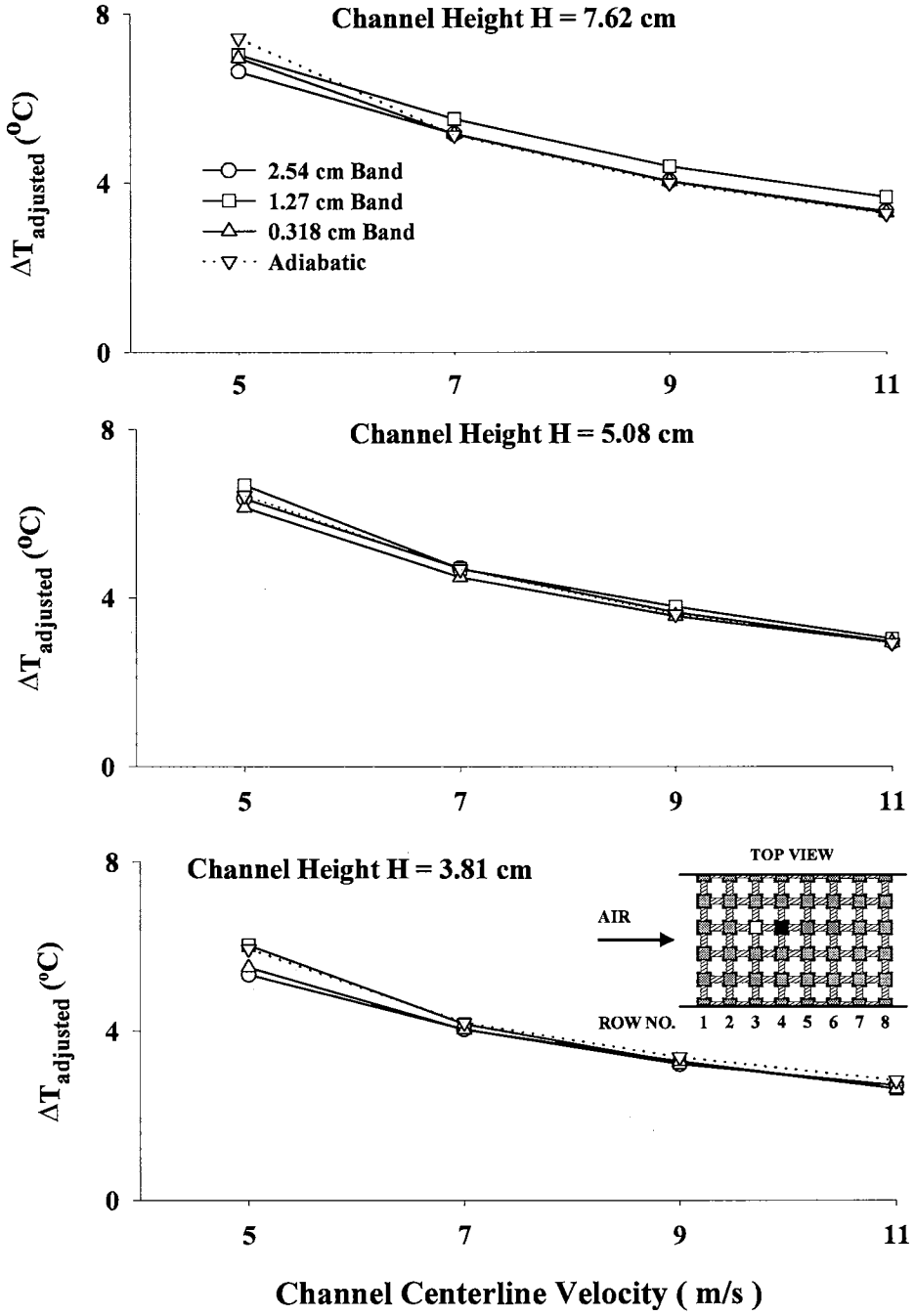

Fig. 3.40 Adjusted ΔT of the module downstream of the heat dissipating module when it was heated with 20 W for three 2 oz conductive and the adiabatic test boards.

of substrate (copper foil) conduction influences on the module temperature rise are shown in Fig. 3.33. The lower the channel centerline velocity, the higher the temperature rise and the greater the exposed copper foil surface area, the higher the temperature rise for module to the left (in the flow direction) of the heat dissipating module. For example, for 1 oz, 2.54cm band test board at channel height of 7.62 cm, the variation of $\Delta T_{adjusted}$ of the module to the left of the heat dissipating module with respect to velocity are tabulated in Table 3.8. Also, the variation of $\Delta T_{adjusted}$ with respect to copper band width (A*) at velocity of 5 m/s for channel height of 7.62 cm are tabulated in Table 3.9.

As demonstrated in Table 3.8, when a module in a regular in-line array is dissipating heat, the higher the cooling air flow velocity, the less the substrate conductivity will help to dissipate the heat. More importantly, as revealed in Table 3.9, the greater the exposed copper surface area (copper tracking), the better the substrate (copper foil) will help to dissipate the heat by distributing the heat to the surroundings.

The heat dissipating module not only dissipated heat through thermal wake to downstream modules but through copper foil conduction to lateral and upstream modules. Since thermal wake influences only the downstream direction, only substrate (copper foil) conduction contributed to the temperature rises of the upstream and two lateral neighboring modules. As Figs. 3.33 to 3.35 illustrate, the trends are clear, substrate conduction affected the temperature rise of the module to the left of the heat dissipating module the same way it affected the module to the right (in the flow direction) and the module upstream of the heat dissipating module. For the module downstream of the heat dissipating module, the behavior of the adjusted temperature rises ($\Delta T_{adjusted}$) were not

Table 3.8

$\Delta T_{adjusted}$ Variation with Respect to Velocity of the Module to the Left of the Heat Dissipating Module for the 1 oz, 2.54 cm Band Test Board at a Channel Height of 7.62 cm.

Module to the **left** of the heat dissipating module **1 oz**, 2.54 cm Band Board, Channel Height H = 7.62 cm		
Channel Centerline Velocity (m/s)	$\Delta T_{adjusted}$ (^oC)	% change from 5 m/s
5	1.86	0
7	1.19	-36 %
9	0.82	-56 %
11	0.62	-67 %

Table 3.9

$\Delta T_{adjusted}$ Variation of the Module to the Left of the Heat Dissipating Module for Three 1 oz and the Adiabatic Test Boards at a Channel Height of 7.62 cm.

Module to the **left** of the heat dissipating module Channel Height H = 7.62 cm		
Copper Band Width (cm)	$\Delta T_{adjusted}$ (^oC)	% change from the Adiabatic Board
0 (Adiabatic)	0.39	0
0.318	0.52	33 %
1.27	1.27	226 %
2.54	1.86	377 %

consistent with respect to the copper foil band width but consistent with respect to the channel centerline velocity which always showed a downward trend with increasing channel centerline velocity. In Fig. 3.36 the $\Delta T_{adjusted}$ data of the downstream module on all test boards clustered together at all three channel heights. For the three passive modules in Figs. 3.33 to 3.35, the thermal wake effect was virtually absent and the conduction effect of the copper foil dominated the heat transfer process. Thus, in Figs. 3.33 to 3.35 (module to the left, right and upstream module) the adiabatic board without any copper foil always had the lowest $\Delta T_{adjusted}$. On the contrary, for the downstream module in Fig. 3.36, the thermal wake had the dominant influence on all test boards. In other words, the heat transfer from the heat dissipating module to the module directly behind it on all six conductive test boards was almost the same with the adiabatic test board. Thermal wake effect on the downstream module of the heat dissipating module can be easily deduced from the comparison between Figs. 3.33 and 3.36.

Similar $\Delta T_{adjusted}$ data for 2 oz and the adiabatic boards were shown in Figs 3.37 to 3.40. The same trends displayed in Figs. 3.33 to 3.36 can be observed in Figs. 3.37 to 3.40. Thus, the same discussion above can also be applied to 2 oz conductive test boards. Due to the fact that only nine modules were monitored for the experiments on the 2 oz conductive test boards, a different module had to be used as the reference to generate the $\Delta T_{adjusted}$ data for 2 oz boards. Instead of using first module of the left column which was not monitored for the 2 oz boards, the second module of the left column was used as the reference. The new reference module (closer to the active module) picking up some heat indirectly (by copper foil conduction) from the active module and compounded with the

deviation from the old reference module produced higher reference ΔTs for the 2 oz test boards. Higher reference ΔTs generated lower $\Delta T_{adjusted}$ data values because the reference ΔT was subtracted from the temperature rise of each neighboring module. This was probably the reason for 2 oz, 0.318 cm band test board to have some $\Delta T_{adjusted}$ data values lower than the adiabatic test board in Figs. 3.37 and 3.38.

The temperature rise ($\Delta T_{adjusted}$) can be seen as an indicator of the conduction effect of the copper foil. Higher ΔTs of neighboring modules were the result of a better conduction heat spread from the heat dissipating module. Consequently, the active module maintained a lower steady state operating temperature. Some examples of steady state operating temperature are given in Table 3.10 at a fixed channel height and channel centerline velocity for all seven test boards.

TABLE 3.10
Steady State Operating Temperature of the Heat Dissipating Module with 20 Watts of Input Power on All Seven Test Boards at a Fixed Channel Height and Channel Centerline Velocity.

Channel Height H = 7.62 cm, V = 5 m/s		
Copper Foil Thickness (oz)	Copper Foil Band Width (cm)	Steady State Operating Temperature of the Heat Dissipating Module (20 W) (^{o}C)
0 (Aiabatic)	0	123.3
1	0.318	118.2
1	1.27	109.8
1	2.54	106.2
2	0.318	111.9
2	1.27	108.2
2	2.54	97.7

3.6 Heat Transfer Correlations

All the Nusselt numbers calculated from the experimental data for the seven modules of the center column at every experimental run were plotted versus the modified Reynolds numbers in Fig. 3.41. The three channel heights (3.81, 5.08 and 7.62 cm) used in the present study gave three different cross sectional areas of the rectangular channel. Therefore, the modified Reynolds number was defined to take the change of the cross sectional area of the rectangular channel into account. Two correlations will be presented in this section. These correlations do not represent an attempt to provide empirical correlations for practical applications but rather to (1) identify the important parameters in the present study, (2) capture the characteristics of these parameters and the interactions between them, and (3) demonstrate the collective influences of these parameters on the Nusselt number. The first correlation is proposed for the data of this present study for the modified Reynolds numbers between 9100 to 26300 :

$$Nu = (0.330 + 0.229\,A^{*}T^{*} + 0.0029\left(\frac{x}{D_h}\right)^{-1.451}) Re^{0.575} \qquad (3.5)$$

where

$$0.0852 \le A^{*} \le 0.682$$

$$0.25 \le T^{*} \le 0.50$$

$$0.11 \le \frac{x}{D_h} \le 5.18$$

$$9100 \le Re \le 26300$$

where x is the stream-wise distance from the center of a module to the beginning of the in-line array and D_h is the hydraulic diameter of the rectangular channel at a specific

channel height.

The correlation represented the experimental data to within +21.2% and -17.5% and had an average absolute deviation of 5.4%. Ninety-seven percent of the experimental data (573 data points) were predicted with better than ±15% deviation (86% within ±10%).

To improve the correlation, one more term was introduced into equation (3.5) to reflect the effect of channel height on the convection heat transfer coefficient. The parameter is a non-dimensional number represented by the channel height (H) divided by the characteristic length of the present study, the module height (t). The second correlation for all the heated modules for Reynolds numbers between 9100 to 26300 is:

$$Nu = (0.593 + 0.410\,A^{*}T^{*} + 0.0035\left(\frac{x}{D_h}\right)^{-1.697})\left(\frac{H}{t}\right)^{-0.140} Re^{0.526} \qquad (3.6)$$

where

$$0.0852 \le A^{*} \le 0.682$$

$$0.25 \le T^{*} \le 0.50$$

$$0.11 \le \frac{x}{D_h} \le 5.18$$

$$1.5 \le \frac{H}{t} \le 3.0$$

$$9100 \le Re \le 26300$$

The correlation represented the experimental data to within +19.2% and -14.1% and had an average absolute deviation of 4.5%. Ninety-nine percent of the experimental data (584 data points) were predicted with better than ±15% deviation (90% within ±10%).

The two correlations are presented graphically in Fig. 3.42. It is noticeable in Fig. 3.42 that the difference between the two correlations is substantial. As shown in the figure, before the term (H/t) was added, the correlation predicted data points scattered over a much wider range. On the contrary, after the term (H/t) was added, the spread of the predicted data points was narrower and the predicted data points fell upon each other more instead of side by side. It looks as if that after the term (H/t) was added, the number of the predicted data points were reduced.

Referring to the two correlations, there are two trends can be concluded.

1. After introducing the term (H/t) into equation (3.5), the results of both correlations improved at least by 17% in the average absolute deviation. This suggested that channel height is one of the important geometric parameters in the present study.
2. Under adiabatic, forced convection conditions, the correlations from previous research were of the general form of $Nu = C_1 Re^{C_2}$. For this present study , the ratios of the coefficients of the term A*T* to the leading constant coefficients in the two correlations are (0.229/0.330) and (0.410/0.593) respectively. These ratios are consistently all about 70%. Although the coefficient of A*T* was depended on how the A* and T* were defined, the trend shown in the correlations should not be disregarded. This trend indicated that exposed copper foil area and thickness of copper foil are other, if not, the most significant parameters in the conjugate heat transfer process.

In summary, these correlations indicated that the modified Reynolds number is a good hydrodynamic characteristic descriptor of the channel cooling air flow, for at least

86% of the experimental data points of the present study were predicted within ±10% deviation by either correlation. Still, the term (H/t) was needed to further improve the prediction of equation (3.5). As discussed previously, this illustrated that channel height is another essential parameter. Similarly, from the previous discussion, the exposed copper foil surface area ratio (A*) and the copper foil thickness ratio (T*) are yet two other important parameters. For the two correlations, equations (3.5) and (3.6), the term (x/D_h) was not a substantial factor in either correlation, except for the first two rows. For after the second row, the x/D_h values became greater than unity and would be greater for even larger row numbers, and with an exponent of -1.451 (equation. 3.5) or -1.697 (equation 3.6), the influence of the x/D_h term would be quickly diminishing.

The modified Reynolds number (Re) proposed in the present study is one of the dominant parameters for the conjugate heat transfer process in turbulent flow regime. The modified Reynolds number complemented by the non-dimensional channel height (H/t) would do an even better job of predicting the Nusselt number. The exposed copper surface area ratio (A*) and the copper thickness ratio (T*) of the test boards as discussed in the previous section were closely associated with each other. The term A*T* can be seen as one of the most influential parameters in the conjugate heat transfer process even when compared with the modified Reynolds number.

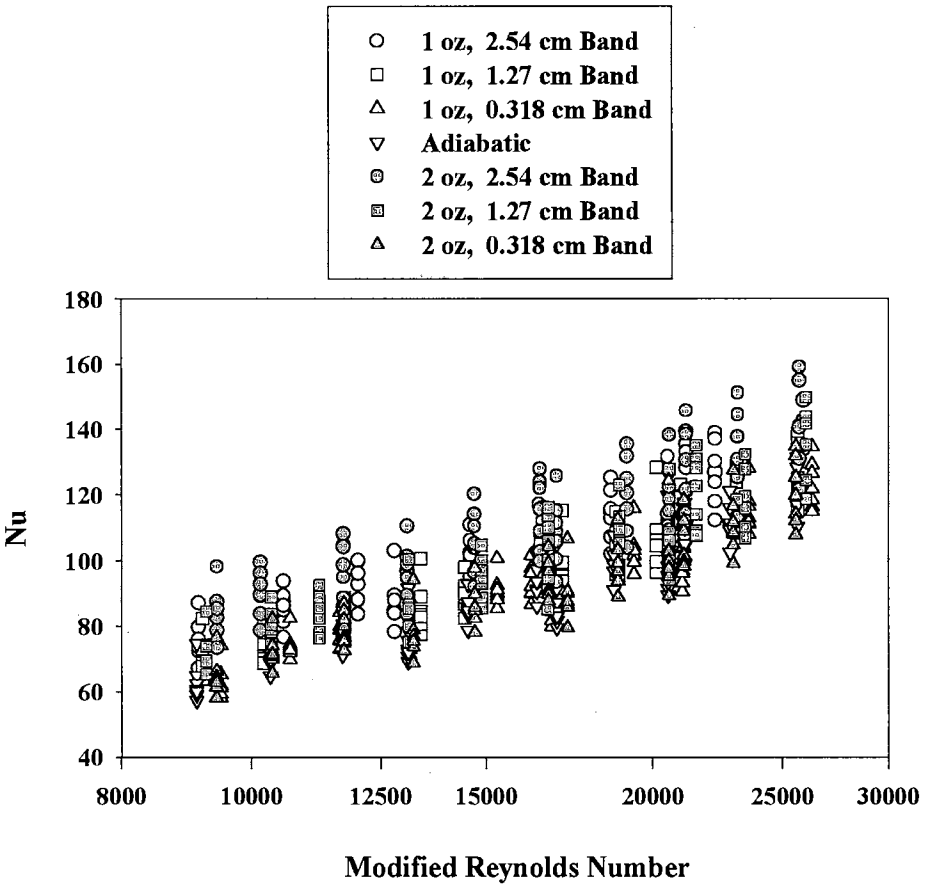

Fig. 3.41 Nusselt numbers of all seven test boards versus modified Reynolds number.

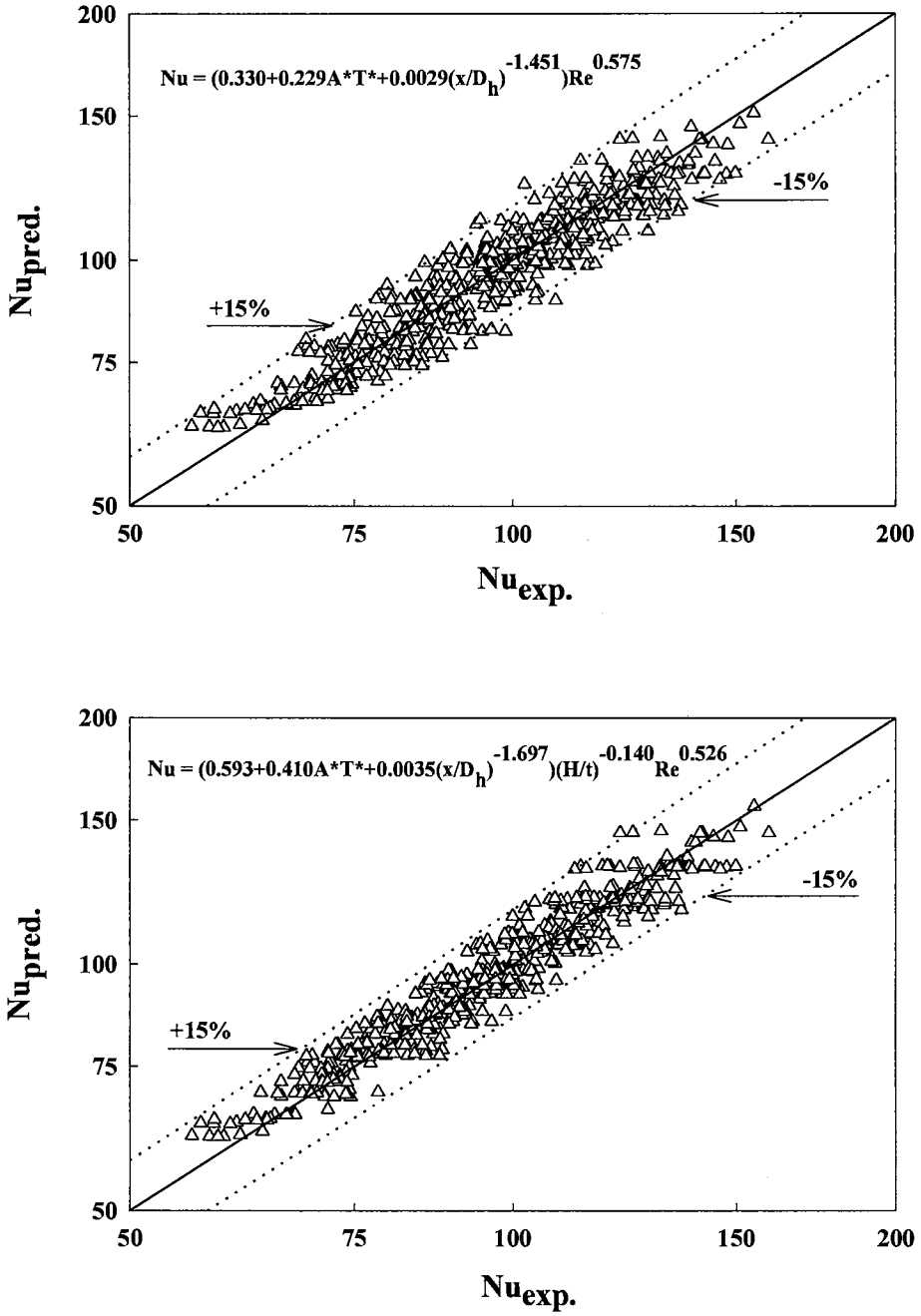

Fig. 3.42 Nusselt numbers predicted by two different correlations versus Nusselt numbers calculated from experimental data.

CHAPTER IV

SUMMARY, CONCLUSIONS AND RECOMMENDATIONS

4.1 Summary

As discussed in Chapter I, experimental study of the conduction effects of the conductive substrate which is a layer (or several layers) of copper foil serves as the electric power distribution plane in printed circuit boards is relatively scarce in the literature. This experimental study was designed to fill in the void of the quantitative experimental study on the conduction effects of the copper foil in PCBs. The present research was concerned with a single heat dissipating cubic module in an in-line array of the same kind of modules on conductive test boards. It was configured to idealize a single air-cooled one-sided printed circuit board with heat dissipating electronic components as found in today's computers or many electronic devices. Experiments were carried out in a horizontal rectangular wind tunnel on seven test boards (six conductive and one adiabatic) for three channel heights (7.62, 5.08 and 3.81 cm) at four channel centerline velocities (5, 7, 9 and 11 m/s). The experiments were performed by heating one single module at a time and then the temperature measurements were taken for that specific module. For seven modules in a specific column of eight modules, the measurements were taken for each of the seven test boards at a fixed velocity and channel height. Each of the seven modules was heated with a power level of 10 Watts one at a time. Only the

third module of the center column was also heated with a power level of 20 Watts to generate the temperature rise data. When the third module was heated with 20W of input power, the temperatures of either the twenty-four modules of three columns (including the third module itself) or the eight surrounding modules and the heat dissipating module were monitored, and recorded when a steady state condition was reached.

Real printed circuit board blanks were etched with the same pattern but different connecting band widths to generate different copper foil (copper tracking) covered surface areas for six conductive test boards. A "bare" printed circuit board (without any copper foil on it) was used as the adiabatic test board for comparison purposes. An approach was devised to systematically and quantitatively investigate the conduction effects of the copper foil in the printed circuit boards which has not been focused on in previous research. Beginning with a serious search for an appropriate way to consummate the task, conductive test boards made of real copper clad circuit board blanks etched with the designed pattern were used in the experiments. This is believed to be the first time that this approach was used to specifically study the effects of copper foil conduction in PCBs quantitatively. Real pre-cut copper clad circuit boards (25.4 × 38.1 cm) were exposed with an ultra violet fluorescent light source, developed in a heated solution, and then etched in the Ferric Chloride etchant with constant agitation to produce the conductive test boards with designed copper foil pattern on them. Three connecting copper foil band widths were designed to reflect the copper foil distributions on the printed circuit boards found in real applications. They were separated copper foils of 2.54 cm squares connected by different widths (2.54, 1.27 and 0.318 cm) and the same length

(2.54 cm) of copper foil bands both in stream-wise and span-wise directions. Two sets of conductive test boards with two thicknesses (1 and 2 oz FR-4 Epoxy Glass) and exactly the same copper foil pattern with three different connecting band widths were used in the study. The convection heat transfer coefficient and temperature distribution information of this conjugate heat transfer process was obtained by performing more than ninety-six experimental runs (750 lab hours).

An arduous experimental investigation has been carried out to fulfill the objectives laid out in Chapter I. Specific measures were taken to achieve each objective of the study as listed below:

1) One of the most important objectives of the present study was to investigate the effects of the exposed (to the cooling air flow) surface area of the conductive substrate (copper foil) on this combined modes of heat transfer. The previously mentioned technique of etching the designed pattern on the conductive test boards was put together specifically to accomplish this objective in the present study. The Nusselt numbers calculated from the experimental measurements at four velocities and three channel heights for all seven test boards were further reduced by normalizing the Nusselt numbers of the six conductive test boards with the Nusselt numbers of the adiabatic test board. The normalized Nusselt numbers (of seven modules, rows 1 to 7) of each conductive test board with different exposed copper foil surface area ratio (A*) were then analyzed to study the influence of the exposed copper foil surface area in the conductive test boards on the conjugate heat transfer process.

2) The investigation of the influence of the thickness of the conductive substrate (copper foil) on this combined modes of heat transfer was conducted by running the same experiments on two sets (two copper foil thicknesses) of conductive test boards. Each set of the conductive test boards consisted of exactly the same copper foil distribution pattern with three different connecting band widths (three A*s). The results of these two sets of conductive test boards were then studied by comparing them with the results of the adiabatic test board and each other.

3) The heat transfer coefficients of the module when heated with 20 Watts were also compared with the coefficients of the same module when heated with 10 Watts under the same conditions (the same channel height and channel centerline velocity on the same test board) for each of the seven test boards at four velocities and three channel heights. This was done to study the effect of the variation of the input power on the heat transfer process.

4) The conduction effects of the copper foil in the test boards were also shown by collecting data on a specified module heated with 20 Watts of input power. The temperatures of twenty-four modules were monitored at the same time and recorded when steady state conditions were reached at four velocities and three channel heights for three 1 oz conductive and the adiabatic test boards. Only nine (eight neighboring and the heat dissipating) modules were monitored for three 2 oz conductive test boards. The temperature measurements were then reduced and analyzed to demonstrate the heat spread through the conduction of the copper foil from the heat dissipating module to

the neighboring modules (upstream, downstream, and two lateral modules of the heat dissipating module) and the surroundings.

5) The present experimental study was also dedicated to the accumulation of a useful and reliable database for future research. Additional measurements and experiments were conducted in order to ensure the data of the present study can be used as a database for Computational Fluid Dynamic and Heat Transfer problems. The consistency (repeatability) of the experimental data was checked and satisfactory results were found by repeating the same experiments on the 1 oz, 2.54 cm band width conductive test board for three channel heights at four centerline velocities. The same confirmation was obtained for both the channel centerline velocity measurements and the module temperature measurements which were also routinely checked.

6) Two correlations (one with the non-dimensional channel height H/t parameter, the other without) were developed. These correlations were developed to recognize the important parameters of this conjugate heat transfer process, capture the characteristics of these parameters and their influences on Nusselt number of a heat dissipating module.

The next section is devoted to the conclusions reached by this experimental investigation.

4.2 Conclusions

The most important conclusions of the present study are summarized as follows:

1) The substrate (copper foil) conduction in the real printed circuit boards can notably affect the conjugate heat transfer process which clearly should not be neglected.

Specific conclusions that can be made regarding the substrate conduction effect are:

- The copper foil bands connecting the heat dissipating module to the surrounding modules played a significant role as the "extended" module surfaces were exposed to the cooling air flow. Thus, the copper foil bands improved the overall convection heat transfer yielding a higher convection heat transfer coefficient of the heat dissipating module. The wider the band width (the greater the exposed copper foil surface ratio, A*), the greater the improvement on the convection heat transfer coefficient.
- The copper foil bands of an active module aid in distributing the heat from the heat dissipating module to the lower temperature neighboring passive modules. Consequently, lower steady state operating temperatures were recorded. As a result of wider band widths, the temperature rises of passive neighboring modules also increased considerably. For the adiabatic test board, this effect was absent, thus the highest steady state operating temperatures were recorded.
- Increase of the copper foil thickness enhances the heat transfer on an real printed circuit board. However, the enhancement was closely associated with the width of the copper foil bands connecting the modules in term of the heat transfer coefficient. The wider the band width, the greater the enhancement because of a thicker copper foil.

2) The modified Reynolds number was one of the most dominant parameters in the present study. The flow regimes of all the experiments of this present study were

turbulent (Re = 9100 to 26300). Accordingly, the Reynolds number governed the conjugate heat transfer process under forced convection mode. The following conclusions were revealed by the experimental results considering the modified Reynolds number:

- The higher the modified Reynolds number, the higher the convection heat transfer coefficient of a heat dissipating module. A higher modified Reynolds number was the result of a higher channel centerline air velocity, or a lower channel height, or the combination of both which was a higher velocity at a lower channel height.
- In contrast, the higher the modified Reynolds number, the less significant the conduction effect of the substrate (copper foil) in printed circuit boards. The lower the modified Reynolds number, the more significant the conduction effect of the substrate (copper foil) in printed circuit boards.

3) The most influential parameters in the conjugate heat transfer process were the modified Reynolds number (Re) proposed in this study which took into account the change of cross sectional area associated with different channel heights, the exposed copper surface area ratio (A*), the copper foil thickness ratio (T*), and the non-dimensional channel height (H/t). The thickness of the copper foil (T* in the study) as mentioned earlier could play a significant role in this conjugate heat transfer process but was closely associated with the width of the copper band width (the same thing as A* in the study). As the copper band width decreased, the influence of copper foil thickness diminished.

4) The convection heat transfer coefficient was independent of input power variation in this conjugate heat transfer process under the configuration of the present study.
5) The effects of the conductive substrate (both exposed surface area and thickness of the copper foil) in the printed circuit boards diminish with increasing channel centerline velocity.

Through all the efforts and conclusions reported above, the overall objective of the present experimental study was to help to formulate a more complete understanding of the conjugate heat transfer in electronic equipment. Consequently, this experimental study has contributed to our understanding of some of the issues in electronic cooling technology. Specifically, the achievements of the present study are highlighted as follows:

1) In the present study, the etching technique was employed to make different exposed copper foil surface area ratio (A*) conductive test boards out of real copper clad circuit board blanks. The combination of etching technique and using real circuit board blanks enables the researchers to control all the parameters that influence the conduction effects of the copper foil in printed circuit boards by designing all kinds of patterns of the copper foil distribution (copper tracking). Thus, systematic and quantitative studies of the conductive characteristics of real printed circuit boards can be pursued. Also, using the standard real circuit board blanks in electronic cooling research can eliminate the waste of time of searching for the right materials and fabrication method to produce the test boards for different researches. Consequently, the consistency of the test boards used in electronic cooling research will increase the scope for comparing results from different researches.

2) The quantitative heat transfer results of the different exposed copper foil surface area in the conductive test boards reported by the present study is the first set of data of such kind. As discussed previously, the results can serve as a benchmark database for future numerical works. For future experimental works, they can serve as a foundation for the future studies of copper foil conductive characteristics in PCBs to be built upon.

3) The correlations developed by the present study identified four essential parameters (A*, T*, Re and H/t) of the conjugate heat transfer process under the configuration of the present study. New parameters proposed by the present study showed promising results in the correlations (90% of data points were predicted within 10% deviation when H/t were included in the correlations). These four parameters can be incorporated into the work of future researchers for further development of more complicated practical correlations for electronic cooling applications. They can also be used as references to future researchers for waiving these proven parameters and concentrating their efforts on identifying new influential parameters in this kind of conjugate heat transfer process.

4.3 Recommendations

There are many parameters involved in the heat transfer process of an array of electronic components mounted on an real printed circuit board cooled by passing air. The main theme of the present study was to understand the conduction effects of copper foil in PCBs. In the study, the etching technique was applied to the standard printed circuit board blanks to accomplish the task.. Combining all kinds of copper foil

distribution patterns that can be generated by etching technique with other parameters involved, there can be plenty of opportunities to improve the understanding of this conjugate heat transfer on real printed circuit boards used in electronics. Those parameters like the dimensions and shape of the module, the orientation of the test board and the location and number of heat dissipating modules... etc. The following are recommendations for future work in this area:

1) Apply the etching technique to industry standard PCB blanks to prepare the test boards in electronic cooling research.
2) Examine the effects of different copper foil distribution patterns. The following are further categorized details:
    i) Different uniform array spacing (2.54 cm was investigated by the study).
    ii) Non-uniform array spacing.
    iii) Multiple copper bands connecting neighboring modules (a single band connecting neighboring modules was used in the study). Mainly, this is to examine whether the influences of four 0.64 cm bands, two 1.27 cm bands and a single 2.54 cm band are the same, for example.
    iv) Different orientations of the connecting copper bands (straight bands either perpendicular or parallel to the cooling air flow was used in the study). Inclined bands instead of straight bands can be used or diagonal bands can be used to connect four diagonal neighboring modules (of the heat dissipating module), for example.
3) Examine the effects of different arrangements of the array of modules (in-line array was used in the study). Staggering array can be used or the orientation of each module

in the array can be changed, for example.

4) Examine the effects of different orientations of the test boards (the test boards was perpendicular to the gravitational force). The test boards can be arranged to be parallel to the gravitational force , for example. In that case, the approaching velocity of the cooling air and the backside conduction heat loss of the test board are two of the most important parameters to be studied.

5) Examine the effects of the contact resistance between the bottom surface of a heated module and the copper foil surface underneath. Several related parameters can be investigated:

    i) Different method of mounting a module to the test board (hollow nylon bolt and nut were used in the study), like soldering the module to the test board.

    ii) Different pressure applied to the contact surface between the module and copper foil, if this is applicable to the mounting method.

6) Examine the effects of geometric parameters of the test module (cubic module was used in the study). Different heights of modules or different shapes of modules can be studied, for example.

7) Examine the effects of multiple active (heat dissipating) modules in the array (a single module was active in the study).

8) Run the experiments with more channel height values (7.62, 5.08 and 3.81 cm were used in the study). The channel height was found to be an important parameter in the study. Expanding the data base with more channel height values will help to develop a more accurate model which can predict the effects of channel height variation. For multiple test boards experiments, the channel height becomes the spacing between

two test boards.

9) Run experiments to measure the pressure drop across a module, local velocity, and provide flow visualization results. Understanding of the fluid dynamics of an array of modules on a conductive boards is another essential factor beside heat transfer measurements to fully comprehend this conjugate heat transfer process.

10) Conduct numerical simulations to predict this conjugate heat transfer process on real printed circuit boards (a fiberglass board with conductive copper foil). Experimental and numerical works are complementary to each other.

REFERENCES

Arabzadeh, M. (1993), "Experimental Study of Geometric Effects and Conduction Loss on Forced Air-Cooling of Regular In-Array of Electronic Components," Ph.D. Thesis, Oklahoma State University, Stillwater, Oklahoma.

Arabzadeh, M., Ogden, E.L. and Ghajar, A.J (1993). "Conduction Heat Transfer Measurements for an Array of Surface Mounted Heated Components," Enhanced Cooling Techniques for Electronics Applications, ASME HTD-Vol. 263, pp. 69-78.

Arvizu, D.E. and Moffat, R.J. (1981), "Experimental Heat Transfer from an Array of Heated Cubical Elements on an Adiabatic Channel Wall," Rept. No. HMT-33, Thermosciences Division, Department of Mechanical Engineering, Standford University, Standford, CA.

Arvizu, D.E. and Moffat, R.J. (1982), "The Use of Superposition in Calculating Cooling Requirements for Circuit Board Mounted Electronic Components," Proceedings of the 32nd Electronic Components Conference, San Diego, CA, pp. 133-144.

Azar, K. and Moffat, R.J. (1991), "Heat Transfer Coefficient and Its Estimation in Electronic Enclosures," Proceedings of the 1991 National Electronics Packaging and Production Conference (East), Boston, MA.

Biber, C.R. and Sammakia, B.G. (1986), "Transport from Discrete Heated Components in a Turbulent Channel Flow," ASME Preprint 86-WA/HT-68.

Chang, M.J., Shyu, R.J. and Fang, L.J. (1987), "An Experimental Study of Heat Transfer From Surface Mounted Components to a Channel Airflow," ASME Preprint 87/HT-75.

Chung, J., (1987), "Maximizing Heat Transfer from PCBs," Machine Design, pp. 87-92.

Copeland, D.W. (1988), "Effects of Channel Height and Planar Spacing on Air Cooling of Electronic Components," Proceeding of the 8th Annual International Electronics Packaging Society, Baltimore, MD, pp. 321-328.

Davalath, J. and Bayazitoglu (1987), Y., "Forced Convection Cooling Across Rectangular Blocks," Journal of Heat Transfer, Vol. 109, pp. 321-328.

Faghri, M., Lessmann, R.C., Sridhar, S., Schmidt, R., and Asako, Y. (1989), "A Preliminary Experimental Study of Forced Air-Cooling of Rectangular Blocks Encountered in Electronic Equipment," Collected Papers in Heat Transfer, ASME HTD-Vol. 123, pp. 1-6.

Graham, K. and Witzman, S. (1988), "Analytical Correlation of Thermal Design of Electronic Packages," Cooling Technology for Electronic Equipment, W. Aung, editor, Hemisphere Publishing Corporation, New York, pp. 249-264.

Incropera, F.P. and DeWitt, D.P. (1990), Introduction to Heat Transfer, Second Edition, John Wiley & Sons, Inc.

Kline, S.J. and McClintock, F.A. (1953), "Describing Uncertainties in Single-Sample Experiments," Mechanical Engineering, pp. 3-8.

Kraus, A.D. and Bar-Cohen (1983), A., Thermal Analysis and Control of Electronic Equipment, Hemisphere Publishing Corporation, New York.

Lehmann, G.L. and Wirtz, R.A. (1985), "The Effect of Variation in Stream-Wise Spacing and Length on Convection From Surface Mounted Rectangular Components," Heat Transfer in Electronic Equipment, ASME HTD-Vol. 48, pp. 39-48.

Lohan, J.M. and Davies, M.R.D. (1996), "Thermal Interaction Between Electronic Components," Heat Transfer in Electronic Equipment ASME HTD-Vol. 329, pp. 73-82.

Moffat, R.J., Arvizu, D.E. and Ortega, A. (1985), "Cooling Electronic Components: forced Convection Experiments with an Air-Cooled Array," Heat Transfer in electronic Equipment, ASME HTD-Vol. 48, pp. 17-27.

Nakayama, W. and Park, S.-H. (1996), "Conjugate Heat Transfer From a Single Surface-Mounted Block to Forced Convective Air Flow in a Channel," Journal of Heat Transfer, Vol. 118, pp. 301-309.

Ortega, A. and Moffat, R.J. (1986a), "Buoyancy Induced Convection in a Non-Uniformly Heated Array of Cubical Elements on a Vertical Channel Wall," Heat Transfer in Electronic Equipment, ASME HTD-Vol. 57, pp. 123-134.

Ortega, A. and Moffat, R.J. (1986b), "Experiments on Buoyancy-Induced Convection Heat Transfer From an Array of Cubical Elements on a Vertical Channel Wall," Rept. No. HMT-38, Thermosciences Division, Department of Mechanical Engineering, Standford University, Standford, CA.

Ortega, A., Ulrich, S.W., and Kim, J.K. (1994), "Conjugate Forced Convection From a Discrete Heat Source on a Plane Conducting Surface: a Benchmark Experiment," Heat Transfer in Electronic Equipment, ASME HTD-Vol. 292, pp. 25-36.

Peterson, G.P. and Ortega, A. (1990), "Thermal Control of Electronic Equipment and Devices," in Advances in Heat Transfer, Vol. 20, Academic Press, New York, pp. 181-314.

Rajagopalan, M. (1991), "A Micrpcomputer-Based Data Acquisition System and Software for Research in Electronic Cooling," M.S. Report, Oklahoma State University, Stillwater, Oklahoma.

Roeller, P.T.and Webb, B.W. (1992), "A Composite Correlation for Heat Transfer From Isolated Two- and Three-Dimensional Protrusions in Channels," International Journal of Heat and Mass Transfer, Vol. 35, pp. 987-990.

Sparrow, E.M., Niethhammer, J.E. and Chaboki, A. (1982), "Heat Transfer and Pressure Drop Characteristics of Arrays of Rectangular Modules Encountered in Electronic Equipmnt," International Journal of Heat and Mass Transfer, Vol. 25, pp. 961-973.

Sparrow, E.M., Cook, D.S. and Chrysler, G.M. (1982), "Heat Transfer by Natural Convection From an Array of Short, Wall-Attached Horizontal Cylinders," Journal of Heat Transfer, Vol. 104, pp. 125-131.

Wagner, G.R. (1984), "Circuit Board Material/Construction and its Effect on Thermal Management," Section 3,Chapter 2 in Thermal Management Concepts in Microelectronic Packaging: From Component to System, ISHM Technical Monograph Series 6984-003, S.S. Furkay, R.F. Kilburn and G. Monti, Editors, Published by the International Society for Hybrid Microelectronics, Silver Spring, MD.

Wirtz, R.A. (1996), "Forced Air Cooling of Low-Profile Package Arrays,", Chapter 3 in Air Cooling Technology for Electronic, S.J. Kim and S.W. Lee, Editors, Published by the CRC Press, Inc., Boca Raton, FL.

Wirtz, R.A. and Dykshoorn, P. (1984), "Heat Transfer from Arrays of Flat Packs in Channel Flow," Proceedings of the 4th Annual International Electronics Packaging Society Conference, New York, pp. 318-326.

Yamamoto, H., Seki, N. and Fukusako, S. (1979), "Forced Convection Heat Transfer on Heated Bottom Surface of a Cavity," Journal of Heat Transfer, Vol. 101, pp. 475-479.

APPENDIX A

UNCERTAINTY ANALYSIS

APPENDIX A

UNCERTAINTY ANALYSIS

The uncertainties in the calculations for convection heat transfer coefficient and channel centerline velocity are presented here. The reader is referred to Kline and McClintock (1953) for a more complete discussion concerning uncertainty analysis theory.

A. 1 Convection Heat Transfer Coefficient (h)

Total Input Power

The total input power to the heat dissipating module is calculated using the equation:

$$Q_t = I \times Volt \qquad (A.1)$$

where I = the current in ampere measured by the Radio Shack 22-163 LCD auto range digital multimeter

Volt = voltage drop across the heat dissipating resistor in volt measured by the HP 3466A digital multimeter.

Following the procedure outlined in Kline and McClintock (1953), the uncertainty interval for the total input power calculations can be obtained from the following equation:

$$\omega_{Q_t} = \left[\left(\frac{\partial Q_t}{\partial I} \omega_I \right)^2 + \left(\frac{\partial Q_t}{\partial \text{Volt}} \omega_{\text{Volt}} \right)^2 \right]^{1/2} \tag{A.2}$$

where ω_I = the uncertainty interval for the current

and ω_{Volt} = the uncertainty interval for the voltage drop.

Taking the derivative of (A.1) with respect to I and Volt, it can be shown that

$$\frac{\partial Q_t}{\partial I} = \text{Volt} \tag{A.3}$$

and

$$\frac{\partial Q_t}{\partial \text{Volt}} = I \tag{A.4}$$

Now, substituting (A.3) and (A.4) into (A.2), dividing by Q_t, and multiplying by 100 yields an equation for the percentage uncertainty of the input power calculation:

$$\frac{\omega_{Q_t}}{Q_t} = \left[\left(\frac{\omega_I}{I} \right)^2 + \left(\frac{\omega_{\text{Volt}}}{\text{Volt}} \right)^2 \right]^{1/2} \tag{A.5}$$

The percentage uncertainty for the current ($\frac{\omega_I}{I}$) is ±1.5% from the Radio Shack digital multimeter owner's manual, the percentage uncertainty for the voltage drop ($\frac{\omega_{\text{Volt}}}{\text{Volt}}$) is ±0.03% from the Hewlett Packard digital multimeter operating manual. Substituting these values into (A.5) gives percentage uncertainty for the input power calculations due to inaccuracies in the current and voltage drop measurements:

$$\frac{\omega_{Q_t}}{Q_t} = 1.5\ \% \tag{A.6}$$

It is obvious that the greatest influence on the percentage uncertainty for the total input power is seen to be the current measurements by the Radio Shack digital multimeter.

Thermal Resistance of the Channel Floor

The thermal resistance of the channel floor was defined as:

$$R_w = \frac{1}{A_k}\left(\frac{t_1}{k_1} + \frac{t_2}{k_2} + \frac{t_3}{k_3}\right) \tag{2.3}$$

Now substituting all the corresponding values listed in Chapter II into (2.3), the equation for calculating the thermal resistance of the channel floor becomes

$$R_w = \frac{\frac{t_1}{A_k}}{k_1} + \frac{\frac{t_2}{A_k}}{k_2} + \frac{\frac{t_3}{A_k}}{k_3} \tag{A.7}$$

where

$$\frac{t_1}{A_k} = 0.0532 \text{ in (1/m)}$$

$$\frac{t_2}{A_k} = 2.480 \text{ in (1/m)}$$

$$\frac{t_3}{A_k} = 19.69 \text{ in (1/m)}$$

Following the procedure outlined in Kline and McClintock (1953), the uncertainty interval for the thermal resistance of channel floor calculations can be obtained from the following equation:

$$\omega_{R_w} = \left[\left(\frac{\partial R_w}{\partial k_1}\omega_{k_1}\right)^2 + \left(\frac{\partial R_w}{\partial k_2}\omega_{k_2}\right)^2 + \left(\frac{\partial R_w}{\partial k_3}\omega_{k_3}\right)^2\right]^{1/2} \tag{A.8}$$

Substituting the values $\frac{t_1}{A_k}$, $\frac{t_2}{A_k}$ and $\frac{t_3}{A_k}$ into (A.7) and then take the derivative of (A.7) with respect to k_1, k_2 and k_3, it can be shown that

$$\frac{\partial R_w}{\partial k_1} = \frac{-0.0532}{k_1^2} \tag{A.9}$$

$$\frac{\partial R_w}{\partial k_2} = \frac{-2.480}{k_2^2} \tag{A.10}$$

$$\frac{\partial R_w}{\partial k_3} = \frac{-19.69}{k_3^2} \tag{A.11}$$

Now, substituting (A.9), (A.10) and (A.11) into (A.8), dividing by R_w, and multiplying by 100 yields an equation for the percentage uncertainty of the thermal resistance of the channel floor calculations:

$$\frac{\omega_{R_w}}{R_w} = 100 \left\{ \left[\frac{(0.0532)}{R_w k_1} \left(\frac{\omega_{k_1}}{k_1} \right) \right]^2 + \left[\frac{(2.480)}{R_w k_2} \left(\frac{\omega_{k_2}}{k_2} \right) \right]^2 + \left[\frac{(19.69)}{R_w k_3} \left(\frac{\omega_{k_3}}{k_3} \right) \right]^2 \right\}^{1/2} \tag{A.12}$$

The uncertainty for each variable was estimated as follows:

$\frac{\omega_{k_1}}{k_1}$: the percentage uncertainty for the thermal conductivity of pure copper was estimated to be 10%, Ortega and Moffat (1986).

$\frac{\omega_{k_2}}{k_2}$: the percentage uncertainty for the fiberglass was estimated to be 10%, Anderson and Moffat (1990).

$\frac{\omega_{k_3}}{k_3}$: the percentage uncertainty for commercial plexiglas was estimated to be 10%,.

Substituting the above uncertainty values along with the following values into (A.12)

$R_w = 110.5$ °C/W $\qquad\qquad$ $k_1 = 401$ W/m-°C

$k_2 = 0.293$ W/m-°C $\qquad\qquad$ $k_3 = 0.193$ W/m-°C

the percentage uncertainty for the thermal resistance of the channel floor due to inaccuracies in the thermal conductivities of pure copper, fiber glass, and commercial plexiglas is:

$$\frac{\omega_{R_w}}{R_w} = 9.3\ \%$$

The greatest influence on the percentage uncertainty for the thermal resistance of the channel floor is seen to be the thermal conductivity of the commercial plexiglas.

Vertical Conduction Heat Loss Through the Channel Floor

The estimated vertical conduction heat loss through the channel floor was defined by the following equation in Chapter II:

$$Q_k = (T_m - T_\infty) / R_w \tag{2.2}$$

or

$$Q_k = \frac{\Delta T}{R_w} \tag{A.13}$$

where $\Delta T = T_m - T_\infty$.

Following the procedure outlined in Kline and McClintock (1953), the uncertainty interval for the vertical conduction heat loss through the channel floor can be obtained from the following equation:

$$\omega_{Q_k} = \left[\left(\frac{\partial Q_k}{\partial \Delta T} \omega_{\Delta T} \right)^2 + \left(\frac{\partial Q_k}{\partial R_w} \omega_{R_w} \right)^2 \right]^{1/2} \tag{A.14}$$

Taking the derivative of (A.13) with respect to ΔT and Q_k, it can be shown that

$$\frac{\partial Q_k}{\partial \Delta T} = \frac{1}{R_w} \tag{A.15}$$

$$\frac{\partial Q_k}{\partial R_w} = \frac{-\Delta T}{R_w^2} \tag{A.16}$$

Now, substituting (A.15) and (A.16) into (A.14), dividing by Q_k, yields an equation for the percentage uncertainty of Q_k calculations:

$$\frac{\omega_{Q_k}}{Q_k} = \left[\left(\frac{\omega_{\Delta T}}{\Delta T} \right)^2 + \left(\frac{\omega_{R_w}}{R_w} \right)^2 \right]^{1/2} \tag{A.17}$$

The greatest influence on the percentage uncertainty for the estimated vertical conduction heat loss through the channel floor is seen to be the thermal resistance of channel floor.

ΔT (T_m - T_∞)

Following the procedure outlined in Kline and McClintock (1953), the uncertainty interval for ΔT (T_m - T_∞) calculations can be obtained from the following equation:

$$\omega_{\Delta T} = \left[\left(\frac{\partial \Delta T}{\partial T_m} \omega_{T_m} \right)^2 + \left(\frac{\partial \Delta T}{\partial T_\infty} \omega_{T_\infty} \right)^2 \right]^{1/2} \tag{A.18}$$

Taking the derivative of ΔT (T_m - T_∞) with respect to T_m and T_∞, it can be shown that

$$\frac{\partial \Delta T}{\partial T_m} = 1 \tag{A.19}$$

$$\frac{\partial \Delta T}{\partial T_\infty} = -1 \tag{A.20}$$

Now, substituting (A.19) and (A.20) into (A.18), dividing by ΔT, yields an equation for the percentage uncertainty of ΔT calculations:

$$\frac{\omega_{\Delta T}}{\Delta T} = \left[\left(\frac{\omega_{T_m}}{\Delta T} \right)^2 + \left(\frac{\omega_{T_\infty}}{\Delta T} \right)^2 \right]^{1/2} \tag{A.21}$$

The influence on the percentage uncertainty for ΔT (T_m - T_∞) is seen to be equally distributed between the temperature of the heat dissipating module (T_m) and the surrounding air (T_∞).

Radiation Heat Loss

The estimated radiation heat loss to the surroundings from the heat dissipating module was defined by the following equation in Chapter II:

$$Q_r = \sigma \varepsilon A_m (T_m^4 - T_\infty^4). \tag{2.4}$$

Now substituting all the corresponding values listed in Chapter II into (2.4), the equation for calculating the estimated radiation heat loss to the surroundings from the heat dissipating module becomes

$$Q_r = 1.109 \times 10^{-11} (T_m^4 - T_\infty^4). \tag{A.22}$$

where the coefficient 1.109×10^{-11} is in W/K^4.

Following the procedure outlined in Kline and McClintock (1953), the uncertainty interval for the estimated radiation heat loss to the surroundings from the heat dissipating module calculations can be obtained from the following equation:

$$\omega_{Q_r} = \left[\left(\frac{\partial Q_r}{\partial T_m} \omega_{T_m} \right)^2 + \left(\frac{\partial Q_r}{\partial T_\infty} \omega_{T_\infty} \right)^2 \right]^{1/2} \quad \text{(A.23)}$$

Taking the derivative of (A.22) with respect to T_m and T_∞, it can be shown that

$$\frac{\partial Q_r}{\partial T_m} = 4.436 \times 10^{-11} T_m^3 \quad \text{(A.24)}$$

$$\frac{\partial Q_r}{\partial T_\infty} = -4.436 \times 10^{-11} T_\infty^3. \quad \text{(A.25)}$$

Now, substituting (A.24) and (A.25) into (A.23), dividing by Q_r, yields an equation for the percentage uncertainty of Q_r calculations:

$$\frac{\omega_{Q_r}}{Q_r} = \left[\left(\frac{4.436 \times 10^{-11} T_m^3 \omega_{T_m}}{Q_r} \right)^2 + \left(\frac{4.436 \times 10^{-11} T_\infty^3 \omega_{T_\infty}}{Q_r} \right)^2 \right]^{1/2} \quad \text{(A.26)}$$

The percentage uncertainty of the radiation heat loss to the surroundings from the heat dissipating module is seen to be equally influenced by the temperature of the heat dissipating module (T_m) and the surroundings air (T_∞).

Convection Heat Transfer Coefficient

The convection heat transfer coefficient is defined as:

$$h = \frac{Q_m}{A_m (T_m - T_\infty)} \quad \text{(2.5)}$$

where $$Q_m = Q_t - Q_k - Q_r \quad \text{(2.1)}$$

Now substituting (2.1) into (2.5), the equation for calculating convection heat transfer coefficient (h) becomes

$$h = \frac{Q_t - Q_k - Q_r}{A_m \ \Delta T} \tag{A.27}$$

where $\Delta T = T_m - T_\infty$.

Following the procedure outlined in Kline and McClintock (1953), the uncertainty interval for the convection heat transfer coefficient calculations can be obtained from the following equation:

$$h = \left[\left(\frac{\partial h}{\partial Q_t} \omega_{Q_t} \right)^2 + \left(\frac{\partial h}{\partial Q_k} \omega_{Q_k} \right)^2 + \left(\frac{\partial h}{\partial Q_r} \omega_{Qr} \right)^2 + \left(\frac{\partial h}{\partial \ \Delta T} \omega_{\Delta T} \right)^2 \right]^{1/2} \tag{A.28}$$

where ω_{Q_t} = the uncertainty interval for Q_t

ω_{Q_k} = the uncertainty interval for Q_k

ω_{Q_r} = the uncertainty interval for Q_r

and $\omega_{\Delta T}$ = the uncertainty interval for ΔT

Taking the derivative of (A.27) with respect to Q_t, Q_k, Q_r and ΔT, it can be shown that

$$\frac{\partial h}{\partial Q_t} = \frac{1}{A_m \ \Delta T} \tag{A.29}$$

$$\frac{\partial h}{\partial Q_k} = \frac{-1}{A_m \ \Delta T} \tag{A.30}$$

$$\frac{\partial h}{\partial Q_r} = \frac{-1}{A_m \ \Delta T} \tag{A.31}$$

$$\frac{\partial h}{\partial \ \Delta T} = \frac{-(Q_t - Q_k - Q_r)}{A_m \ \Delta T^2} \tag{A.32}$$

Now, substituting (A.29), (A.30), (A.31) and (A.32) into (A.28), dividing by h (equation 2.5), and multiplying by 100 yields an equation for the percentage uncertainty of the convection heat transfer coefficient calculations:

$$\frac{\omega_h}{h} = 100 \left\{ \left[\frac{Q_t}{Q_m} \left(\frac{\omega_{Q_t}}{Q_t} \right) \right]^2 + \left[\frac{Q_k}{Q_m} \left(\frac{\omega_{Q_k}}{Q_k} \right) \right]^2 + \left[\frac{Q_r}{Q_m} \left(\frac{\omega_{Q_r}}{Q_r} \right) \right]^2 + \left[\frac{\omega_{\Delta T}}{\Delta T} \right]^2 \right\}^{1/2} \quad \text{(A.33)}$$

The uncertainty for each variable was estimated as follows:

$\frac{\omega_{Q_t}}{Q_t}$: the percentage uncertainty for the total input power was analyzed earlier and calculated to be 1.5% (see equation A.6).

$\frac{\omega_{Q_k}}{Q_k}$: the percentage uncertainty for the estimated vertical conduction heat loss through channel floor was analyzed earlier and may be estimated from equation (A.17).

$\frac{\omega_{Q_r}}{Q_r}$: the percentage uncertainty for the estimated radiation heat loss to the surroundings from the heat dissipating module was analyzed earlier and may be estimated from equation (A.26).

$\frac{\omega_{\Delta T}}{\Delta T}$: the percentage uncertainty for ΔT was analyzed earlier and may be estimated from equation (A.21).

Substituting the above values and equations along with the following values into (A.33)

$Q_t = 10.0$ W $\quad Q_k = 0.1829$ W $\quad Q_r = 0.0252$ W

$Q_m = 9.792$ W $\quad T_\infty = 294.08$ K (20.93°C) $\quad T_m = 314.28$ K (41.13°C)

gives the maximum percentage uncertainty for the convection heat transfer coefficient:

$$\frac{\omega_h}{h} = 3.8\ \%\ \text{(maximum)} \qquad \text{(A.34)}$$

The greatest influence on the percentage uncertainty for the convection heat transfer coefficient is seen to be the difference between the module temperature and the measured approaching air temperature (T_m-T_∞).

A. 2 Channel Centerline Velocity (Air)

The channel centerline air velocity was calculated in the computer program VELAIR. The equation was derived from applying the Bernoulli's equation to the Pitot-static probe used in this study:

$$V = \sqrt{\frac{2\,\Delta P^*}{\rho}} \tag{A.35}$$

where V = channel centerline velocity in m/s

ΔP^* = the differential pressure measured by the pressure transducer in Pascals (Pa)

ρ = the approaching air flow density in kg/m^3 at T_∞

and T_∞ = the approaching air temperature in K.

From ideal gas law,

$$\rho = \frac{P^*_{atm}}{RT_\infty} \tag{A.36}$$

where P^*_{atm} = atmospheric pressure in Pa

$R = 287$, the gas constant of air in J/kg-K.

Before substituting these values into (A.35), first, making all the units consistent:

so $$\Delta P^* = \frac{25.4}{13.6} \times \frac{101325}{760} \Delta P \text{ in Pa.} \tag{A.36a}$$

where ΔP in inches of water column.

and

$$P^*_{atm} = \frac{101325}{760} P_{atm} \text{ in Pa.} \tag{A.36b}$$

where P_{atm} in mm Hg.

Now, substituting (A.36a), (A.36b) and (A.36) into (A.35), the equation to calculate the channel centerline velocity becomes:

$$V = 32.7419\sqrt{\frac{\Delta P \; T_\infty}{P_{atm}}} \tag{A.37}$$

Following the procedure outlined in Kline and McClintock (1953), the uncertainty interval for the channel centerline velocity calculations can be obtained from the following equation:

$$\omega_V = \left[\left(\frac{\partial V}{\partial \Delta P}\omega_{\Delta P}\right)^2 + \left(\frac{\partial V}{\partial T_\infty}\omega_{T_\infty}\right)^2 + \left(\frac{\partial V}{\partial P_{atm}}\omega_{P_{atm}}\right)^2\right]^{1/2} \tag{A.38}$$

where $\omega_{\Delta P}$ = the uncertainty interval for the differential pressure

and $\omega_{T\infty}$ = the uncertainty interval for the approaching air.

Taking the derivative of (A.37) with respect to ΔP, T_∞ and P_{atm}, it can be shown that

$$\frac{\partial V}{\partial \Delta P} = \frac{32.7419}{2}\sqrt{\frac{T_\infty}{\Delta P \; P_{atm}}} \tag{A.39}$$

$$\frac{\partial V}{\partial T_\infty} = \frac{32.7419}{2}\sqrt{\frac{\Delta P}{T_\infty \; P_{atm}}} \tag{A.40}$$

$$\frac{\partial V}{\partial P_{atm}} = -\frac{32.7419}{2}\sqrt{\frac{\Delta P \; T_\infty}{P_{atm}^3}} \tag{A.41}$$

Now, substituting (A.39), (A.40) and (A.41) into (A.38), dividing by V, and multiplying by 100 yields an equation for the percentage uncertainty of the channel centerline velocity calculations:

$$\frac{\omega_V}{V} = 100\left[\left(\frac{1}{2}\frac{\omega_{\Delta P}}{\Delta P}\right)^2 + \left(\frac{1}{2}\frac{\omega_{T_\infty}}{T_\infty}\right)^2 + \left(\frac{1}{2}\frac{\omega_{P_{atm}}}{P_{atm}}\right)^2\right]^{1/2} \qquad \text{(A.42)}$$

The value of the term $\frac{\omega_{\Delta P}}{\Delta P}$ for the differential pressure is ±15.3% which includes the uncertainty of the pressure transducer ±0.3% from the MKS pressure transducer instruction manual and estimated 15% uncertainty because of the installation (the vertical and horizontal positions and alignments with the air flow) of the pitot static probe when every time the channel centerline velocity was measured. The uncertainty interval for the approaching air temperature is estimated to be ±0.5 K(°C) whereas the uncertainty interval for the reading of the atmospheric pressure from the barometer is estimated to be ±1 mm Hg. Substituting these values and the following values for T_∞ and P_{atm} into (A.42)

$$T_\infty = 293.85\text{K } (20.7°\text{C}) \qquad P_{atm} = 725.5 \text{ mm Hg}$$

gives the maximum percentage uncertainty for the channel centerline velocity calculations due to inaccuracies in the pressure readings and temperature measurements:

$$\frac{\omega_V}{V} = 7.7\ \% \text{ (maximum)} \qquad \text{(A.43)}$$

The greatest influence on the percentage uncertainty for the channel centerline velocity is seen to be the differential pressure readings from the pressure transducer.

APPENDIX B

LOCAL VELOCITY MEASUREMENT RESULTS

APPENDIX B

LOCAL VELOCITY MEASUREMENT RESULTS

A set of typical data for three channel heights and four channel centerline velocities at three vertical locations on the center plane (span-wise) are presented and discussed here. The data were taken during some experimental runs of this study. Fig. B.1 illustrates the velocity profiles for the three channel height settings. The profiles at the location of 6 cm upstream of the leading row of modules can be categorized as follows:

for channel height H = 7.62 cm, developing flow,

for channel height H = 5.08 cm, further developed but still developing flow,

for channel height H = 3.81 cm, fully developed flow.

The greater the channel height, the greater the hydraulic diameter of the rectangular channel, thus longer distance was needed to reach fully developed flow. As shown in Fig. B.1, the velocity profiles of four channel centerline velocities appeared flat at the center core for H = 7.62 cm, parabolic for H = 3.81 cm and in between H = 7.62 and 3.81 cm for H = 5.08 cm.

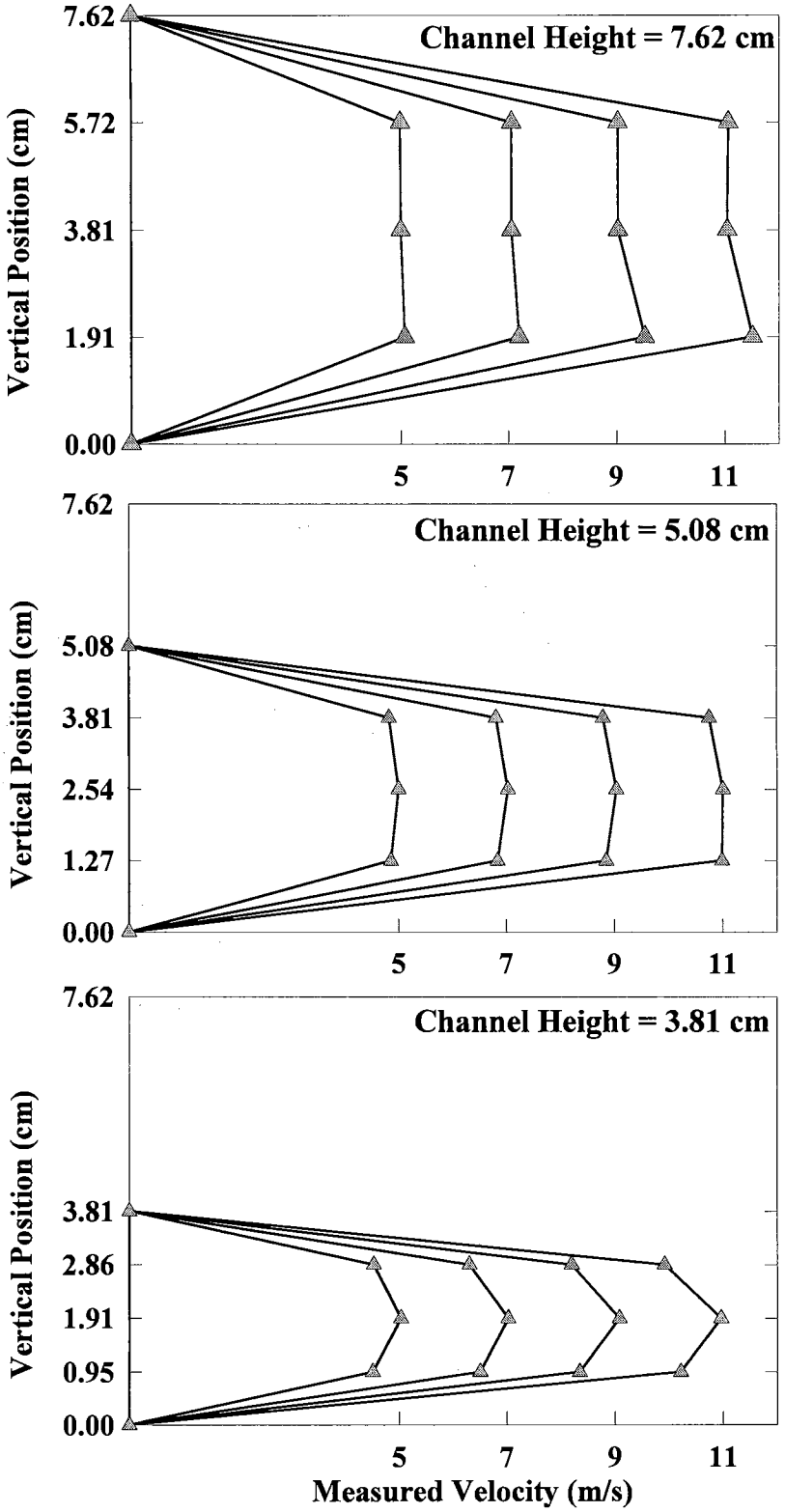

Fig. B.1 Velocity measurement of the rectangular channel at three vertical positions for three channel heights.

APPENDIX C

SAMPLES OF EXPERIMENTAL DATA

APPENDIX C

SAMPLES OF EXPERIMENTAL DATA

Due to the volume of the data collected in this study only a small sample of the data is presented. The complete data of this study are available from Professor A. J. Ghajar at the School of Mechanical & Aerospace Engineering of Oklahoma State University, 218 Engineering North, Stillwater, OK 74078. Telephone number: 405-744-5900.

A sample data file from the data reduction computer program, RED40, is presented in the following page for the experiments on the first module (row 1) of the center column when it was heated with a power level of 10 Watts at a channel centerline velocity (air) of 5 m/s and a channel height of 7.62 cm (3.0 in.) on the **1** oz, 2.54 cm copper band width conductive test board. This data file displays the average, lowest, and highest temperatures of each channel which usually consists of ten sets of raw data from the ECD-5100 digital data logger. Channel 2 is the steady state temperature of the first module of the right column (in the flow direction), channel 3, the second module and so on. Channel 10 is the steady state temperature of the first module of the center column, and channel 18 is the first module of the left column (in the flow direction). Channel 26 is the temperature of the approaching air. Both channels 1 and 27 were connected to dummy thermocouples. The data collected from channels 1 and 27 were not used in the data reduction processes of this study.

INPUT DATA FILE =B:4B1-511.H30 OUTPUT DATA FILE =B:T4B1-511.H30

****
THE RESULTS ARE

INLINE ARRANGEMENT WAS USED
THE TEMPERATURES ARE IN DEG C

CHANNEL NO.	MEAN TEMP	LOWEST TEMP	HIGHEST TEMP
1	24.91	24.70	25.00
2	25.36	25.30	25.40
3	25.00	24.90	25.10
4	24.99	24.80	25.10
5	24.95	24.80	25.10
6	25.01	24.90	25.10
7	24.80	24.70	24.90
8	24.76	24.60	24.80
9	24.69	24.60	24.80
10	58.23	58.20	58.30
11	27.25	27.10	27.40
12	25.98	25.90	26.20
13	25.34	25.20	25.40
14	25.35	25.30	25.50
15	24.78	24.70	24.80
16	25.08	25.00	25.20
17	24.65	24.60	24.70
18	25.02	24.90	25.10
19	24.26	24.20	24.40
20	24.51	24.40	24.60
21	24.21	24.10	24.30
22	24.58	24.40	24.70
23	24.10	24.00	24.20
24	24.63	24.50	24.80
25	24.15	24.10	24.20
26	24.31	24.20	24.40
27	24.21	24.10	24.30

THE START TIME (HRS AND MINS) =23.51
THE FINAL TIME (HRS AND MINS) = .09
DURATION OF EXPERIMENT (HRS AND MINS) = .18

EXPERIMENT WAS CONDUCTED ON 07/02/96 BY TANG
****

A sample data file from the data reduction computer program, RED40, is presented in the following page for the experiments on the first module (row 1) of the center column when it was heated with a power level of 10 Watts at a channel centerline velocity (air) of 5 m/s and a channel height of 7.62 cm (3.0 in.) on the **2** oz, 2.54 cm copper band width conductive test board. Only the heat dissipating and the eight neighboring modules were monitored for all three 2 oz conductive test boards so the monitored channel numbers reduced to twelve. Channels 2 to 4 are the steady state temperatures of the three neighboring modules of the right column (in the flow direction). Channels 5 to 7 are the steady state temperatures of the three modules of the center column, and channels 8 to 10 are the three neighboring modules of the left column (in the flow direction). Channel 11 is the temperature of the approaching air. When the first module of the center column was heated, no upstream module was monitored so channel 5 became the channel for first module and channel 7, the third module of the center column. Both channels 1 and 12 were connected to dummy thermocouples. The data collected from channels 1 and 12 were not used in the data reduction processes of this study.

INPUT DATA FILE =B:4B2-511.H30 OUTPUT DATA FILE =B:T4B2-511.H30

****
THE RESULTS ARE

INLINE ARRANGEMENT WAS USED
THE TEMPERATURES ARE IN DEG C

CHANNEL NO.	MEAN TEMP	LOWEST TEMP	HIGHEST TEMP
1	26.04	25.90	26.20
2	26.55	26.40	26.70
3	25.70	25.60	25.80
4	25.74	25.60	25.90
5	55.53	55.40	55.60
6	28.24	28.10	28.40
7	26.60	26.40	26.80
8	26.40	26.30	26.60
9	25.30	25.20	25.40
10	25.33	25.20	25.40
11	25.60	25.40	25.70
12	25.47	25.30	25.60

THE START TIME (HRS AND MINS) =15.25
THE FINAL TIME (HRS AND MINS) =15.34
DURATION OF EXPERIMENT (HRS AND MINS) = .09

EXPERIMENT WAS CONDUCTED ON 02/24/97 BY TANG
****

Two sample tables from the Microsoft Excel is presented in the following page for the experimental runs of the first seven modules (rows 1 to 7) of the center column when each of them was heated with a power level of 10 Watts at a channel centerline velocity (air) of 5 m/s and a channel height of 7.62 cm (3.0 in.) on the 1 and 2 oz, 2.54 cm copper band width conductive test boards. Only the third module (row 3) was also heated with a power level of 20 Watts (denoted as 3* in the tables). Each table represents an experimental run in this study.

Using the Excel spreadsheet, the temperature measurement data from the program RED40 were further reduced to calculate Qcond (estimated vertical conduction heat loss), Qrad (estimated radiation heat loss), Qconv (equivalent convection heat transfer rate), h (equivalent convection heat transfer coefficient) and Nu (Nusselt number) for each heat dissipating module. In these tables, Tc is the steady state heat dissipating module temperature and Tinfin is the approaching air temperature. k in these tables is the thermal conductivity of the approaching air evaluated at the average of the two temperatures listed in the last column. V listed in the last column of each table is the velocity measured during an experimental run in m/s, P is the measured atmospheric pressure in mm Hg and T is the approaching air temperature when the velocity measurement was taken in °C. Re in bold is the modified Reynolds number for that experimental run.

	1 oz, 2.54 cm band, H=7.62cm, V=5 m/s				k =	0.02613	W/(m.k)	
Row	Tc (C)	Tinfin (C)	Qcond (W)	Qrad (W)	Qconv (W)	h (W/m^2.C)	Nu	V7=5.017
1	58.23	24.31	0.1506	0.0469	9.803	89.6	87.1	P=718.8
2	61.87	24.86	0.1643	0.0522	9.784	81.9	79.7	T=29.3
3	66.65	26.09	0.1800	0.0589	9.761	74.6	72.5	Re =7571.7
4	70.57	26.79	0.1943	0.0650	9.741	69.0	67.0	V1=4.920
5	68.23	27.64	0.1802	0.0598	9.760	74.5	72.5	P=718.8
6	67.02	28.22	0.1722	0.0570	9.771	78.1	75.9	T=24.4
7	68.87	28.95	0.1772	0.0594	9.763	75.8	73.7	Re=7643.3
3*	106.16	25.46	0.3582	0.1414	19.500	74.9	72.8	**Re=9129**

	2 oz, 2.54 cm band, H=7.62 cm, V=5 m/s				k =	0.02595	W/(m.k)	
Row	Tc (C)	Tinfin (C)	Qcond (W)	Qrad (W)	Qconv (W)	h (W/m^2.C)	Nu	V7=4.926
1	55.53	25.60	0.2710	0.0411	9.688	100.3	98.2	T=23.3
2	59.89	25.62	0.3102	0.0481	9.642	87.2	85.4	P=732.2
3	61.42	24.32	0.3359	0.0521	9.612	80.3	78.6	Re=7846.4
4	63.08	23.49	0.3584	0.0559	9.586	75.1	73.5	V1=5.001
5	58.84	23.45	0.3204	0.0489	9.631	84.4	82.6	P=731.2
6	56.90	23.46	0.3027	0.0458	9.652	89.5	87.6	T=25.3
7	57.63	23.37	0.3102	0.0470	9.643	87.3	85.4	Re=7862.3
3*	97.72	23.87	0.6686	0.1235	19.208	80.6	78.9	**Re=9425**

VITA

Wen-chieh Tang

Candidate for the Degree of

Doctor of Philosophy

Thesis: AN EXPERIMENTAL STUDY OF HEAT TRANSFER OF A SINGLE HEATED MODULE ON CONDUCTIVE BOARDS IN THE TURBULENT REGION FOR AN IN-LINE ARRAY OF SURFACE MOUNTED CUBIC MODULES IN A HORIZONTAL RECTANGULAR CHANNEL

Major Field: Mechanical Engineering

Biographical:

Personal Data: Born in Taipei, Taiwan, On March 11, 1961, the son of Fan Tang and A-fan Lee.

Education: Graduated from Cheng Gung High School, Taipei, Taiwan, in June, 1980; received the Diploma in Mechanical Engineering from National Taipei Institute of Technology, Taipei, Taiwan, in June, 1984; received the Master of Science degree in Mechanical Engineering from New Jersey Institute of Technology, Newark, New Jersey, in January, 1990; completed the requirements for the Doctor of Philosophy degree at Oklahoma State University in July 1997.

Professional Experience: Teaching Assistant, School of Mechanical and Aerospace Engineering, Oklahoma State University, 1991 to 1996.

Professional Memberships: American Society of Mechanical Engineers, American Institute of Aeronautics and Astronautics.